THERMODYNAMIC MODELING OF COMPRESSIBLE HYDRATES AND CALCULATIONS OF MULTIPHASE EQUILIBRIUM DIAGRAMS

Iuri Soter Viana Segtovich

Tese de Doutorado apresentada ao Programa de Pós-graduação em Engenharia de Processos Químicos e Bioquímicos, da Universidade Federal do Rio de Janeiro, como parte dos requisitos necessários à obtenção do título de Doutor em Engenharia de Processos Químicos e Bioquímicos.

Orientadores: Frederico W. Tavares
Charlles R. de A. Abreu

Rio de Janeiro

Novembro de 2018

THERMODYNAMIC MODELING OF COMPRESSIBLE HYDRATES AND CALCULATIONS OF MULTIPHASE EQUILIBRIUM DIAGRAMS

Iuri Soter Viana Segtovich

TESE SUBMETIDA AO CORPO DOCENTE DO CURSO DE PÓS-GRADUAÇÃO EM ENGENHARIA DE PROCESSOS QUÍMICOS E BIOQUÍMICOS DA ESCOLA DE QUÍMICA (EPQB) DA UNIVERSIDADE FEDERAL DO RIO DE JANEIRO COMO PARTE DOS REQUISITOS NECESSÁRIOS PARA A OBTENÇÃO DO GRAU DE DOUTOR EM CIÊNCIAS EM ENGENHARIA DE PROCESSOS QUÍMICOS E BIOQUÍMICOS.

Examinada por:

Prof. Frederico Wanderley Tavares, D. Sc.

Prof. Charlles Rubber de Almeida Abreu, D. Sc.

Prof. Papa Matar Ndiaye, D. Sc.

Prof. Eduardo Rocha de Almeida Lima, D. Sc.

Prof. Marcelo Castier, Ph. D.

Prof. Márcio Luis Lyra Paredes, D. Sc.

Alexandre Mussumeci Valim de Freitas, Ph. D.

RIO DE JANEIRO, RJ – BRASIL

NOVEMBRO DE 2018

Segtovich, Iuri Soter Viana

Thermodynamic modeling of compressible hydrates and calculations of multiphase equilibrium diagrams/ Iuri Soter Viana Segtovich. – Rio de Janeiro, 2018.

xix, 141 p.

Orientadores: Frederico W. Tavares
Charlles R. de A. Abreu

Tese (doutorado) – Universidade Federal do Rio de Janeiro, Escola de Química, Programa de Engenharia de Processos Químicos e Bioquímicos, 2018.

1. Statistical Thermodynamics. 2. Natural Gas Hydrates. 3. Phase Equilibrium Algorithm. 4. Thermodynamic Modeling. 5. Solid Solution Compressibility. I. Tavares, Frederico W. (orient.) II. Abreu, Charlles R. de A. (coorient.) III. Título.

Ceci n'est pas une thèse

- Uma referência a René Magritte

Ó mar salgado, quanto do teu sal
São lágrimas de Portugal!
Por te cruzarmos, quantas mães choraram,
Quantos filhos em vão rezaram!
Quantas noivas ficaram por casar
Para que fosses nosso, ó mar!

Valeu a pena? Tudo vale a pena
Se a alma não é pequena.
Quem quer passar além do Bojador
Tem que passar além da dor.
Deus ao mar o perigo e o abismo deu,
Mas nele é que espelhou o céu.

- Mar português, de Fernando Pessoa

Agradecimentos

Aos meus professores orientadores desde os útimos perídos de graduação até a conclusão desse doutorado, Amaro, Charlles e Fred, pela solicitude, amizade e transmissão de conhecimento e experiências.

Ao apoio do pessoal atual e former members do laboratório ATOMS, professor Papa, professora Carla, professor Pedro, professor Cauê, professor Filipe, Dr. Gabriel, Dr[a]. Jéssica, Dr. Troner, Dr[a]. Ana, Aninha, Arthur, Cliff, Fellipe, Ingrid, Marlon, Thales, Vinicius, Vítor, Caio, Gerson, Hugo, Isabela, Mariana, Thiago, *Vanessa*, Yamara, *Wilfred*, Leo T. G., Renata, Hermes, *José*, *Jürgen*, Amanda, Maria Rosa, Thiago Marinho, Tiago Lemos, Felipe Coelho, José Torraca pelas discussões e, também, pelas descontrações.

À amigos do período de pós graduação em outros laboratórios, Dr. Leonardo Silva, e Dr. Gabriel Ferreira, Denis Dias, Felipe Gomide, Ataíde Neto, Daniel Tomaz, Afrânio, Otto e Flávio Lins pelas interdisciplinaridades e outros papos.

A Nathália, pela sua gestão e gerenciamento de projetos e, também, pelas descontrações.

Ao Leo da informática por resolver os nosso problemas de hardware e sua amizade.

Ao meu grande amigo Fernando Medeiros, que trouxe e desenvolveu grandes ideias em nossos projeto e pesquisa em hidratos, e em nosso grupo.

Enfaticamente, aos meus maiores amigos no laboratório ao longo desses anos: Rafael Pereira, Guilherme Carneiro e, novamente, Fernando Medeiros.

Aos meus pais e a minha namorada, pela paciência e pelo apoio incondicional.

A todos meus professores ao longo da minha vida e, novamente, a meus pais, pela formação.

Resumo da Tese apresentada ao EPQB/UFRJ como parte dos requisitos necessários para a obtenção do grau de Doutor em Ciências (D.Sc.)

THERMODYNAMIC MODELING OF COMPRESSIBLE HYDRATES AND CALCULATIONS OF MULTIPHASE EQUILIBRIUM DIAGRAMS

Iuri Soter Viana Segtovich

Novembro/2018

Orientadores: Frederico W. Tavares
Charlles R. de A. Abreu

Programa: Engenharia de Processos Químicos e Bioquímicos

Esta tese investiga a termodinâmica de equilíbrio de fases de hidratos. As principais contribuições são o desenvolvimento de um novo modelo termodinâmico para clatratos compressíveis e de um novo algoritmo para flash multifásico incluindo fases sólidas.

Este trabalho estende o modelo original de van der Waals e Platteuw para clatratos compressíveis dispensando a suposição de raio de cavidades constantes. Os resultados obtidos com este modelo incluem: (i) um desvio de pressão entre clatrato e estrutura não ocupada de referência, (ii) volume molar dependente do ocupante, (iii) dilatação da rede induzida pela adsorção sob aumento da pressão e (iv) equilíbrio isoestrutural com diferentes ocupâncias e volume de rede. Essa abordagem não introduz novos parâmetros empíricos. O modelo proposto apresenta características não relatadas na literatura, o que pode auxiliar na compreensão de diferentes cenários de formação de hidratos e projeto de processos.

O algoritmo para cálculos de equilíbrio multifásico proposto se baseia na generalização das equações flash de Rachford e Rice e de análise de estabilidade relacionadas à distância do plano tangente. Usando fatores K com múltiplas referências, o algoritmo aceita considerar componentes excluídos de alguma fase. As expressões reconhecem a modelagem de hidratos, em que fugacidade, pressão e temperatura são variáveis de entrada, e a composição é calculada. A generalidade deste algoritmo permite a geração de uma variedade de diagramas de fase. Devido às simplificações no sistema de equações, esse algoritmo é mais rápido e robusto do que a referência anteriormente proposta na literatura.

Abstract of Thesis presented to EPQB/UFRJ as a partial fulfillment of the requirements for the degree of Doctor of Science (D.Sc.)

THERMODYNAMIC MODELING OF COMPRESSIBLE HYDRATES AND CALCULATIONS OF MULTIPHASE EQUILIBRIUM DIAGRAMS

Iuri Soter Viana Segtovich

November/2018

Advisors: Frederico W. Tavares
Charlles R. de A. Abreu

Department: Chemical Engineering

This thesis investigates the thermodynamics of phase equilibrium of hydrates. The major contributions are the development of a new thermodynamic model for compressible clathrates and of a new algorithm for multiphase flash including solid phases.

This work extends the original van der Waals and Platteeuw model for compressible clathrates by dispensing with the assumption of constant cages radii. The results obtained with this model include: (i) a pressure shift between the clathrate and the empty lattice reference, (ii) guest dependent molar volume of the lattice, (iii) swelling of the lattice under increasing pressure and (iv) isostructural phase equilibrium with different cage occupancy and lattice volume. This approach introduces no empirical parameters. The proposed model presents features not previously reported in the literature which can aid in understanding different scenarios of hydrate formation and processes design.

The algorithm for multiphase equilibrium calculations proposed is based on the solution of a generalization of the flash equations from Rachford and Rice and of stability analysis equations related to the the tangent plane distance criteria. Using multi-reference K-values the algorithm handles components that are excluded from phases. The expressions for K-values acknowledge hydrate modeling where pressure, temperature and guest component fugacities are input variables, from which composition is calculated. The generality of this algorithm allows the generation of a variety of phase diagrams. Because of simplifications in the system of equations, this algorithm is faster and more robust than the reference previously proposed in the literature.

Contents

List of Figures **xii**

List of Tables **xv**

List of Symbols **xvi**

List of Abbreviations **xix**

1 Introduction **1**

1.1 General motivation 2

1.1.1 Phase equilibrium behavior of hydrates 3

1.1.2 Thermodynamic model for hydrates 4

1.1.3 High pressure environments 4

1.2 Objectives 4

1.3 Contributions 5

1.4 Structure of the text 6

2 Literature review **7**

2.1 Empirical correlations 7

2.2 Statistical thermodynamics and the van der Waals and Platteeuw model 8

2.3 Phase equilibria algorithms 8

2.3.1 Degrees of freedom in thermodynamic systems 9

2.3.2 Algorithm for hydrate formation condition 9

2.4 Thermodynamic modeling for a multiphase system 10
2.4.1 Flash calculations 12
2.4.2 Stability analysis 13
2.5 Modifications and extensions for variations in the lattice volume . 14
2.6 Negative apparent compressibility 16
2.7 Isostructural phase equilibrium 16
2.8 Final remarks 17

3 Thermodynamic modeling of gas hydrates 18
3.1 The van der Waals and Platteeuw basic principles 18
3.2 The partition function 19
3.3 The empty lattice reference 20
3.4 Cell theory and the Langmuir coefficients 21
3.5 Derived properties from the semi-grand-canonical partition function 23

4 Hydrate phase equilibrium calculations 26
4.1 Equations for the simultaneous multiphase flash and stability analysis calculations 27
4.2 Algorithm for the isothermal-isobaric flash. 29
4.3 NewtonRaphson loop 31
4.4 Successive substitution loop 34
4.5 Extension of the algorithm for incipient phase points 34
4.6 Initial guesses 37
4.7 Phase diagram sequential calculations 38

5 Results and discussion on Phase diagrams 41
5.1 Single guest hydrates 41
5.2 Low water content gas streams 43
5.3 Aqueous systems containing thermodynamic inhibitors 44

5.4 Phase diagram for a mixture of water, methane and propane . . . 46
5.5 Phase diagram for a mixture of water, ethane and propane 51
5.6 Phase diagram for a mixture of water, carbon dioxide and iso-butane 54

6 A natural pressure shift 56

6.1 Geometry relation between cages radii and lattice molar volume . 62
6.2 Volumetric properties for the empty lattice 65
6.3 Thermodynamic properties for compressible hydrates 66
6.3.1 Hydrate pressure 66
6.3.2 Chemical potential of the host component 68
6.4 The Clapeyron equation 69
6.5 Dissociation enthalpy 71
6.6 Parameterization 73
6.7 Pressure shift solution algorithm 73

7 Results and discussion of the pressure shift model 76

7.1 Lattice volume, cages radii and Langmuir coefficients. 76
7.2 Predictions of guest dependent lattice volume 78
7.3 Disambiguation of parameters for large guests 82
7.4 Phase equilibrium 84
7.5 Swelling of the hydrate lattice 96
7.6 Iso-structural phase equilibrium 98
7.7 Final remarks 103

8 Conclusions 104

Bibliography 106

A Derivation of the equations used in the multiphase flash algorithm 112

A.1 Gibbs energy minimization 112

A.2 Stationary point calculation 115
A.3 Generalized RachfordRice equation 117

B Derivation of the pressure shift model **121**

B.1 The semi-grand canonical partition function 121
B.2 The empty lattice reference 122
B.3 Cell theory and Langmuir coefficients 122
B.4 Derivation of thermodynamic properties from the partition function 124
B.5 Number of guest component molecules 128
B.6 Hydrate pressure 130
B.7 Chemical potential of the host component 132
B.8 Internal energy 133

C Parameterization of the hydrate modeling framework **134**

C.1 Formation properties for the empty lattice 134
C.2 Cell theory cages radii and Kihara potential 135
C.3 Volumetric properties of the empty lattice 136
C.3.1 Volume shift algorithm 138
C.4 Guest component fugacity 140
C.5 Volumetric properties for liquid water 140

List of Figures

1.1 Clathrate hydrate cages and crystal structures 2

2.1 Model framework for hydrate phase equilibrium calculations . . . 11

4.1 Flowchart of the procedures to systematically generate phase diagrams from a multiphase equilibrium algorithm. 40

5.1 Single hydrates formation boundary lines 42

5.2 Phase diagram for single guest methane hydrate in high and low water content 43

5.3 Phase diagram for single guest methane hydrate with and without ethanol. 45

5.4 Phase diagram for the system [H2O, C1, C3] with the global mole composition of $[0.40, 0.30, 0.30]$. 49

5.5 Highlight α from phase diagram of the system [H2O, C1, C3] with the global mole composition of [0.40, 0.30, 0.30]. 50

5.6 Highlight β from P.T phase diagram for the system [H2O, C1, C3] with the global mole composition of [0.40, 0.30, 0.30] 50

5.7 Highlight γ from P.T phase diagram of the system [H2O, C1, C3] with the global mole composition of [0.40, 0.30, 0.30] 51

5.8 Phase diagram for the system water/ethane/propane in the mixture composition of 0.5/0.15/0.35 52

5.9 Phase diagram for the system water/ethane/propane in the mixture composition of 0.40/0.30/0.30 52

5.10 Phase diagram for the system water/ethane/propane in the mixture composition of .990/0.005/0.005 53

5.11 Phase diagram for the system [H2O, CO2, iC4] with the global mole composition of [0.40, 0.58, 0.02] 55

6.1 Representation of the pressure shift model featuring volume difference for hydrates of different guests at a same pressure. 59

6.2 Cell theory potentials based on the Kihara intermolecular potential 61

6.3 Geometric relation between lattice edge length, number of molecules, extensive volume and molar volume. 63

6.4 Consistency test with the Clapeyron equation 70

6.5 Analysis of the pressure shift algorithm for given hydrate pressure 74

7.1 Lattice molar volume and cage radii and Langmuir coefficients as function of empty lattice pressure. 77

7.2 Pressure shift, lattice molar volume and occupancy of probe molecule hydrates versus the the hard-core size cage potential parameter 78

7.3 Pressure shift, lattice molar volume and occupancy of probe molecule hydrates versus the the soft-core size cage potential parameter 79

7.4 Pressure shift ($\Delta P^{\mathrm{H-EL}}$), lattice molar volume ($\overline{V}^{\mathrm{EL}}$) and occupancy Θ_{ij} of a single hydrate of a probe guest versus the energy cage potential parameter 80

7.5 Disambiguation of molecular size parameters with the pressure shift model at the standard temperature and pressure. 83

7.6 Comparison of different lattice behavior modeled in literature and proposed here 85

7.7 Phase equilibrium behavior of methane hydrates for the 6 models under analysis 88

7.8 Thermodynamics properties of methane hydrates for the 6 models under analysis. 89

7.9 Phase equilibrium behavior of carbon dioxide hydrates for the 6 models under analysis 91

7.10 Thermodynamics properties of carbon dioxide hydrates for the 6 models under analysis. 92

7.11 Phase equilibrium behavior of ethane hydrates for the 6 models under analysis 93

7.12 Thermodynamics properties of ethane hydrates for the 6 models under analysis. 94

7.13 Phase equilibrium behavior of a hydrates with a single type of cage for the pressure shift and standard models and different values of σ_i that generate the same values for Langmuir coefficient at P_0. 95

7.14 Swelling of hydrates at high pressure conditions using the proposed pressure shift model 96

7.15 Prediction of iso-structural phase equilibria for hydrates 99

7.16 Detailing iso-structural phase equilibria for a Carbon dioxide hydrate. 101

7.17 Critical behavior of the iso-structural phase equilibria. 102

C.1 Volume calculations for the volume shift algorithm 140

List of Tables

C.1 Formation properties for the empty lattice with respect to ice and pure liquid water. 135

C.2 Parameters for the Kihara cage potential. 136

C.3 Parameter from the methane hydrate molar volume correlation . . 137

C.4 Parameters of the molar volume correlation for pure liquid water . 141

List of Symbols

A	Absolute extensive Helmholtz energy, p. 19
N^{c}	Number of cages in the hydrate phase for each type of cage, p. 18
N^{g}	Number of particles in the hydrate phasevfor each guest component, p. 18
N_{w}	Number of molecules of water in the phase, p. 18
N_{ij}	Number of molecules for each guest type in each cage type, p. 24
P	Pressure, p. 7
Q	Canonical partition function, p. 19
R	ideal gas constant, p. 8
S	absolute extensive Entropy, p. 20
U	Absolute extensive internal energy, p. 20
V	extensive volume, p. 18
Z	Coordination number (number of waters in a hydrate cage), p. 23
Ψ	Absolute extensive semi-grand canonical thermodynamic potential, p. 19
Ξ	Semi-grand canonical partition function, p. 19
k_{B}	Boltzmann constant, p. 20
ϵ_i	Well depth parameter in the intermolecular potential, p. 23
$\overline{H}$	molar enthalpy, p. 10

$\overline{V}$	molar volume, p. 10
σ_i	Soft-core size parameter in the intermolecular potential, p. 23
TPD	Tangent plane distance, p. 13
TPD*	stationary point Tangent plane distance, p. 13
$\boldsymbol{K}$	K-values (distribution coefficient vector), p. 7
	matrix of Langmuir coefficients for each guest in each cage, p. 8
$\boldsymbol{\Theta}$	matrix of occupancy of each guest in each cage, p. 8
$\boldsymbol{\beta}$	mole basis phase ammount for each phase in a multiphase system, p. 9
$\hat{\boldsymbol{\phi}}$	fugacity coefficient vector, p. 12
$\hat{\boldsymbol{f}}$	fugacity vector, p. 8
γ	activity coefficients (symmetric convention), p. 11
$\boldsymbol{\lambda}$	Absolute activity, p. 19
$\boldsymbol{\mu}$	absolute chemical potential vector, p. 8
$\boldsymbol{\nu}$	number of cages to water molecules in a hydrate unit cell vector, p. 8
$\boldsymbol{\theta}$	vector of stability variables for each phase, p. 13
$\boldsymbol{x}$	composition matrix for each component in each phase, p. 9
$\boldsymbol{y}$	gas phase composition vector, p. 7
$\boldsymbol{z}$	overall composition vector for each component in a multiphase system, p. 9
T	Temperature, p. 7
REF	index of the reference phase with respect to mass balance, p. 28
a_i	Hard-core size parameter in the intermolecular potential, p. 23

b	index of an incipient phase in the multiphase system, p. 35
c	enumeration of components in the system, p. 28
n^{c}	Number of types of cages for a hydrate structure, p. 18
n^{g}	Number of types of guest components, p. 18
p	list of index of assumed present phases solved whose amount is solved in the multiphase flash, p. 28
N_{w}^{uc}	Number of water molecules in unit cell, p. 64
P_0	Reference condition pressure, p. 72
R	cages radii, p. 21
T_0	Reference condition temperature, p. 72
V^{uc}	Unit cell volume, p. 64
Φ	product of the configurational integral for internal degrees of freedom and particle momentum integral (thermal de Broglie wavelength), p. 21
$\overline{H}$	Molar enthalpy, p. 56
$\overline{U}$	Molar internal energy, p. 56
RES	Numerical method residue, p. 75
TOL	Numerical method tolerance, p. 75
a^{uc}	Unit cell edge parameter, p. 64
q	canonical partition function for a single enclathrated guest component molecule in a hydrate cage, p. 21
r	radial coordinate, p. 21
w	spherically symmetric cage potential, p. 21
C_P	Heat capacity, p. 72

List of Abbreviations

Aq	aqueous solution, p. 11
EL	empty lattice reference, p. 8
H	hydrate phase, p. 8
Lnp	liquid phase rich in non-polar components, p. 12
Pw	pure water phase, p. 11
ref	reference condition, p. 10
sat	saturation phase equilibrium condition, p. 12
uni	univariant phase equilibrium condition, p. 10
V	vapor, p. 12
Vw	pure water in vapor condition, p. 12
w	water, p. 8
I	Conventional ice, p. 45

Chapter 1

Introduction

Hydrates are solids first observed in laboratory experiments in 1810. These solids are composed of water and molecular species commonly known as the guest components. Some usual guest components are methane, ethane, propane, carbon dioxide, hydrogen sulfide, and iso-butane. Hydrates may form at conditions where water and at least one guest component are present. The formation of hydrates is favored at conditions of low temperature and high pressure.

Research of hydrate science and technology has been primarily of interest to the oil and natural gas processing industry since 1934 due to flow assurance issues. However, more recently, there has been intense research on natural reserves of methane hydrates and separation processes based on hydrate formation. As the production and processing of oil and gas operate with streams of mixtures with several guest components and water, the occurrence of gas hydrates in pipelines is a common concern. As hydrates are solid phases, their formation may cause pipeline blockage, if the particles are able to grow and agglomerate. Consequently, risks of accidents and need of expensive remediation measures arises.

Natural gas hydrates occurring in seafloor are a potential reserve of energy for some countries. These may occur at depths of 300-800 m in regions where there has been historical accumulation of organic matter and activity of methanogen bacteria, and also in continental areas in Russia.

Hydrate technology may be explored in separation processes involving water or guest components as industrial gas purification or water desalination. In the former, different affinities of different guest components to the hydrate phase lead to a difference in the composition of the feed gas and of the dissociation product. This can be explored in stages to accomplish a desired level of separa-

tion. For the latter, the process is equivalent to a separation of water by freezing. However, by using a hydrate promoter component, it is possible to achieve solidification of the water into a hydrate phase at mild conditions of temperature and pressure.

In 1949, microscopic investigation of hydrate systems has determined that the hydrate phase is a crystalline solid composed of a water lattice and cages which the molecules of the guest components can occupy. This allowed the development of the original model of van der Waals and Platteeuw, in 1959, as a successful application of statistical thermodynamics to phase equilibrium calculations in an engineering context.

Hydrate phases having different crystalline structures exist, as structures s^I, s^{II} and s^H shown in Figure 1.1. Each structure differs in number and geometry of the cages that compose it.

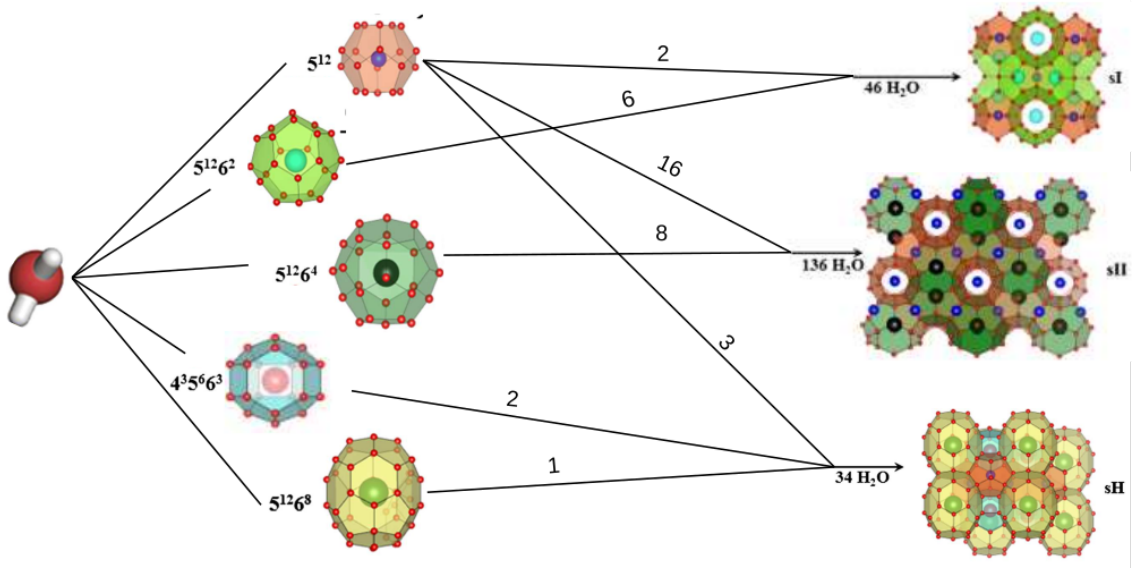

Figure 1.1: Clathrate hydrate cages and crystal structures s^I, s^{II} and s^H (Source: WARRIER *et al.*, 2016).

1.1 General motivation

For the purpose of design or optimization of processes, it is desired to have computational models to calculate thermodynamic properties and phase equilibrium behavior of relevant streams. In special, the flow assurance research field requires calculations of hydrates stability region, with respect to stream compositions and thermodynamic condition. In order to study the stability conditions for hydrates, equilibrium thermodynamics provides basis for the modeling of

properties and phase equilibrium.

1.1.1 Phase equilibrium behavior of hydrates

The standard scenario for discussing phase equilibrium behavior of hydrates is the three-phase equilibrium of a binary mixture between water and a guest component from natural gas. In this scenario a gas phase rich in the guest component, a liquid phase rich in water and the hydrate phase in a known structure are in equilibrium at a condition given by temperature and pressure along an univariant line.

Upon reduction of temperature, an ice phase becomes more stable than a liquid water phase, therefore there exists a four-phase coexistence condition, named a quadruple point, where phase transition between ice and liquid water takes place. Similarly, upon increase in pressure, the gas phase rich in guest components become less stable than a phase with those in liquid condition, therefore a second quadruple point exists, where phase transition for the condensation of the phase rich in guest component takes place. Depending on the guest component and on the range of temperature and pressure, a hydrate phase having either one or other structure might be present at the stable equilibrium condition. In the case of a mixture of different guest components, there may exist a region of coexistence of a liquid and a gas phase rich in the guest components or a region of coexistence of hydrate phases in different structures.

The algorithm of PARRISH and PRAUSNITZ (1972) is the standard method to calculate the incipient formation condition for scenarios where the guest components are found stable in either a liquid or vapor phase, and each hydrate structure can be tested separately. However, in order to handle the case of coexistence of fluid phases rich in the guest components or of the coexistence of hydrate phases in different structure the formalism of a multiphase flash algorithm is necessary. Furthermore, where it is not possible to safely assume which phases are present at the equilibrium condition, a stability analysis technique is essential to solve the stable phase equilibrium problem. In order to be able to calculate phase equilibrium involving hydrates in scenarios with different number of phases and phases in different physical states, this thesis investigates multiphase flash calculations, stability analysis and aspects of these type of calculations involving hydrate phases.

1.1.2 Thermodynamic model for hydrates

At first, the phase equilibrium calculations were based on empirical correlations regressed to experimental data of temperature and pressure of formation condition in the standard scenario for gas phases of different guest components. After the original van der Waals and Platteeuw model was published, it became the standard way of calculating thermodynamic properties of hydrates - chemical potentials, in special. From those calculations, phase equilibrium criteria could be solved rigorously using an appropriate algorithm.

1.1.3 High pressure environments

For high pressure conditions as in production of natural gas from deep sea floor hydrate layers or in flow assurance in deepwater oil fields, additional challenges become noticeable. Regarding modeling, it has been observed that the standard van der Waals and Platteeuw model calculations accuracy is not satisfactory. This inadequacy is atributed to compressibility of clathrates and distortion of cages in such conditions. As for algorithm adequacy, regions of coexistence and transition of stable hydrate phases in different structures require use of the multiphase flash and stability analysis formalism noted before. The works of Ballard and collaborators (BALLARD, 2004; BALLARD and SLOAN JR., 2004, 2002) are a milestone in both thermodynamic modeling and algorithm areas. During the study of hydrate phase equilibria at high pressure in this thesis, a thermodynamic inconsistency became apparent. In order to propose an improved model for hydrates at high pressure, considering the compressibility of lattices and consequent distortion of cages, this thesis investigates the assumptions of the original van der Waals and Platteeuw model and the derivations of expressions for thermodynamic properties from the model.

1.2 Objectives

The general goal of this thesis is investigating hydrate systems with respect to calculation of thermodynamic properties, phase equilibrium and kinetics of formation. Specifically, this thesis puts effort into the following aspects of hydrate formation:

- fundamentals of statistical thermodynamics needed to derive a thermodynamic model for a clathrate solution and the assumptions made in the

original van der Waals and Platteeuw model,

- propose a thermodynamically consistent extension to contemplate compressible clathrates,
- phase equilibrium algorithm and aspects of these type of calculations involving multiple phases including hydrate phases,
- the fundamentals of stability analysis and application to phase equilibrium including hydrate phases.

1.3 Contributions

The main contributions of this thesis are primarily to hydrate science and engineering. Nevertheless, some aspects of the phase equilibrium algorithm and specially of the compressible clathrate model are also applicable to other systems such as in adsorption science and engineering. Specifically, this thesis brings the following contributions from its development and results:

- A multiphase equilibrium algorithm with simultaneous stability analysis for systems involving hydrates, and which constitute an improvement over the works in the literature (BALLARD and SLOAN JR. (2004)).
  - The decoupling of generalizations of the Rachford and Rice equations from the stability analysis equations makes this algorithm faster and more robust than the reference work because it involves solution of a system of approximately half the number of equations, and with an issue of singularity at incipient condition calculations solved analytically.
  - Using multi-reference K-values the algorithm handles components that are assumed excluded from one or more phases.
  - The expressions for the updating of composition and fugacities acknowledge hydrate phases being modeled with the van der Waals and Platteeuw model, where pressure, temperature and guest component fugacities are input variables, from which composition and fugacities are calculated.

  The algorithm developed in this thesis and a discussion on phase diagram behavior of hydrate systems generated with this algorithm have been published on Fluid Phase Equilibria, (SEGTOVICH *et al.*, 2016a,b).

- A thermodynamic model for compressible clathrates which was derived here making a modification in the partition function and which constitute a new model with features not present in the previous literature.
  - phase equilibrium calculations pass a test based on the Clapeyron equation showing the model is thermodynamically consistent,
  - a pressure shift between the clathrate and the empty lattice isochoric reference,
  - varying water basis lattice volume for clathrates of different types of guest at the same temperature and pressure,
  - swelling of the hydrate lattice in equilibrium with a gas phase under increasing pressure,
  - isostructural phase equilibrium involving hydrate phases with different cage occupancy and water basis lattice volume,
  - this approach introduces no empirical parameters.

  The model developed in this thesis was presented at the XI Iberoamerican conference on phase equilibria and fluid properties for process design - EQUIFASE-2018 (SEGTOVICH *et al.*, 2018).

1.4 Structure of the text

A review on thermodynamic modeling and phase equilibrium of gas hydrates is presented on Chapter 2. Then this thesis describes the development of an algorithm for phase equilibrium calculations specifically suited to hydrate systems, also investigating limitations and proposing improvements and extensions. These are discussed in Chapters 4 and 5, and Appendix A. After, this thesis describes the thermodynamic modeling of hydrates, based on the original model of van der Waals and Platteeuw, investigating limitations and proposing improvements and extensions. These are discussed in Chapters 3, 6 and 7, and Appendix B and C.

Chapter 2

Literature review

This chapter presents a review on thermodynamic modeling and phase equilibrium of gas hydrates. This text shows the advancements of methods for calculating hydrate formation condition starting from the empirical methods, to the thermodynamic method based on the van der Waals and Platteeuw model, to aspects of phase equilibrium and stability analysis using the thermodynamic modeling, the modifications and extensions to the van der Waals and Platteeuw model and establishing the state-of-the art in clathrate modeling.

2.1 Empirical correlations

The earliest method for predicting the formation of natural gas hydrates are the *K*-values method of WILCOX *et al.* (1941). The method uses correlations for *K*-values, which represent the ratio between dry basis mole fraction of the feed gas and the hydrate as a function of temperature and pressure. The calculation of formation condition for hydrates is analogous to calculation of dew point calculations according to Eq. 2.1.

$$1 - \sum_i \left(\frac{y_i}{K_i(T,P)} \right) = 0 \tag{2.1}$$

where $\boldsymbol{y}$ is the vector of composition for the vapor phase and $\boldsymbol{K}$ is the vector of distribution coefficients for each component between the vapor and hydrate phases for a given temperature (T) and pressure (P).

2.2 Statistical thermodynamics and the van der Waals and Platteeuw model

Between the years of 1949 and 1952, experimental determination of the crystal structure of hydrates and the classification of these phases as clathrates was achieved. With this knowledge, VAN DER WAALS and PLATTEEUW (1959) developed a model based on statistical thermodynamics. In their model the chemical potential of water in the clathrate phase is expressed with respect to the theoretical empty lattice condition as a function of the cage occupancy according to Eq. 2.2.

$$\Delta\mu_{\mathrm{w}}^{\mathrm{H-EL}} = R\ T\ \ln\left(\prod_{j}\left(\left(1-\sum_{i}\left(\Theta_{ij}\right)\right)^{\nu_j}\right)\right) \tag{2.2}$$

where $\Delta\mu_{\mathrm{w}}^{\mathrm{H-EL}}$ is the change in chemical potential for water between the conditions of hydrate and empty lattice, $\boldsymbol{\Theta}$ is the cage occupancy matrix for each species in each cage, R is the ideal gas constant and $\boldsymbol{\nu}$ is the ratio between number of cages of each type and the number of water molecules in a hydrate unit cell for a given structure.

The cage occupancy is calculated analogously to the Langmuir adsorption theory from the fugacity of the guest component and an affinity coefficient named the Langmuir coefficients according to Eq. 2.3. The coefficients are calculated from the cell theory of LENNARD-JONES and DEVONSHIRE (1937) as a functional of the potential energy model for a guest component particle inside a cage.

$$\Theta_{ij} = \frac{C_{ij}\ \hat{f}_i}{1+\sum_{k}\left(C_{kj}\ \hat{f}_k\right)} \tag{2.3}$$

where $\boldsymbol{C}$ is the matrix of Langmuir coefficients and $\hat{\boldsymbol{f}}$ is the fugacity of each guest component.

2.3 Phase equilibria algorithms

Analysis of degrees of freedom in thermodynamic systems, flash calculations and stability analysis are fundamental in the derivation and discussion of this work. Some key aspects of these topics are covered here.

2.3.1 Degrees of freedom in thermodynamic systems

The number of degrees of freedom required in order to determine all the thermodynamic intensive variables that characterize each phase as pressure (P), temperature (T), and composition ($\boldsymbol{x}$) of a multiphase system in the state of equilibrium, is given by the Gibbs phase rule (Eq. 2.4) for a non-reacting system of n_c components and n_f phases.

$$\nu^{\text{Gibbs}} = n_c - n_f + 2 \tag{2.4}$$

In order to additionally determine the relative amount of matter between these phases, $n_f - 1$ new independent variables, β , together with $n_c - 1$ mass balance equations (Eq. 2.5) are included.

$$\sum_j (\beta_j \, x_{ij}) = z_i \tag{2.5}$$

Consequently, having specified global composition ($\boldsymbol{z}$), the remaining number of degrees of freedom is given by the Duhem theorem (Eq. 2.6).

$$\nu^{\text{Duhem}} = 2 \tag{2.6}$$

However, if ν^{Gibbs} is lower than ν^{Duhem}, being equal to 1 or to 0, then, respectively, the thermodynamic system is denominated univariant or invariant, and 1 or 2 degrees of freedom must be necessarily satisfied by specifying variables also from the multiphase system scope set, as $\boldsymbol{\beta}$ or $\boldsymbol{z}$. Or else the mathematical system will have infinitely many solutions for these variables which characterizes an ill posed problem type denominated indifferent (O'CONNELL and HAILE, 2005).

2.3.2 Algorithm for hydrate formation condition

PARRISH and PRAUSNITZ (1972) developed an iterative scheme for calculating pressure of formation condition using the model of van der Waals and Platteeuw. Their work received outstanding recognition in the literature for providing a clear and reliable algorithm for phase equilibria of hydrate of a given structure, ice or an liquid aqueous solution, and gas rich in hydrate forming components (H-Aq-V).

Alternatively, NG and ROBINSON (1977) used the Clapeyron equation to relate the slope of the univariant equilibrium curve to changes in volume and enthalpy of hydrate formation according to Eq. 2.7.

$$\left(\frac{\partial P}{\partial T}\right)_{\text{uni}} = \frac{\Delta\overline{H}^{\text{uni}}}{T\ \Delta\overline{V}^{\text{uni}}} \tag{2.7}$$

where $\Delta\overline{H}^{\text{uni}}$ is the heat of dissociation for 1 mol of hydrate and $\Delta\overline{V}^{\text{uni}}$ is the change in volume on dissociation of 1 mol of hydrate along the univariant phase equilibrium line.

The Clapeyron equation is an exact relation for univariant phase equilibria and, in the present work, it helped in the assessment of the consistency of the models and algorithms considered.

2.4 Thermodynamic modeling for a multiphase system

For application in phase equilibrium calculations, the chemical potential of water in the empty lattice condition is calculates with reference to the pure water in the stable condition, i.e. water or ice. This calculation is based on classical thermodynamics expression and values for formation properties according to Eq. 2.8.

$$\mathrm{d}\left(\frac{\mu_{\text{w}}^{\text{H}-\text{ref}}}{R\ T}\right) = \left(\frac{-\overline{H}^{\text{H}-\text{ref}}}{R\ T^2}\right)\ \mathrm{d}T + \left(\frac{\overline{V}^{\text{H}-\text{ref}}}{R\ T}\right)\ \mathrm{d}P \tag{2.8}$$

where $\mu_{\text{w}}^{\text{H}-\text{ref}}$, $\overline{H}^{\text{H}-\text{ref}}$ and $\overline{V}^{\text{H}-\text{ref}}$ are differences in chemical potential of water, molar enthalpy and molar volume between the hydrate phase and an arbitrary reference condition, respectively.

For applications in phase equilibrium calculations, the clathrate modeling framework is combined with fluid phase equations of state and condensed phase thermodynamic modeling for calculations of fugacity and this modeling set can be understood as shown in Figure 2.1. Each block therein represents a physical condition and each $\Delta\mu$ expression corresponds to an arrow linking two of these blocks. Fugacities are equivalent to calculations of $\Delta\mu$ with reference to the pure ideal gas reference condition.

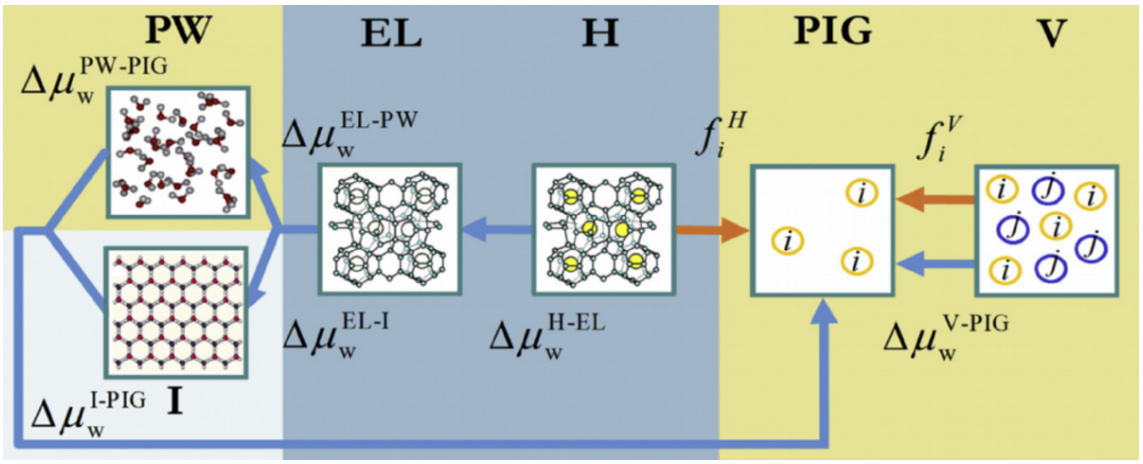

Figure 2.1: Model framework for hydrate phase equilibrium calculations. Each arrow corresponds to a calculation of chemical potential difference ($\Delta\mu$) for water (w) or a guest component (i) between two physical states. Pw stands for pure water, EL stands for empty lattice, H stands for hydrate, pIG stands for pure ideal gas, V stands for vapor, and I stands for conventional ice. The chemical potential difference of a given component in a given condition with respect to the pure ideal gas reference is given by means of its fugacity ($\hat{f}$)

Furthermore if an aqueous solution is to be considered, it is necessary to express the chemical potential of pure water (Pw) with respect to the aqueous solution (Aq), which is conveniently done using activity coefficients (γ) from an excess Gibbs energy model according to Eq. 2.9.

$$\Delta\mu_i^{\text{Aq}-\text{Pw}} = R\ T\ \ln\left(\gamma_i\ x_i\right) \tag{2.9}$$

In order to calculate phase equilibria without liquid water or ice present, it is necessary to calculate the chemical potential of water in the lattice with respect to the gas phase.

Fugacity is a measure of chemical potential with reference to the pure ideal gas state, thus it is a convenient measure for the calculation of H-V equilibria. In this spirit, SLOAN JR. *et al.* (1976) and NG and ROBINSON (1980) described the fugacity of water in the empty lattice (Eq. 2.10) based on an empirical correlation for the saturation pressure of a metastable EL-Vw equilibria, where the parameters of this correlation were obtained from actual hydrate formation data for each structure:

$$\hat{f}_{\text{w}}^{\text{EL}} = P_{\text{w}}^{\text{sat}}\ \hat{\phi}_{\text{w}}^{\text{sat}}\ \int_{P_0}^{P}\left(\frac{\overline{V}_{\text{w}}^{\text{EL}}}{R\ T}\right)\ \text{d}P \tag{2.10}$$

where $\hat{f}_{\text{w}}^{\text{EL}}$ is the fugacity of water in the empty lattice condition, $P_{\text{w}}^{\text{sat}}$ refers to

the saturation pressure of the metastable phase equilibria between the empty lattice and pure water in vapor state (EL-Vw), and $\hat{\phi}_w^{sat}$ is the fugacity coefficient of water in Vw condition at the saturation condition, at temperature T.

Alternatively, BALLARD and SLOAN JR. (2002) proposed to describe the chemical potential of hydrate using formation properties, as in Eq. 2.8, but with direct reference to the pure ideal gas state.

Finally, in order to calculate phase equilibria in mixtures where fluid phases rich in the guest components in liquid (Lnp) or vapor (V) phases coexist, or where hydrate phases in different structure coexist, the formalism of a multiphase flash algorithm is required.

2.4.1 Flash calculations

Flash calculations allow the determination of all intensive variables in a system having the specification of global composition and of two independent intensive variables, provided adequate thermodynamic models for each phase under consideration. In the *PT*-flash , temperature, pressure and global composition are defined, and the solution corresponds to individual phase compositions and relative amount of phases that correspond to the global minimum in Gibbs Energy of the multiphase system as necessary and sufficient condition for equilibrium (TESTER and MODELL, 1997a). The mathematical problem can then be faced as an optimization problem that can be tackled by a variety of mathematical and numerical methods. The most widely known method for flash calculations is the method of RACHFORD JR. and RICE (1952) for liquid vapor equilibria, centered on solving Eq. 2.11.

$$\sum_i \left(\frac{z_i \ (K_i - 1)}{1 + \beta \ (K_i - 1)} \right) = 0 \tag{2.11}$$

where $\boldsymbol{z}$ is the global composition and $\boldsymbol{\beta}$ is the relative amount of vapor in the system.

BISHNOI *et al.* (1989) and BALLARD and SLOAN JR. (2004) proposed advanced algorithms for flash calculations to describe systems presenting hydrates beyond formation condition. Their works were based on Gibbs energy minimization restricted to non-negative phase amount variables.

2.4.2 Stability analysis

When the method for solving phase equilibrium focus on derived necessary conditions for equilibrium, stability analyses are required as tools to assess if the sufficient condition for equilibrium is met at the solution calculated with the chosen approach.

The stability analysis method discussed by MICHELSEN (1982) presents the so-called tangent plane distance (TPD) given by Eq. 2.12. This quantity is associated with the change in Gibbs energy for the creation of an incipient phase with a given composition via the consumption of a small amount of a phase present in the system. In this sense, if the Gibbs energy decreases, it means a new phase with that composition could form spontaneously from the system under consideration, and a multiphase flash considering an additional phase with this composition as initial guess is required.

$$\mathrm{TPD} = \sum_i \left(x_i \ \left(\mu_{ij}(\boldsymbol{x}) - \mu_{ir}(\boldsymbol{z}) \right) \right) \tag{2.12}$$

where μ_{ij} and μ_{ir} are the chemical potential of the species i in the test phase and in the reference phase of the system under analysis, with composition given by $\boldsymbol{x}$ and $\boldsymbol{z}$, respectively.

The method consists on solving an optimization problem in order to find a stationary point of the tangent plane distance (TPD*) with respect to the test phase composition ($\boldsymbol{x}$).

Independently, the multiphase flash method of BISHNOI *et al.* (1989) and BALLARD and SLOAN JR. (2004) presents a so called stability variable ($\boldsymbol{\theta}$, Eq. 2.13). This variable is associated with the ratio of fugacity of any component between a given phase and a reference phase in the system under analysis.

$$\theta_j = \ln\left(\frac{\hat{f}_{ij}}{\hat{f}_{ir}}\right) \quad \texttt{for } i \texttt{ in 1 to } n_\mathrm{c} \tag{2.13}$$

where the value of the phase stability variable θ_j, defined for each phase, in the solution of the phase stability problem dictates the ratio of fugacities $\hat{f}_{ij}$ for all of the components split among that (j) phase and the reference (r) phase.

This variable has value of zero if the phase is present at equilibrium, either as a bulk or as an incipient phase. And it has a positive value if the chemical potential of components in that phase is higher than in the reference case. In such case, the consumption of an infinitesimal quantity of components in the

reference phase, for the creation of an infinitesimal quantity of this phase would increase the global molar Gibbs energy. This solution corresponds to a positive minimum in the TPD, and characterizes a so-called shadow phase, according to the notation from Michelsen. Oppositely, if it has a negative value, this phase would appear spontaneously and, the system is said thermodynamically unstable. In this case, these phase properties would constitute a suitable initial guess for a flash calculation including this phase in addition to previously considered phases.

Additionally, the expression *thermodynamically stable* is used to characterize a *system* for which the solution for the variables associated with each of its phases meets the sufficient conditions for equilibrium, consistently with given specifications. While each *phase* is classified either as *present* or *not present* at equilibrium.

In the present work, an algorithm based on the latter approach is derived. Here, it is observed that the stability variable from this approach corresponds to the dimensionless stationary tangent plane distance (TPD) of Michelsen.

2.5 Modifications and extensions for variations in the lattice volume

The modification and extensions that have been proposed since the publication of the original van der Waals and Platteeuw model concern either the calculation of the chemical potential of the lattice with respect to a suitable reference or the calculations of Langmuir coefficients.

In the original van der Waals and Platteeuw model, the specific volume of the lattice and cage radii are assumed constant. Based on the experimental data of TSE (1987) and of HIRAI *et al.* (2000b), KLAUDA and SANDLER (2000) have used a correlation for the specific volume of the lattice as function of temperature and pressure. More recently, MEDEIROS *et al.* (2018) report an improved correlation for the specific volume of the lattice as function of temperature and pressure based on the experimental data of KLAPPROTH *et al.* (2003) and SHPAKOV *et al.* (1998).

In order to predict changes in the lattice molar volume of the empty lattice and of hydrates of different guests, BELOSLUDOV *et al.* (2002) performed calculations of the free energy of the crystal *within the framework of lattice dynamics in the quasi harmonic approximation*. When comparing the calculations for the empty

lattice with those for actual hydrates, the authors observed what was called an *effective pressure*, the pressure of the empty lattice whose molar volume would be the same as for the actual hydrate molar volume in water basis.

Values for formation properties of the empty lattice reported by varying authors differ significantly because they refer to the theoretical empty lattice and, are determined indirectly by means of regression to actual hydrate phase equilibria (HOLDER *et al.*, 1988).

In an attempt to find reliable values for formation properties for the empty lattice, HANDA and TSE (1986) determined formation properties for Kr and Xe under the hypothesis the structure determined for those small monoatomic species would correspond to a non distorted empty lattice structure.

Several works seek to compensate for deviations in the calculations due to distortion of the lattice using guest-dependent empty lattice expressions.

Assuming that for different guest components, the empty lattice would have different specific volume and therefore different values for formation properties, ZELE *et al.* (1999) and LEE and HOLDER (2002) determined these values independently for several guest components. Similarly, KLAUDA and SANDLER (2000) performed regression of the saturation pressure of the metastable EL-Vw equilibria. In this approach, it is said that the formation properties or saturation pressure involved in the determination of the chemical potential of water in the empty lattice are those of the distorted lattice for each component. This allowed for a better representation of the available data, however at the expense of independent parameters for each guest component and with no direct extension for mixed guest hydrates.

From both experiment (IKEDA *et al.*, 2000) and molecular dynamics (HWANG *et al.*, 1993), it is shown that the unit cell parameter has a different equilibrium value for different kinds of guests.

According to the cell theory, the Langmuir coefficients depend on the cage radii. Considering that changes in the specific volume of the hydrate might affect these dimensions, BALLARD and SLOAN JR. (2002) propose the inclusion of this dependency using a proportionality relation. Additionally, the authors have observed variation in the specific volume of the lattice as large as 3% due to varying guest components. They have used this information empirically in an additional term as function of the proportion of guest components in a correlation for specific volume of the lattice. Similarly, HSIEH *et al.* (2012) used a correlation for Langmuir coefficients depending on the volume of the cages, which

was empirically dependent on pressure. This method, using parameters fitted to hydrate phase equilibrium data allowed improved representation of data at high pressure at the expense of independent parameters for each guest component and each type of cage of each structure and, still with no direct extension for mixed guest hydrates.

Furthermore, this thesis shows that the approach followed by these authors led to phase equilibrium calculations of single or mixed guest hydrates having a thermodynamic inconsistency.

2.6 Negative apparent compressibility

Although a pressure increase would induce a solid matrix into shrinking, in an adsorption system it would also favor the adsorption of more guest particles. On its turn, the increase in adsorbed quantity may induce an expansion of the matrix. The result of this swelling is an apparent negative compressibility of the adsorption system. This phenomenon has been observed in the work of ROZSA and STROBEL (2014) with β-hydroquinone clathrates of hydrogen. There, the authors analyzed the lattice compressibility of the hydrogen clathrates under conditions of varying cage occupancy. According to them, the total unit cell volume of the clathrate increased with an increase in pressure, in the range between 2.4 and 3.0 MPa. Furthermore, anisotropy was observed for the measurements on this material, one of the two characteristic dimensions showed negative apparent linear compressibility over the note range for pressure, while the other showed positive apparent linear compressibility, with the net effect being of negative apparent volumetric compressibility. The authors noted the change in compressibility matches the onset of hydrogen triple occupancy of the β-hydroquinone clathrates. From those observation, it can noted that experimental investigation is needed in order to see whether those properties are present in other clathrate compounds such as hydrates and, whether it is the triple occupancy onset is the responsible for negative compressibility.

2.7 Isostructural phase equilibrium

Experimental observations of HIRAI *et al.* (2000a,b) have shown a change in compressibility of the hydrate phase occurred between 0.7 and 1.5 GPa, although the fundamental crystal structure (s^I) of the methane hydrate was maintained up

to 2.3 GPa. They have observed that the cage occupancy for one type of cages to drop from near 90% to nothing on this transition. According to the authors, the results were not conclusive in strictly determining whether the observed result is stable or metastable behavior. In any case, the measurement of a thermodynamic metastable state, as opposed to kinetically stable states, is of interest to the development and validation of thermodynamic models modeling through correspondence with local minima in Gibbs energy.

In experiments with differential scanning calorimetry, LAFOND *et al.* (2015) observed anomalous melting behavior for clathrate hydrates of Xe. According to the authors, multiple dissociation events were observed, suggesting that more than one hydrate phase was present. However, crystallography experiments only showed one type of crystal structure. The lack of other crystal structures could be an indication of coexistence of different solid phases having the same crystal structure. The authors believe that these phases have different cage occupancy and that this behavior might be explained by strong interdependency between cage occupancy and Langmuir coefficients.

Nonetheless, it has already been shown that metal-organic frameworks can undergo isostructural phase transitions: ZHOU *et al.* (2014) showed that a given metal-organic framework presented negative compressibility together with an unexpected phase transition between phases with the same crystal structure.

2.8 Final remarks

As far as we could tell from current literature, there is no thermodynamic model in the classical thermodynamic equation of state scale that can explain or predict the observations regarding lattice volume changes for hydrates of different guests, effective pressure of hydrates of different guests with respect to an empty lattice, negative apparent compressibility and iso-structural phase equilibrium.

Chapter 3

Thermodynamic modeling of gas hydrates

Here, we present the van der Waals and Platteeuw model and the supporting models required in the clathrate modeling framework for calculations of thermodynamic properties and phase equilibrium. Detailed derivations for the expressions presented here are given in Appendix A, and the parameterization used in the work is given in Appendix B, for reproducibility purposes.

3.1 The van der Waals and Platteeuw basic principles

The original van der Waals and Platteeuw (1959) model is constructed using a partition function for a clathrate phase based on the following assumptions.

1. The hydrate is a solid mixture that can be described by the number of water molecules (N_{w}) and the number of the so-called guest components (N_i^{g}) molecules of a few types (n^{g}), temperature T and volume V^{H} of the phase.

2. There is an a priori description of a lattice of water molecules depending on just the same temperature T, having equal volume ($V^{\mathrm{EL}} = V^{\mathrm{H}}$) and equal number of water molecules (N_{w}), containing N_j^{c} identical cages of a few types (n^{c}).

3. A guest molecule is always located inside some cage, while one individual cage can never hold more than one guest molecule simultaneously.

With these premises, they devise a partition function in the canonical ensemble and, for convenience in dealing with phase equilibrium calculation, transform that into a semi-grand canonical partition function.

3.2 The partition function

The semi-grand canonical partition function (Ξ) represents an ensemble contemplating varying number (N_{ij}) of particles of each guest component (i) in each cage type (j) for a given chemical potential for each guest component (μ_i), a given number of water molecules (N_w) a given temperature (T) and a given phase volume (V). It is expressed as

$$\ln\left(\Xi\right) = \ln\left(Q^{\mathrm{EL}}\right) + \sum_j \left(\nu_j \; N_\mathrm{w} \; \ln\left(\sum_i \left(q_{ij} \; \lambda_i + 1\right)\right)\right) \tag{3.1}$$

where the proportionality factors ($\boldsymbol{\nu}$) relate the number of cages of each type and the number of water molecules in the hydrate phase and depends solely on the a priori described geometry of the lattice. And ($\boldsymbol{\lambda}$) are the so-called absolute activity, defined for each guest component in the hydrate phase from its chemical potential (μ_i), temperature (T) and Boltzmann constant k_B by

$$\mu_i = k_\mathrm{B} \; T \; \ln\left(\lambda_i\right) \tag{3.2}$$

Here, Q^{EL} is the canonical partition function describing the pure water empty lattice, by its temperature, volume and number of water molecules (Section 3.3), and q_{ij} is the single molecule canonical partition function under the mean field cage potential (Section 3.4).

The semi-grand-canonical partition function is associated with the thermodynamic potential we denote by Ψ, resulting from the Legendre transform of Helmholtz energy (A) switching each N_i^g for the corresponding μ_i as done in the transformation of the partition function from the canonical to semi-grand-canonical ensemble under its own formalism. Therefore, these thermodynamic potentials are related with each other and with the partition function by

$$\Psi = \left(A - \sum_i \left(N_i^\mathrm{g} \; \mu_i\right)\right) = \left(-k_\mathrm{B} \; T \; \ln\left(\Xi\right)\right) \tag{3.3}$$

3.3 The empty lattice reference

The van der Waals and Platteeuw model is applied to phase equilibrium calculation at varying T and P by describing the empty lattice Helmholtz energy from theoretical formation properties with respect to a reference condition of the host molecule. The reference condition is usually the spontaneously stable condition at given temperature and pressure. In this section, the reference considered is the pure liquid water. The canonical partition functions are related to Helmholtz energy by

$$\left(A^{\mathrm{EL}}\right) = \left(-k_{\mathrm{B}}\ T\ \ln\left(Q^{\mathrm{EL}}\right)\right) \tag{3.4}$$

where its differentials, from classical thermodynamics are

$$dA^{\mathrm{EL}} = -S^{\mathrm{EL}}dT - PdV^{\mathrm{EL}} + \mu_{\mathrm{w}}^{\mathrm{EL}}dN_{\mathrm{w}} \tag{3.5}$$

from which it can be shown that

$$d\left(\frac{A^{\mathrm{EL}}}{k_{\mathrm{B}}T}\right) = -\frac{U^{\mathrm{EL}}}{k_{\mathrm{B}}T^2}dT - \frac{P^{\mathrm{EL}}}{k_{\mathrm{B}}T}dV^{\mathrm{EL}} + \frac{\mu_{\mathrm{w}}^{\mathrm{EL}}}{k_{\mathrm{B}}T}dN_{\mathrm{w}} \tag{3.6}$$

From these, derived properties as chemical potential, internal energy and pressure can be calculated from the partition function by

$$\mu_{\mathrm{w}}^{\mathrm{EL}} = k_{\mathrm{B}}\ T\ \left(\frac{\partial\frac{A^{\mathrm{EL}}}{k_{\mathrm{B}}\ T}}{\partial N_{\mathrm{w}}}\right)_{T,V^{\mathrm{EL}}} \tag{3.7}$$

$$U^{\mathrm{EL}} = -k_{\mathrm{B}}\ T^2\ \left(\frac{\partial\frac{A^{\mathrm{EL}}}{k_{\mathrm{B}}\ T}}{\partial T}\right)_{V^{\mathrm{EL}},N_{\mathrm{w}}} \tag{3.8}$$

and

$$P^{\mathrm{EL}} = -k_{\mathrm{B}}\ T\ \left(\frac{\partial\frac{A^{\mathrm{EL}}}{k_{\mathrm{B}}\ T}}{\partial V^{\mathrm{EL}}}\right)_{T,N_{\mathrm{w}}} \tag{3.9}$$

These expressions are crucial for the symbolic derivations conducted here, as the canonical partition function for the empty lattice has precisely T, V^{EL} and N_{w} as independent variables. On the other hand, for numerical applications described by pressure instead of volume, it is most convenient to express

the chemical potential from the molar Gibbs energy as function of temperature, pressure and number of moles. This chemical potential is expressed not from an actual empty lattice partition function model but rather as $\Delta\mu_{\mathrm{w}}^{\mathrm{EL-Pw}}$, with reference to pure liquid water at P_0. This relative chemical potential at any T and P is described by $\Delta\mu_{\mathrm{w},T_0,P_0}^{\mathrm{EL-Pw}}$, a chemical potential difference at T_0 and P_0, and a correlation for the molar volume $\overline{V}^{\mathrm{EL}}$ of the pure water lattice as function of T and P, and for relative enthalpy $\Delta\overline{H}_{\mathrm{w},P_0}^{\mathrm{EL-Pw}}$, the latter also with respect to pure liquid water at P_0. The resulting expression is

$$\frac{\Delta\mu^{EL-PW}}{RT} = \frac{\Delta\mu_{00}^{EL-PW}}{RT_0} - \int_{T_0}^{T} \frac{\Delta\bar{H}_0^{EL-PW}}{RT^2} dT + \int_{P_0}^{P} \frac{\bar{V}^{EL}}{RT} dP \tag{3.10}$$

where the superscript $\mathrm{EL-Pw}$ indicates is a difference between empty lattice and the pure liquid water reference. We also note that our equation express the difference in chemical potential for the host molecule at given T, P and N_{w} in lattice condition to a reference condition at a standard pressure P_0, we find this more convenient because then we deal separately with expressions for molar volume of empty lattice here, and of the reference phase elsewhere depending on application.

3.4 Cell theory and the Langmuir coefficients

In order to describe the partition function for a single enclathrated molecule under the mean field cage potential (q_{ij}), additional considerations are necessary (VAN DER WAALS and PLATTEEUW, 1959).

4. Internal degrees of freedom of that guest molecule, are equivalent to those of particles it in the ideal gas state,

5. Translation inside the cage is subject to an mean field water-guest potential based on the approximation of Lennard-Jones and Devonshire.

From those assumptions, q_{ij} is given by a product of a term for internal degrees of freedom configurational integral and thermal wavelength, and a term for a configurational integral for the free volume as in

$$q_{ij} = \Phi_i \int_0^R \left[\exp\left(\frac{-w_{ij}}{k_{\mathrm{B}}T} \right) 4\pi r^2 \right] \mathrm{d}r \tag{3.11}$$

The factor Φ_i represents the configurational integral for internal degrees of freedom (as rotation and vibration) and particle momentum (thermal de Broglie wavelength), which is specific per component and solely a function of temperature. While the free volume integral is evaluated for the mean field cage potential w_{ij} along radial coordinate r in the domain of a cell of radius R_j. Also, the expression for w_{ij} itself depends on the radius R_j and coordination number Z_j of the cell, and on the nature of the guests, in terms of an effective intermolecular interaction potential. In addition, it is useful to relate absolute activity ($\boldsymbol{\lambda}$) to fugacity ($\hat{\boldsymbol{f}}$) using the ideal gas partition function as a reference as in

$$\hat{f}_i = \lambda_i k_\mathrm{B} T \Phi_i \tag{3.12}$$

This expression carries that same factor (Φ_i), in accordance with assumption 4.

Then, Langmuir coefficients (C_{ij}) are defined from

$$q_{ij}\lambda_i = C_{ij}\hat{f}_i \tag{3.13}$$

so that derived properties expressions can be rewritten in terms of finite C_{ij} and $\hat{f}_i$, instead of uncomputable absolute q_{ij} and λ_i, for practical phase equilibrium calculations. We can calculate from the free volume integral, for numerical calculations, as in

$$C_{ij} = \frac{\int_0^R \left[\exp\left(\frac{-w_{ij}}{k_\mathrm{B}T}\right) 4\pi r^2\right] \mathrm{d}r}{k_\mathrm{B}T} \tag{3.14}$$

where the factor (Φ_i) from Eq. (3.11) and Eq. (3.12) cancel out.

We can express q_{ij} from C_{ij}, for convenient symbolic calculations as in

$$q_{ij} = k_\mathrm{B} T \Phi C_{ij} \tag{3.15}$$

We use the cage potential w_{ij} derived from the Kihara pair interaction potential. This cage potential forbids the particle from being closer to the cage boundary by less than a hard-core interaction parameter a_i, thus Eq. 3.14 implementation has this information as $(R_j - a_i)$ built into its upper limit of integration (PRATT *et al.*, 2001).

The resulting expression for w_{ij} is given by MCKOY and SINANOĞLU (1963); PARRISH and PRAUSNITZ (1972); VAN DER WAALS and PLATTEEUW

(1959)

$$\mathtt{D1} = \frac{a_i}{R_j} \tag{3.16a}$$

$$\mathtt{D2} = 1 - \frac{r}{R_j} - \mathtt{D1} \tag{3.16b}$$

$$\mathtt{D3} = 1 + \frac{r}{R_j} - \mathtt{D1} \tag{3.16c}$$

$$\mathtt{DEL}(i) = \frac{\mathtt{D2}^{-i} - \mathtt{D3}^{-i}}{i} \tag{3.16d}$$

$$\mathtt{R1} = \frac{\sigma_i^{12}}{R_j^{11}} \tag{3.16e}$$

$$\mathtt{R2} = \frac{\sigma_i^{6}}{R_j^{5}} \tag{3.16f}$$

$$\mathtt{S1} = \mathtt{DEL}(10) + \mathtt{D1}\ \mathtt{DEL}(11) \tag{3.16g}$$

$$\mathtt{S2} = \mathtt{DEL}(4) + \mathtt{D1}\ \mathtt{DEL}(5) \tag{3.16h}$$

$$w_{ij} = \frac{2\ Z_j\ \epsilon_i\ \left(\mathtt{R1}\ \mathtt{S1} - \mathtt{R2}\ \mathtt{S2}\right)}{r} \tag{3.16i}$$

where a_i, σ_i and ϵ_i are the parameters from the Kihara pair interaction potential of guest component (i) and a water molecule from the lattice. The monospaced symbols used here represent non physically meaningful quantities used for breaking equations into smaller terms.

3.5 Derived properties from the semi-grand-canonical partition function

The hydrate thermodynamic potential is related to Helmholtz energy by Eq. (3.3) and therefore it can be shown that its differential form, from classical thermodynamics is

$$d\frac{\Psi}{k_\mathrm{B}T} = -\frac{U}{k_\mathrm{B}T^2}dT - \frac{P}{k_\mathrm{B}T}dV + \frac{\mu\mathrm{w}}{k_\mathrm{B}T}dN_\mathrm{w} - \sum_i \left[N_i d\ln\left(\lambda_i\right)\right] \tag{3.17}$$

We now proceed to obtain derived properties, specifically relations of guest amount, pressure, chemical potential of water, internal energy and enthalpy. These will have dependencies on empty lattice or ideal gas properties, the references we are carrying.

Inspecting Eq. (3.17), one can relate the number of guest molecules with the partition function

$$N_i = -\left(\frac{\partial \frac{\Psi}{k_B T}}{\partial \ln(\lambda_i)}\right)_{T,V,N_w,\lambda_{\neq i}} \tag{3.18}$$

which can be further decomposed into number of guests per cage type N_{ij}, whose total must recuperate N_i according to

$$N_i = \sum_j \left[N_{ij}\right] \tag{3.19}$$

The number of molecules N_{ij} for each guest type in each cage type is, therefore, given by

$$N_{ij} = \nu_j N_w \frac{q_{ij}\lambda_i}{\sum_i \left[q_{ij}\lambda_i\right] + 1} \tag{3.20}$$

from which it is now convenient to define the occupancy fraction (Θ_{ij}) of type j cages by molecules of type i as

$$\Theta_{ij} = N_{ij}/N_w = \frac{q_{ij}\lambda_i}{\sum_k \left[q_{kj}\lambda_k\right] + 1} = \frac{C_{ij}f_i}{\sum_k \left[C_{kj}f_k\right] + 1} \tag{3.21}$$

and composition can be calculated, for each component i in the guest components list g and for water w using

$$x_i = \frac{\sum_j \left(\nu_j \Theta_{i,j}\right)}{1 + \sum_j \left(\sum_k \left(\nu_j \Theta_{k,j}\right)\right)} \tag{3.22}$$

and

$$x_w = 1 - \sum_{i \text{ in } g} (x_i) \tag{3.23}$$

The chemical potential of water is related to the partition function according to

$$\mu_w = k_B T \left(\frac{\partial \frac{\Psi}{k_B T}}{\partial N_w}\right)_{T,V,\underline{\lambda}} \tag{3.24}$$

This property is essential to phase equilibrium calculations. The derivation for this property expression is presented in the original work of van der Waals and Platteeuw (1959) as

$$\Delta\mu_{\mathrm{w}}^{\mathrm{H-EL}} = k_{\mathrm{B}}T\left(\sum_{j}\left[\nu_j \ln\left(1-\sum_{i}\left[\Theta_{ij}\right]\right)\right]\right) \tag{3.25}$$

where the superscript $\mathrm{H}-\mathrm{EL}$ indicate this is a difference between actual hydrate and empty lattice reference.

Finally, for any phase equilibrium calculation, given guest component fugacities, pressure and temperature, after guest component composition are calculated using Eq. 3.21, 3.22 and 3.23, the fugacity for water is calculated according to

$$\hat{f}_{\mathrm{w}}^{\mathrm{H}} = \hat{f}_{\mathrm{w}}^{\mathrm{Pw}}\ \exp\left(\frac{\Delta\mu^{\mathrm{EL-Pw}} + \Delta\mu^{\mathrm{H-EL}}}{R\ T}\right) \tag{3.26}$$

and fugacity coefficients for guest component are calculated according to

$$\hat{\phi}_{\mathrm{w}}^{\mathrm{H}} = \frac{\hat{f}_{\mathrm{w}}^{\mathrm{H}}}{x_{\mathrm{w}}^{\mathrm{H}}\ P} \tag{3.27}$$

for water, and

$$\hat{\phi}_{i}^{\mathrm{H}} = \frac{\hat{f}_{i}^{\mathrm{H}}}{x_{i}^{\mathrm{H}}\ P} \tag{3.28}$$

for guest components.

Chapter 4

Hydrate phase equilibrium calculations

Here, we propose a modified algorithm for simultaneous multiphase flash and stability analysis calculations, based on the works of GUPTA *et al.* (1991) and of BALLARD and SLOAN JR. (2004). The proposed algorithm performs calculations regarding three kinds of specifications: the isothermal-isobaric-flash $TP-$flash, the incipient phase point temperature or pressure calculation, at given T or P, respectively ($P\beta_1-$flash or $T\beta_1-$flash), which determines a point over a $P \times T$ phase equilibrium diagram boundary line, and the two incipient phases point calculation $\beta_1\beta_2-$flash, which determines a point of intersection between two boundary lines.

We applied this algorithm in calculations of several phase diagrams involving liquid and vapor fluid phases, and ice and hydrates with s^{I} and s^{II} crystalline structures solid phases. These calculations included complex behavior such as single and mixed hydrates retrograde dissociation, hydrate structures coexistence, invariant points, thermodynamic inhibitor induced freezing point depression, low water content gas sublimation line.

Our algorithm depends on fugacity coefficients that have to be calculated by suitable thermodynamic models using input variables from a given iteration. To include hydrates phases within the algorithm calculations, we treat pressure, temperature and guest components fugacities as input variables and present expressions for the calculations of fugacity coefficients for all components included in hydrate phases from these variables.

4.1 Equations for the simultaneous multiphase flash and stability analysis calculations

The key equations used here are: multi-reference K-values, multiphase Rachford-Rice equations, equations for updating the composition, equations for updating the hydrate guests fugacity, and equations for calculating the stability variables. These were derived from Gibbs energy minimization for a $TP-$flash specification, with subsequent reformulations to allow for $T\beta_1-$flash, $P\beta_1-$flash and $\beta_1\beta_2-$flash calculations.

For each thermodynamic model considered, there shall be expressions for the array of fugacity coefficients ($\hat{\phi}_i$) of every component included in the modeled phases. For the sake of clarity, the equations that constitute the thermodynamic model for a given phase are proposed to be regarded by means of two abstractions, which differ in which are the most convenient input variables for each case (Eq. 4.1 and 4.2). The first abstraction applies for the fluid phases considered in this work, as well as ice, identified as thermodynamic models group 1 (TM1), while the second abstraction applies for hydrate phases in structures s^{I} and s^{II}, identified as thermodynamic models group 2 (TM2), as follows:

$$\hat{\phi}_i^{\mathrm{TM1}}\left(T, P, \boldsymbol{x}\right) \tag{4.1}$$

for a normalized composition given by $\boldsymbol{x}$, and

$$\hat{\phi}_i^{\mathrm{TM2}}\left(T, P, \hat{\boldsymbol{f}}^{\mathbf{g}}\right) \tag{4.2}$$

where $\hat{\boldsymbol{f}}^{\mathbf{g}}$ corresponds to guest component fugacities.

For components that are not included in some phase, by definition, e.g. any component other than water in ice phase, or any component unable to occupy hydrate cavities in a hydrate phase, its fugacity coefficient in the excluding phase tends to infinity.

The fugacity coefficients are used to define K-values (distribution coefficients - K_{ij}). We propose the use of multi-reference K-values which allow the consistent handling of such behavior, preventing infinity fugacity coefficients from appearing as numerators in any subsequent equations. This approach allows the methodology to take into consideration phases that exclude one or more components by using the most suitable phase as reference for each component, being it a phase which is assumed as being present and a phase which presents

the highest mole fraction value for that component among the other phases.

$$K_{i,j} = \frac{\phi_{i,ref(i)}}{\phi_{i,j}} \tag{4.3}$$

in which *ref* (i) represents the index of the chosen reference phase for component i.

Let c enumerate indexes for all components in the system, from 1 to n_{c}. Let m enumerate indexes for all modeled phases, from 1 to n_{m}, let $_{REF}$ be the index of the chosen mass balance reference phase, whose relative phase amount (β_{REF}) is considered a dependent variable according to

$$\beta_{REF} = 1 - \sum_{j \neq REF} [\beta_j] \tag{4.4}$$

and let p contain the indexes corresponding to the n_{p} phases assumed present, excluding the mass balance reference phase. Stability analysis and equilibrium criteria originate the following nonlinear residue equations for assumed present phases:

$$Res_j^{\mathrm{p}} = \sum_{i \ \mathtt{in} \ c} \left[\frac{z_i \left(K_{i,j} - K_{i,REF} \right)}{K_{i,REF} + \sum\limits_{l \ \mathtt{in} \ p} \left[\beta_l \left(K_{i,l} - K_{i,REF} \right) \right]} \right] = 0 \tag{4.5}$$

and the following explicit equation for assumed shadow phase stability variables:

$$\theta_j = \ln \left(\frac{\sum\limits_{i \ \mathtt{in} \ c} \left[\dfrac{z_i \left(K_{i,REF} \right)}{K_{i,REF} + \sum\limits_{l \ \mathtt{in} \ p} \left[\beta_l \left(K_{i,l} - K_{i,REF} \right) \right]} \right]}{\sum\limits_{i \ \mathtt{in} \ c} \left[\dfrac{z_i \left(K_{i,j} \right)}{K_{i,REF} + \sum\limits_{l \ \mathtt{in} \ p} \left[\beta_l \left(K_{i,l} - K_{i,REF} \right) \right]} \right]} \right) \tag{4.6}$$

Composition for group TM1 phases are related to mass balance variables and K-values as follows:

$$x_{i,ref(i)} = \frac{z_i}{K_{i,REF} + \sum\limits_{l \ \mathtt{in} \ p} \left[\beta_l \left(K_{i,l} - K_{i,REF} \right) \right]} \tag{4.7}$$

and

$$x_{i,j} = x_{i,ref(i)} K_{i,j} e^{\theta_j} \tag{4.8}$$

Additionally, for the group TM2, the following equation is proposed for updating fugacity of guest components as function of mass balance variables and K-values:

$$f_{i,j} = \frac{z_i K_{i,j} e^{\theta_j}}{K_{i,REF} + \sum\limits_{l \text{ in } p} \left[\beta_l \left(K_{i,l} - K_{i,REF}\right)\right]} \phi_{i,j} P \tag{4.9}$$

The complete derivation of these equations is presented in Appendix A.

4.2 Algorithm for the isothermal-isobaric flash.

The algorithm proposed here is considered as a simultaneous multiphase flash and stability analysis methodology. This is supported by the same characteristic present in the original works (BALLARD and SLOAN JR., 2004; GUPTA *et al.*, 1991), which is that phase amount and stability variable solutions are searched for simultaneously in the iterative scheme, as opposed to the methodology of MICHELSEN (1982), as discussed below.

These algorithms work with a definite number of modeled phases, that are phases that may be present at equilibrium in thermodynamic conditions close to the simulated condition, according to experience. The algorithm shall provide the information of whether each of these phases will be in fact present at equilibrium or not. In case a modeled phase is conclude not to be present, the variables corresponding to this phase may converge to a shadow phase solution or to a trivial solution. As the hydrate phases are modeled by a different set of equations than the fluid phases, and using different parameters for each structure, the variables corresponding to this phase may converge to a shadow phase solution, but not to a trivial solution.

As the algorithm progresses, these phases are either assumed as present or as shadow phase, which determines the independent variables and equations for the numerical method. The assumption for each phase and, therefore, the independent variables and equations, may change between iterations depending on values of stability and phase amount variables. On the other hand, in the approach used by Michelsen, a flash calculation with a definite set of phases assumed present at equilibrium is converged, and then an independent stability analysis loop is conducted to test whether another phase should be considered in a augmented flash calculation or not.

We should note that when a hydrate phase is not present at equilibrium, the variables in the system of equations that correspond to their properties will approach values that characterize a shadow phase solution. That is sure to occur because the hydrate modeling is done using different equations than the equation of state used for the fluid phases modeling (eos-phases). Conversely, the eos-phases variables may converge to trivial or shadow phase solutions, depending on thermodynamic conditions and initial guess for composition.

Here, we extend the concept of shadow phases to treat hydrate phases, having the guest component fugacities as the independent variables. However, the assurance of convergence of the stability analysis for eos-phases is very sensitive to initial guesses and the well understood technique of stability analysis discussed by Michelsen can be applied in combination with our algorithm for post-calculations analysis of stability of these fluid phases.

It should be noted that our successive substitution equation (Eq. 4.7) for the updating of composition values, when applied to an assumed shadow phase, works similarly to the one used by Michelsen for solution of stationary TPD composition. They are equivalent at the solution, however, differ in three aspects that will influence convergence:

First, our equation is similar to the one used in a flash calculation, in which the composition of the analyzed phase is updated according to its K-value and to every other present phase amounts and K-values. On the other hand, the equation used by Michelsen is similar to the one used in a bubble point equation, in which the composition of the analyzed phase is updated according to its K-value considering 1 reference phase. This difference will vanish in the limiting case of calculations involving a shadow phase and a single assumed present bulk phase.

Second, we used multi-reference K-values, in order not to have any division by numbers close to zero in the system of equations for the general case.

And third, we first calculate stability variables and then calculate normalized composition for the analyzed phase. In contrast, Michelsen approach calculates n_c not-normalized molar faction -like variables, from which they compute actual molar fractions and TPD.

The algorithm used consist of a loop for solution of the β_j variables for assumed present phases, given constant values of x_{ij} and $\hat{f}_{ij}$ solving multiphase Rachford Rice equations (Res_j^{p}), with proposed multi-reference K-values, using NewtonRaphson method. The θ_j variables are calculated after the Newton-

Raphson method. And x_{ij} or $\hat{f}_{ij}$, depending on the group to which each phase belongs, are updated in an outer loop using a successive substitution method. The multi reference K-values are evaluated from definition using the thermodynamic models when necessary, i.e. when its values are required and any of x_{ij} or $\hat{f}_{ij}$, T or P have been updated after its last evaluation.

After K_{ij} evaluations, a verification of convergence must be performed. If the values of composition and volume of an eos-phase (a fluid phase modeled with an equation of state) converge to the same values as the variables corresponding to another eos-phase in the list (which is denominated a trivial solution), the variables and equations related to that phase need to be removed from the system of equation system, because it is not be possible to independently calculate the β_j variables for two exactly equal phases and the Jacobian matrix in the NewtonRaphson method would become singular.

In the current approach, there is no possibility of reappearance of a phase that was eliminated as result of the trivial solution criteria. If desired to test for a phase with characteristics similar to the phase that was removed, a new phase must be created, at first assumed as a shadow phase with a new initial guess for composition.

4.3 NewtonRaphson loop

In a Newton-Raphson step, some variables are regarded as constant, while the others, regarded as independent variables v_j for residue functions Res_j and are updated according to the following expression in matrix notation:

$$\boldsymbol{v}^{[k+1]} = \boldsymbol{v}^{[k]} - \boldsymbol{J}^{-1}\boldsymbol{Res} \tag{4.10}$$

In which $\boldsymbol{J}$ is the Jacobian matrix, defined from the partial derivatives of each residue equation Res_j with respect to each independent variable v_j.

$$J_{n,j} = \left(\frac{\partial Res_n}{\partial v_j}\right)_{[v_{\neq j}]} \tag{4.11}$$

Originally, in the reference works (BALLARD and SLOAN JR., 2004; GUPTA *et al.*, 1991), all of the residue equations Res^{E} and Res^{S} that are presented in Appendix C, or equivalent versions of these, were solved in the Newton-Raphson method block, for all β_j and θ_j variables. However, we noticed prob-

lems in the convergence of that block caused by equations corresponding to the Res_j^{S} in incipient phase point calculations, when both β_j and θ_j for a given phase are equal to zero.

Here, based on the triviality of a solution for Res_j^{S} for either one of β_j or θ_j when the other one is assumed different from zero, it is proposed that this set of equations is implicitly solved analytically in the assembling of a reduced equation system being intended for numerical evaluation.

In this approach, the phases characterized as present or not present may be checked after every or after a couple of iterations. When a phase changes category the system of equations is reassembled before the algorithm moves on.

Also, being able to decouple Res^{E} for assumed present phases (Res^{P}) from the ones for shadow phases, θ_j variables for shadow phases are solved explicitly outside the Newton-Raphson block. And, therefore, only the equations Res^{P} are used to assemble the Res array of the Newton-Raphson method, and only β_j variables for assumed present phases are used to assemble the independent variable vector, while θ_j of these phases are zero, to meet the corresponding equation Res^{S} analytically, and θ_j of shadow phases is calculated after the Newton-Raphson loop. The management of which β_j variables should be calculated in the Newton-Raphson loop is done by an appearance/disappearance event handling with a presence list for the phases under consideration.

Hence, the proposed independent variable vector and residue functions that shall be solved in the Newton-Raphson loop, v_j and Res_j are, for a $TP-$flash:

$$\boldsymbol{v} = \left[\beta_j \texttt{ for each } j \texttt{ in } p\right] \tag{4.12a}$$

and

$$\boldsymbol{Res} = \left[Res_j^p \texttt{ for each } j \texttt{ in } p\right] \tag{4.12b}$$

where p lists the index of the phases that are assumed present in a given calculation step, among all the modeled phases, excluding the phase which is reference for the mass balance.

This system consists of a number variables and equations equal to the size of the p list, which is the number of assumed present phases, except the mass balance reference phase. This is an equation system with less than half the size of the equation system solved in then Newton-Raphson block in the reference works, which was twice all modelled phases (β_j and θ_j for each) except the mass balance reference phase.

Therefore, this modification contributes to improving the algorithm speed. By removing the equations Res^{S} known for causing numerical instability in the method, this modification also contributes to the algorithm robustness.

For the Jacobian matrix evaluation, the derivatives of equations Res^{P} with respect to the independent variables in the Newton-Raphson method are the following:

$$\left(\frac{\partial Res_n^p}{\partial \beta_j}\right)_{[\beta_{k\neq j}]} = -\sum_{i \text{ in } c}\left[\frac{z_i\left(K_{i,n}-K_{i,REF}\right)\left(K_{i,j}-K_{i,REF}\right)}{\left(K_{i,REF}+\sum_{l \text{ in } p}\left[\beta_j\left(K_{i,l}-K_{i,REF}\right)\right]\right)^2}\right] \tag{4.13}$$

After every step of the Newton-Raphson method, all the θ_j variables for the assumed shadow phases are calculated (Eq. 4.6) and 4 verification of convergence are performed:

- Step restriction is used such that β_j variables are not allowed to change more than 25% of its original values. In case the variable value is close to zero, the relative step approach becomes problematic. Tehrefore, if the limiting step size was lower than 1×10^{-5}, a limiting step of this fixed size was used instead.

- If any phase amount variable assumed negative value in a given iteration, the phase is removed from the present phases list, i.e., $\beta_j = 0$, and the element corresponding to this phase in the phase presence list is set to indicate that this phase is no longer assumed present and its stability variable should be calculated in the next iterations of the algorithm, while the phase amount is held constant and equal to zero. And if it is the reference phase β_{REF} to assume negative value, another phase is chosen as reference.

- If the stability variable for any phase assumes negative value while the phase amount for that phase is defined as zero, this phase is reinserted in the present phases list, i.e. $\theta_j = 0$ and its phase amount is reinitialized as $\beta_j = 1 \times 10^{-9}$, and it should be calculated in the next iterations of the algorithm, while the stability variable is held constant and equal to zero.

Here, we propose the use of an appearance/disappearance management that must not allow exceeding of $n^{c} + 1$ phases simultaneously present for a $TP-$flash calculation. The reason for that is that, while having more than n_c

present phases, the equation system becomes indifferent, i.e. the system will have infinitely many solutions for these variables, according to previous discussion. However, while equilibrium K-values are not obtained, as many as n_c of β_j variables can be calculated for assumed present phases in an iteration, besides the reference phase, without the problem of solutions. Otherwise, the consequences in the numerical method are that if there are too many phases present during Newton-Raphson iterations, the Jacobian matrix becomes singular. In case it is not possible to reinsert a phase without inflicting this rule, iterations proceed with the negative θ_j until disappearing of another phase is detected in the appearance/disappearance management.

4.4 Successive substitution loop

An outer loop is used to update and verify convergence in composition or fugacity using successive substitution method and the values provided from the NewtonRaphson loop for relative phase amounts and stability variables. More specifically, considering group TM1 phases according to the abstraction of Eq. (4.1), the composition is updated using explicit expressions for composition (Eq. 4.7 and 4.8), while, on the other hand, in this work, being group TM2 phase model regarded according to the abstraction presented in Eq. 4.2, it is proposed that fugacity is updated according to Eq. 4.9. Then thermodynamic models for group TM1 phases can use the new composition values and the ones for group TM2 can use the new fugacity values to provide updated fugacity coefficient values and K-values. In this way, the updating methodology is valid for simulations whereas the reference phase is a phase from group TM1 or TM2, unlike in the reference work BALLARD and SLOAN JR. (2004) in which the reference phase was required to be a fluid phase. Moreover, a step control is used so that the maximum allowed variation in the successive substitution is of 25% of the variable value in that iteration (or a minimum of 1×10^{-5}).

4.5 Extension of the algorithm for incipient phase points

Given the specification of determined phase amount and one of either T or P, the equation system is completely specified and then the remaining one of P or T can be calculated. For the determination of a boundary of the phase

envelope in the $P \times T$ diagram, i.e. a $T\beta_1-$flash or $P\beta_1-$flash, the β_j variable for determined phase is specified as zero, both the θ_j variable and the Res_j equation for that phase become obsolete, as the incipient phase is in equilibrium with the present phases, by definition; one of the T or P variables is specified and the remaining one is included in the NewtonRaphson equation system.

The partial derivatives of the equations Res^{p}, with respect to T or P are expressed analytically with respect to a dummy variable ξ, equivalent to T or P:

$$\mathtt{N1} = z_i \left(K'_{i,n} - K'_{i,REF} \right) \tag{4.14a}$$

$$\mathtt{D1} = K_{i,REF} + \sum_{l \ \mathtt{in} \ p} \left[\beta_l \left(K_{i,n} - K_{i,REF} \right) \right] \tag{4.14b}$$

$$\mathtt{N2} = z_i \left(K_{i,n} - K_{i,REF} \right) \left(K'_{i,REF} + \sum_{l \ \mathtt{in} \ p} \left[\beta_l \left(K'_{i,n} - K'_{i,REF} \right) \right] \right) \tag{4.14c}$$

$$\left(\frac{\partial Res_n^{\mathrm{p}}}{\partial \xi} \right)_{v \neq \xi} = \sum_{i \ \mathtt{in} \ c} \left[\frac{\mathtt{N1}}{\mathtt{D1}} - \frac{\mathtt{N2}}{\mathtt{D1}^2} \right] \tag{4.14d}$$

In which $K'_{i,n}$ is the partial derivative of $K_{i,n}$ with respect to ξ:

$$K'_{i,n} = \frac{1}{\phi_{i,n}} \left(\frac{\partial \phi_{i,ref(i)}}{\partial \xi} \right) - \frac{\phi_{i,ref(i)}}{\left(\phi_{i,n} \right)^2} \left(\frac{\partial \phi_{i,n}}{\partial \xi} \right) \tag{4.15}$$

This expression, in turn, depends on the derivatives of the fugacity coefficients with respect to the same variable. Considering a generalized algorithm for any thermodynamic models, this partial derivative are evaluated numerically using the central point finite difference method.

$$\left(\frac{\partial \phi_{i,ref(i)}}{\partial \xi} \right) = \frac{\phi_{i,ref(i)}(\xi + \delta) - \phi_{i,ref(i)}(\xi - \delta)}{2\delta} \tag{4.16}$$

for each component and phases in which they are included. Otherwise, for each component in phases from which they are excluded, it is equal to zero, where δ is an arbitrary perturbation, having magnitude much smaller than ξ and, at the same time, higher than numerical tolerance used in these calculations (e.g. $\delta = 1 \times 10^{-5}\xi + 1 \times 10^{-10}$).

Let b_1 be the index for an assumed incipient phase. This index should be removed from the p array, as the phase amount for an incipient phase is zero, and this variable will be fixed in calculations of condition (T or P) for incipient point.

Hence, the proposed independent variable vector and residue functions that shall be solved in the NewtonRaphson loop, v_j and Res_j are, for a $T\beta_1-$flash or a $P\beta_1-$flash.

$$v^{\mathrm{b}_1} = \left[T \texttt{ or } P, \ \left(\beta_j \texttt{ for each } j \texttt{ in } p\right)\right] \tag{4.17}$$

and

$$Res^{\mathrm{b}_1} = \left[Res^{\mathrm{p}}_{b_1}, \ \left(Res^{\mathrm{p}}_{j} \texttt{ for each } j \texttt{ in } p\right)\right] \tag{4.18}$$

In the same way, by specifying two phase amounts, i.e. a $\beta_1\beta_2-$flash, the T and P pair that satisfy the specification can be calculated, by specifying these two phases as incipient, one can find the T and P pair that marks the intersection between the phase diagram boundaries for two distinct incipient phases.

Let b_2 be the index for a second assumed incipient phase, remove also this index from the p array. The proposed independent variable and equation system is then as follows.

$$v^{\mathrm{b}_1,\mathrm{b}_2} = \left[T, \ P, \ \left(\beta_j \texttt{ for each } j \texttt{ in } p\right)\right] \tag{4.19}$$

and

$$Res^{\mathrm{b}_1,\mathrm{b}_2} = \left[Res^{\mathrm{p}}_{b_1}, \ Res^{\mathrm{p}}_{b_2}, \ \left(Res^{\mathrm{p}}_{j} \texttt{ for each } j \texttt{ in } p\right)\right] \tag{4.20}$$

In summary, the T or P can be solved for the $T\beta_1-$flash, $P\beta_1-$flash or $\beta_1\beta_2-$flash calculations using the same set of residue functions as for the $TP-$flash, just by differentiating those with respect to the different desired set of variables.

The maximum number of assumed present phases allowed by the appearance/disappearance management increases to $n^{\mathrm{c}}+2$ and $n^{\mathrm{c}}+3$ in the $T\beta_1-$flash or $P\beta_1-$flash and in the $\beta_1\beta_2-$flash, respectively, as the specified β_j variables for the b_1 and b_2 phases are specified, and not calculated in the Newton-Raphson method.

The algorithm is summarized as follows. The decisions involved in the block diagram are based on flash specifications or on each phase thermodynamic

model group.

Function `multiphaseFlash()`**:**
- **input:** z_i, CalculationMode, 2 of {T,P,β_j} accordingly
- **guess:** x_{ij}, $\hat{f}_{ij}$, T, P, β_j, θ_j
- Assemble v_j according to Eq. (4.12a, 4.17 or 4.19)
- **do**
  - **do**
    - Calculate K_{ij} from x_{ij},$\hat{f}_{ij}$,T,P (Eq. 4.3).
    - Calculate RES_j^{NR} according to Eq. (4.12b, 4.18 or 4.20).
    - Calculate Jac according to Eq. (4.11, 4.13, 4.14d and 4.15).
    - Update v_j in a Newton Raphson method step (Eq. 4.10)
    - Update β_j, T and P, accordingly to the definition of v_j
    - Update θ_j according to the explict equation Eq. 4.6
    - **if** $\beta_{REF} < 0$ **then**
      - change reference;
      - reassemble v;
    - **else if** $\beta_j < 0$ **then**
      - reassemble v;
    - **end**
    - **if** $\theta_j < 0$ **then**
      - reassemble v;
    - **end**
  - **loop while** abs $\left(RES^{NR}\right) > 1 \times 10^{-9}$;
  - Update x_{ij} for phases in TM1, according to Eq. (4.7 and 4.8)
  - Update $\hat{f}_{ij}$ for phases in TM2, according to Eq. (4.9)
  - Calculate $RES^{SS} \leftarrow \sum_{i,j1} \left([x_{i,j1}]^k - [x_{i,j1}]^{k-1}\right) + \sum_{i,j2} \left([\hat{f}_{i,j2}]^k - [\hat{f}_{i,j2}]^{k-1}\right)$
- **loop while** abs $\left(RES^{SS}\right) > 1 \times 10^{-9}$;

return x_{ij}, $\hat{f}_{ij}$, T, P, β_j, θ_j

4.6 Initial guesses

As not to violate Gibbs phase rule in the initial guess, n^c, $n^c + 1$ and $n^c + 2$ phases, where all the components are included in at least one of them, are assumed present for the $TP-$flash, $T\beta_1-$flash or $P\beta_1-$flash and $\beta_1\beta_2-$flash specifications, respectively. For the β_j variables, the initially guessed present phases may be initialized as present in equal amounts, while the θ_j values for the initially absent phases may be any positive number, but usually lower than 1. Also, initial guess values for K_{ij} can be obtained from correlations, ideal behavior as-

sumption or evaluations of the thermodynamic models using initial guesses for the thermodynamic models inputs, that is, composition of fluid phases and fugacity of guests in hydrate phases. Initial guess for composition of fluid phases are taken empirically according to MICHELSEN (1982) suggestions and to experience. Initial guess for fugacity of guests is equal to the fugacity of components in an assumed present fluid phase, as calculated from the corresponding equation of state.

4.7 Phase diagram sequential calculations

We assemble phase diagrams from recursive usage of the presented algorithm. For one given phase as in incipient condition, determining the pressure at a given temperature ($T\beta_1-$flash) or temperature at a given pressure ($P\beta_1-$flash) corresponds to points belonging to line segments of phase boundary curves. While finding the pressure and temperature for the specification of two incipient phases ($\beta_1\beta_2-$flash) corresponds to the point of intersection between two line segments.

The phase diagram is composed of line segments that correspond to one phase in incipient condition. We generate these line segments using incipient conditions calculations recursively, following a grid in pressure or in temperature.

We initialize the calculations using a $TP-$flash at the minimum temperature and minimum pressure in the range of interest. Then, knowing what are the phases that are present in bulk amount in the edge of the range of interest, we perform a $T\beta_1-$flash to find the pressure at which either one of these phases will disappear, or a different phase will appear. The solution corresponds to the first point in the diagram under study. Then we increase the specified temperature following a grid that extends to the maximum temperature in the range of interest and perform additional $T\beta_1-$flash sequentially. We use the solutions for the calculation of one point as initial guess for the next. Depending on the slope of the curve being calculated, we change the choice of which is the specified variable. While the slope is close to zero, temperature is used as the specified variable. If the slope becomes higher than a given limit, pressure is used as the specified variable $P\beta_1-$flash, following a grid that extends to the maximum or minimum pressure in the range of interest, according to the trend observed in the previous few points. The limit used was based empirically on the scale of

the plot in the region of interest:

$$\left(\left(\frac{\partial \ln P}{\partial T}\right)_{\text{eq}}\right)^{\text{lim}} = 1 \tag{4.21}$$

At a condition over some line segment, all phases that are present in either of the separate regions will be present. An incipient phase line may consist of a few adjacent line segments joined at 2- or 3-line connections. Some of the 4 or 6 segments that meet at these connections superpose if they are univariant.

At some point the algorithm will indicate either that one of the bulk phases that was present in a previous point is no longer present or that a bulk phase that was not present in a previous point is now present (the stability variables corresponding to one phase changes from positive to zero and the phase amount changes from zero to a positive value between two points in the calculation grid). That indicates that a curve for one incipient phase has intercepted with the curve for a different incipient phase. The precise values of the points of intersection are calculated using $\beta_1\beta_2-$flash specification. After an intersection, the slope of the curve for an incipient phase changes discontinuously, possibly requiring a reversal in the pressure and/or temperature grids.

The calculations for the curve for that one incipient phase terminate when the calculations reach the limits of the range of interest. Then the calculations for a different incipient phase are conducted, starting from each intersection encountered. The most convenient choice of the grid for these lines depends on the phases that appear at those intersections. We summarize this procedure in Figure 4.1

At last, we assemble these lines in a single plot to generate a phase diagram for the simulated mixture in the desired pressure and temperature ranges. The regions are labeled according to the phases that are present in those pressure and temperature conditions, at equilibrium. The determination of which are the set of phases that are present in a region of the diagram follows from a $TP-$flash calculations at any point inside a labeled region.

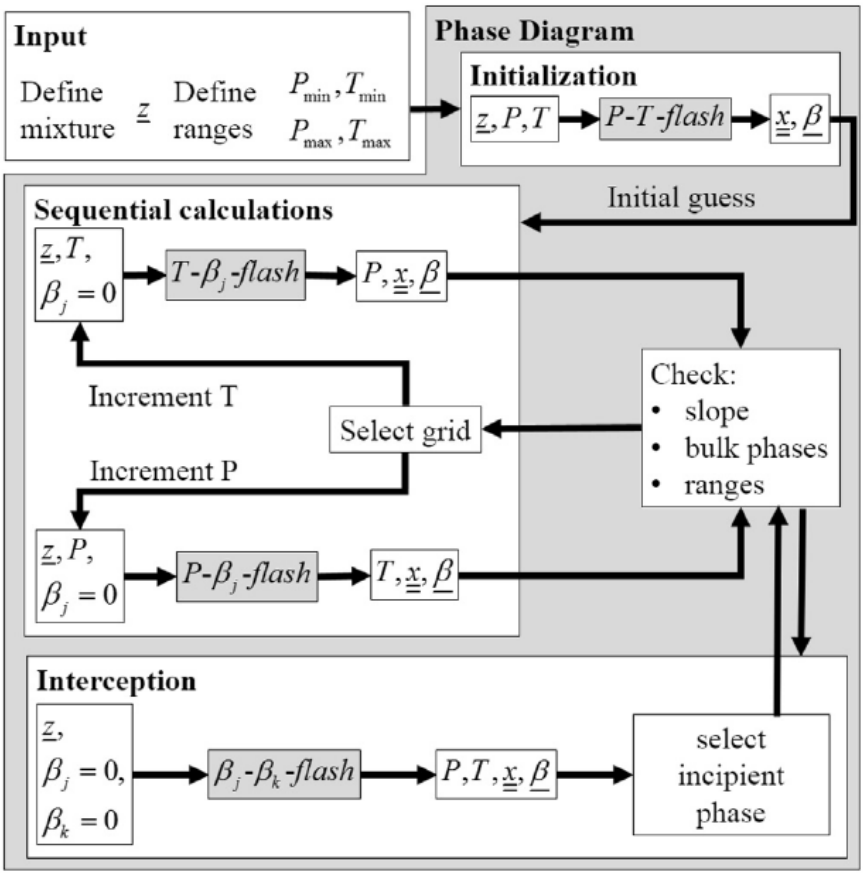

Figure 4.1: Flowchart of the procedures to systematically generate phase diagrams from a multiphase equilibrium algorithm.

Chapter 5

Results and discussion on Phase diagrams

The results and discussion are presented accordingly to different phase equilibrium scenarios analyzed. Note that the phase diagrams have labels given for regions in the $P \times T$ plane, so that the phases present at any line are the same phases present in at least one of the two regions that are separated by that line.

5.1 Single guest hydrates

Phase diagrams for hydrates in water and single guest mixtures were generated. The 3phase lines calculated represent coexistence of ice, vapor and hydrates, (I+V+H) or liquid water, vapor or liquid phases rich in the hydrate-forming component and hydrates (Lw+V+H or Lw+Lhf+H). These results are presented in Figure 5.1.

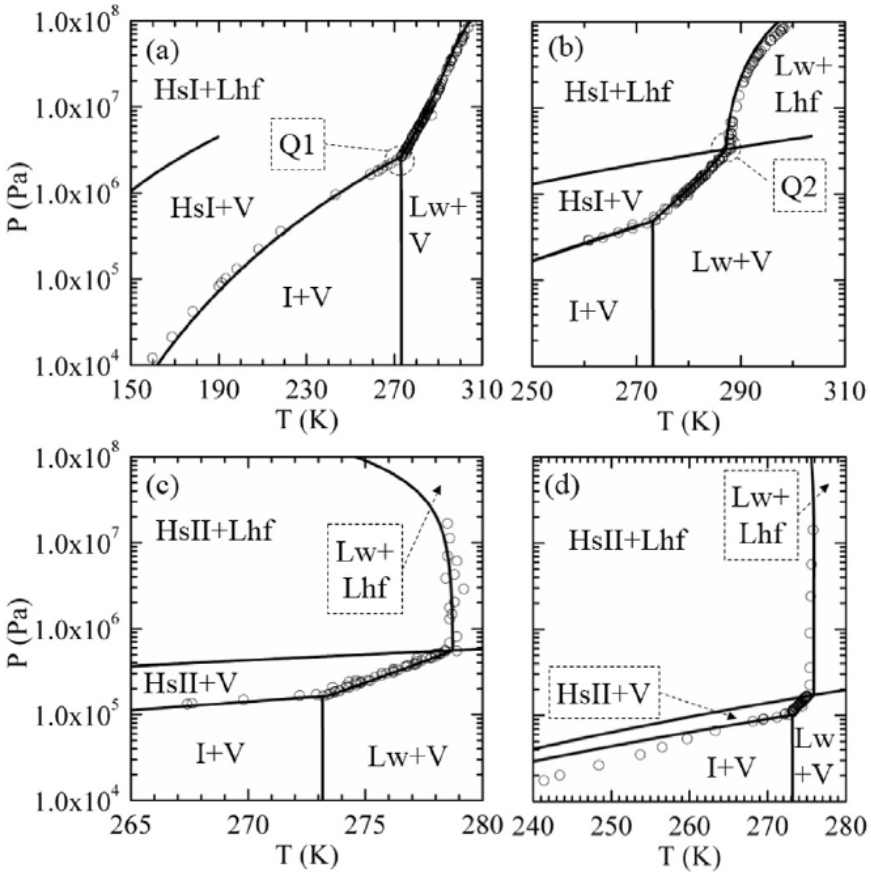

Figure 5.1: Single hydrates formation boundary lines for (a) Methane in sI, (b) ethane in sI, (c) propane in sII, (d) i-butane in sII. Circles are experimental data from literature (SLOAN JR and KOH, 2007). HsI stands for hydrate in structure I, HsII stands for hydrate in structure II, Lw stands for liquid water, with trace amount of guest components in phase equilibrium composition, Lhf stands for Liquid phase rich in hydrate forming components, V stands for vapor, I stands for conventional ice. Q1 and Q2 stands for first and second quadruple points

The results presented in this topic show both the level of adequacy of the thermodynamic model implementation using parameters from the literature and the capacity of the proposed algorithm to perform calculations involving three phase equilibrium involving I, Lw, Lhf, V, HsI and HsII phases. The quantitative representation depends on thermodynamic model parameters, which have not been optimized in this work. The following different qualitative behavior calculated here are identified: mixture (a) showing a single quadruple point, mixtures (b to d) showing two distinct quadruple points, and mixture (c) showing retrograde dissociation. A quadruple point in binary mixtures is a special case of intersection between phase equilibrium boundary lines, in which the lines are 3phase equilibrium loci, therefore univariant and the point is a 4phase equilibrium locus, therefore invariant. These intersections were observed naturally from sequential calculations of lines having different incipient phase specifica-

tions. After, each quadruple point precise value was calculated using $\beta_1\beta_2-$flash specifications.

5.2 Low water content gas streams

A system composed of a hydrateforming component and sufficiently low water content will typically present a (V), a (I+V) and a (H+V) region. Figure 5.2 shows the $P \times T$ phase diagram for a mixture with water mole fraction equal to 1×10^{-4} (black lines), superposed to shadowed regions corresponding to the phase equilibrium regions as divided by the univariant lines observed for a system with sufficient water content for Lw-V equilibrium occurrence.

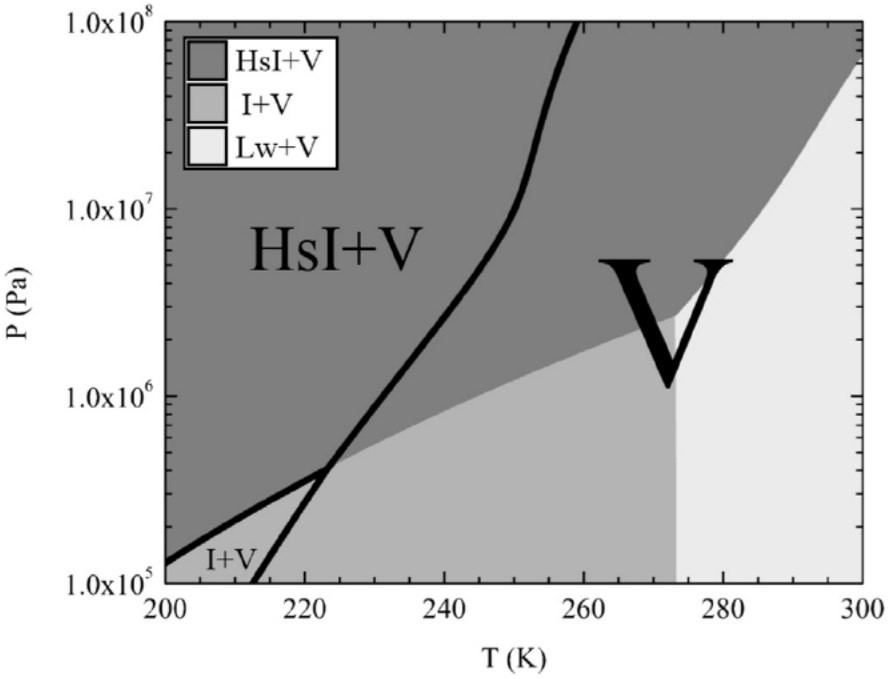

Figure 5.2: Phase diagram for single guest methane hydrate in high and low water content. The shadowed regions represent the two phase equilibrium loci, as divided by the three phase equilibrium univariant lines observed for a system with sufficient high water content for Lw+V equilibrium to occur in the range of temperature and pressure shown. The black lines divide the distinct phase equilibrium regions for the mixture with water mole fraction equal to 1×10^{-4}, as identified by the letters over the plot.

The I+H+V line for the low water content mixture coincides with the high water content case because, at that locus, the system is univariant, having 3 phases and 2 components.

It should be noted that the proposed algorithm handles these one- or two-phase-equilibrium scenarios using the same numerical methods and treating these phases with the same thermodynamic modeling used in the three-phase-equilibrium scenarios. The stability analysis detects that liquid state water is not present, that is, always presenting positive value for the stability variable, for any condition in the range shown in this diagram.

5.3 Aqueous systems containing thermodynamic inhibitors

A system composed of one hydrateforming component, water and one thermodynamic aqueous phase soluble hydrates thermodynamic inhibitor, as is ethanol, will typically present a region of Lw-V, of I-Lw-V and of H-Lw-V equilibrium. Figure 5.3 shows the $P \times T$ phase diagram for a mixture with global mole proportion of ethanol/water equal to $3/7$ (black lines), superposed to shadowed regions corresponding to the phase equilibrium regions as divided by the univariant lines observed for a system with no ethanol.

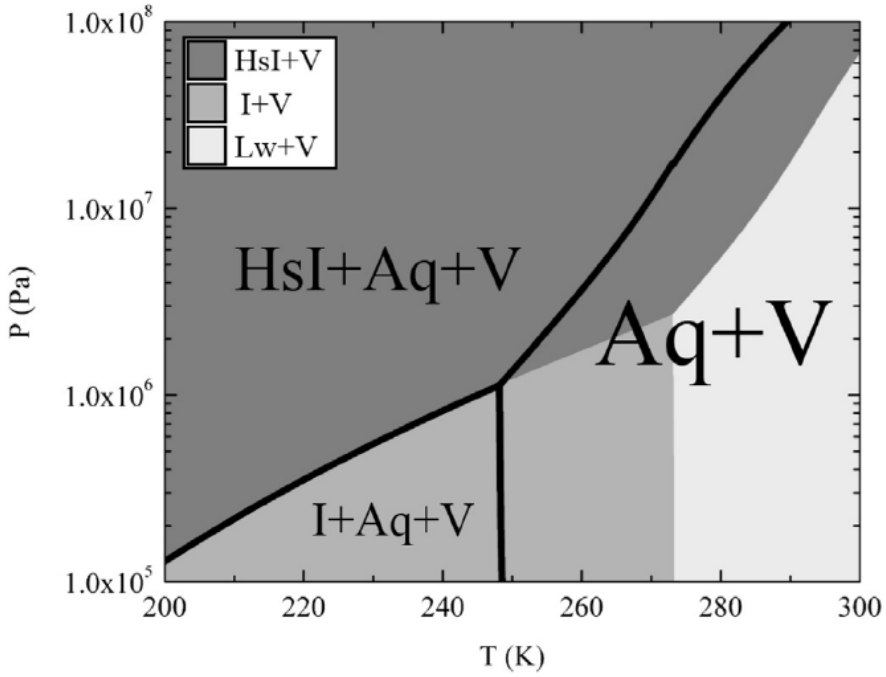

Figure 5.3: Phase diagram for single guest methane hydrate with and without ethanol. The shadowed regions present Hydrate (H), Vapor (V) Liquid water (Lw) and/or Ice (I) phases in equilibrium, as divided by the univariant lines observed for a system with no ethanol, while the black lines divide the distinct phase equilibrium regions for the mixture with global mole proportion of ethanol/water equal to 3/7, (Aq) corresponds to aqueous solution containing ethanol.

As there are three components in the system, the boundary line of Lw+V/I+Lw+V is not univariant, and it separates a region of 3phase equilibrium from a region of 2phase equilibrium. The I+Lw+V+H line is a univariant locus, having 4 phases and 3 components. It approximately coincides with the no-inhibitor case because, at that locus, as the vapor phase contains negligible ethanol quantity and our hydrate model does not account for ethanol participation as guests, there are three out of these four phases composed basically by only two components, that are the same phases and components as in the no-inhibitor case (I+H+V containing only water, only water and methane, and approximately only methane, respectively).

The stability analysis detects either 2 or 3 phase equilibrium regions, based on stability variable values for each modeled phase. Consistent modeling of the reference conditions assures no discontinuities are observed in the phase diagrams.

5.4 Phase diagram for a mixture of water, methane and propane

We generated a $P \times T$ phase diagram for the system [water, methane, propane] with the global mole composition of $[0.4, 0.3, 0.3]$ (Figure 5.4). This composition is in a range that corresponds to excess of guest components in relation to water, in comparison to the approximate composition of the hydrate phase. Therefore, the complete formation of hydrates takes place with the consumption of all water from the aqueous liquid or ice phases.

This diagram presents regions of phase equilibrium involving ice (I), water rich liquid (Lw), hydrate forming components rich liquid (Lhf), vapor (V) and hydrate in sII structure (HsII). In contrast with phase diagrams for single guest hydrates, it presents a phase envelope associated with the condensation of the gas phase (V) originating the liquid phase Lhf. We call the line that separates the regions in which hydrate phases are present from the ones in which these are not present as the hydrate formation line. In this phase diagram, this line crosses the Lhf-V equilibrium phase envelope. In more details, at relatively low pressure range, (approximately 1×10^5 - 1×10^6 Pa) the hydrate line determines Lw + H + V coexistence, at higher pressure (approximately 1×10^6 - 1×10^7 Pa) this line determines coexistence of (Lw + H + V + Lhf), and at even higher pressure (above approximately 1×10^7 Pa) this line determines coexistence of (Lw + H + Lhf). The highlights α, β and γ of Figure 5.4 show, in the ranges in which these intersections occur, some regions of 2- and of 3-phase-equilibrium, some 3- and some 4-phase equilibrium lines. The 3-phase regions correspond to equilibrium conditions in which only part of the water in the water rich phase, i.e. ice or aqueous liquid, has changed in physical state and participated in the hydrate phase formation. The 4-phase lines correspond to superposition of a line segments calculated for one incipient phase and a line segments calculated for a different incipient phase.

In this diagram, we present our calculations together with experimental data of univariant 4-phase equilibrium from literature as made available by NIST hydrate data viewer (KROENLEIN *et al.*, 2015).

Figures 5.5 to 5.7 show the highlights α, β and γ. Accompanying each highlight, we present an abstraction representing the phase equilibrium lines. The abstractions have the purpose of making clearer how segments connect and overlap. Each line formatting (continuous black, continuous light gray and dashed dark gray) represents a segment of an isopleth corresponding to a given phase

as incipient for the mixture with the defined composition. The dashed circles mark the locations where different segments intersect. Thinner lines are used in the portions where two segments overlap, while at the same time representing them side by side, so that they can be visualized with no ambiguity. A locus in which line segments overlap is a locus of univariant equilibrium.

Figure 5.5 shows highlight α. It corresponds to the portion of the phase diagram above the Lhf-V phase envelope, in which HsII, Lhf, Lw and V phases may be present.

The V phase boundary line is the bubble point line of the Lhf-V phase envelope. Above it, the boundary line for Lw as incipient and the one for H as incipient delimit a three phase region (Lw + H + Lhf). In the segment AB, the lines for Lw and the line for V coincide, meaning that segment is an univariant, and the HsII, Lw, Lhf and V phases coexist. In this segment, either Lw or V phases or none may be in incipient condition. In a univariant condition, pressure and temperature are not independent variables, so the solution for the relative amount of these phases will depend on the value for some intensive thermodynamic property related to the multiphase scope, as is the overall molar enthalpy or overall molar volume of the multiphase system. Below the point B from the bubble point line, these segments for Lw and for HsII coincide because the four phases (Lw + H + Lhf + V) coexist. However, in this segment, either HsII or Lw phases or none are in incipient condition, while V and Lhf are necessarily bulk phases.

Figure 5.6 shows Highlight β, this corresponds to the portion of the phase diagram just below the Lhf-V phase envelope. In this region, the HsII, Lhf, Lw and V phases may be present. The Lhf phase boundary line corresponds to the dew point line of the Lhf-V phases envelope. The boundary line with Lw as incipient phase and the one with H as the incipient phase delimit a three phase region (Lw + H + V). Above point C these lines coincide because four phases coexist (Lw + H + Lhf + V). The system is univariant along this segment and either Lw or HsII phases or none can be in incipient condition. In the segment CD, the coexistence of the Lw + H + Lhf + V phases also occur, however in this segment, Lw and Lhf are the two phases from which either one can be in incipient condition. In fact, the univariant line observed in highlight β is the continuation of the univariant line observed in highlight α. The 3- phase region (Lw + Lhf + HsII) from highlight β is only clear in the abstraction Figure 5.6b, while not being discernible in the calculated plot Figure 5.6a. However, this region extends to the region of highlight γ (Figure 5.7) In the scaling used in Figure 5.7, the Lw + Lhf + HsII phase equilibrium region is clear without the

need of graphical artifacts.

Figure 5.7 shows highlight γ, which corresponds to the portion of the global phase diagram (Figure 5.4) close to the normal freezing point of water. In this region, the HsII, Lw, I and V phases may be present. The continuous light gray line corresponds to the hydrate formation curve. In the calculated phase diagram Figure 5.7a, there is, apparently, a single line separating the regions of Lw-V and I-V equilibrium. However, that is not a univariant line, according to Gibbs phase rule regarding the whole system. The lines for Lw as incipient phase (dashed, dark gray) or I as incipient phase approximately overlap. That happens in these calculations because Lw phase, as a natural consequence of the equation of state used, is composed approximately of pure water. That being, the Lw-I phases equilibrium, behave approximately as 1-component 2-phase equilibrium, which is a univariant equilibrium. Geometrically, both as a matter of scaling and as a matter of solubility of the gases in the liquid water phase, as the points F and G approach, the line segment EG tends to a vertical orientation, as show in the calculated diagram Figure 5.7a.

These 3-phase regions are the most simple example of complex behavior involving hydrates that only become possible to calculate when using a multiphase algorithm. This kind of algorithm allows to model phase equilibrium beyond initial hydrate formation conditions.

These highlights show rather narrow regions of three-phase equilibrium conditions. Regarding physico-chemical coherence of the regions present here, it is in accordance with Gibbs phase rule that they must exist. For a system presenting three components and three phases, the number of degrees of freedom from the Gibbs phase rule is two; therefore, pressure and temperature can be independently specified yielding solutions of three phase equilibrium varying in composition of each phase. Furthermore, satisfying the Duhem theorem, for a given mixture composition, these solutions vary in the amount of each phase.

All of these three-phase-equilibrium regions are bounded by at least two lines of three-phase-equilibrium, in which one of the phases is in incipient condition. That is, one line equivalent to a dew point calculation coupled to a two-phase flash calculation, in which the two bulk phases are Lw and V. The determination of the composition of each phase requires a flash calculations, and the determination of the temperature or pressure requires a dew point like calculation. Being the 'dew' phase a hydrate crystal, this is the usual line of calculations of hydrate formation condition. The other line is equivalent to a bubble point calculation coupled to a two-phase flash calculation, in which the two bulk

phases are H and V, and the 'bubble' phase is an aqueous phase droplet.

Following the analogy, the bubble point calculation solution occurs consistently at slightly lower temperature or slightly higher pressure than the dew point calculation solution. It is important to point out that these combined calculations were performed implicitly, because our algorithm uses the equations that characterize these equilibria in a unified procedure.

In addition, regarding numerical aspects of these calculations, to vouch for the robustness of the methods that we used and the tolerances that we applied, we verified the solutions for one or another incipient phase in univariant equilibrium lines, where according to Gibbs phase rule both solutions must overlap. In fact, our results coincide to several significant figures: 95% of values for absolute relative deviation between bubble-point-like calculations and dew-point-like calculations of pressure belongs to the interval $(1 \times 10^{-15}, 1 \times 10^{-10})$ while this deviation measurement for points belonging to two distinct boundary lines above the univariant Lw-HsII-Lhf-V line region were higher than 1×10^{-2}, and below the univariant Lw-HsII-Lhf-V line region were higher than 1×10^{-5}.

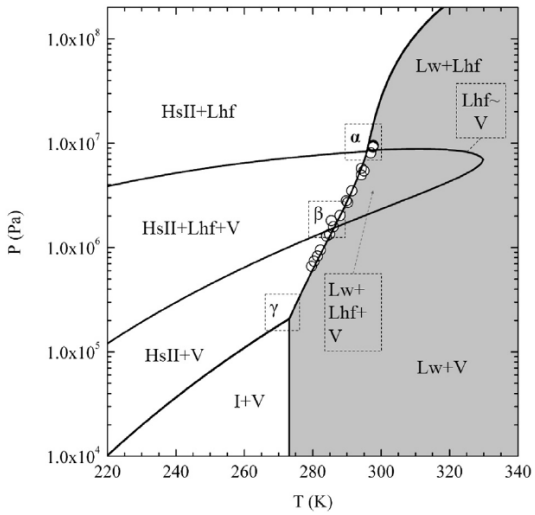

Figure 5.4: Phase diagram for the system [H2O, C1, C3] with the global mole composition of $[0.40, 0.30, 0.30]$. The regions present Ice (I), Hydrate in structure sII (HsII), water rich liquid (Lw), hydrate forming components rich liquid (Lhf) and/or Vapor (V) phases in equilibrium. Experimental data from literature available in NIST hydrate data viewer (KROENLEIN *et al.*, 2015).

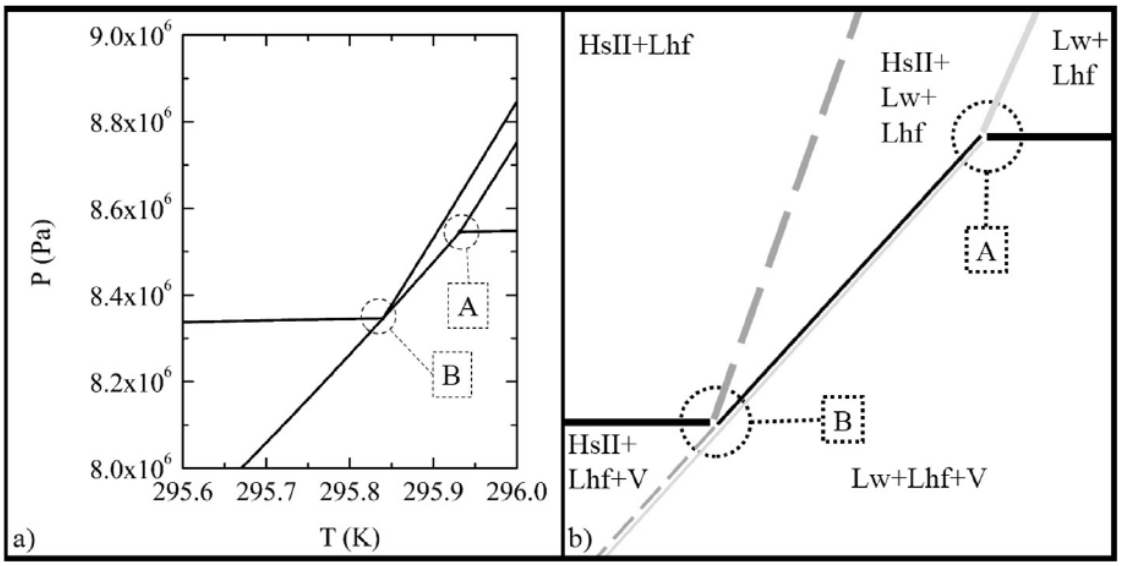

Figure 5.5: Highlight α from phase diagram of the system [H2O, C1, C3] with the global mole composition of [0.40, 0.30, 0.30] in the region of intersection between boundary lines for Lhf vaporization and for HsII formation. The boundary lines represent condition of incipient phase for Hydrate in structure sII (HsII - continuous light gray line), water rich liquid (Lw - dashed dark gray line), and Vapor (V - continuous black line). All the regions in this range present hydrate forming components rich liquid phase (Lhf) in equilibrium.

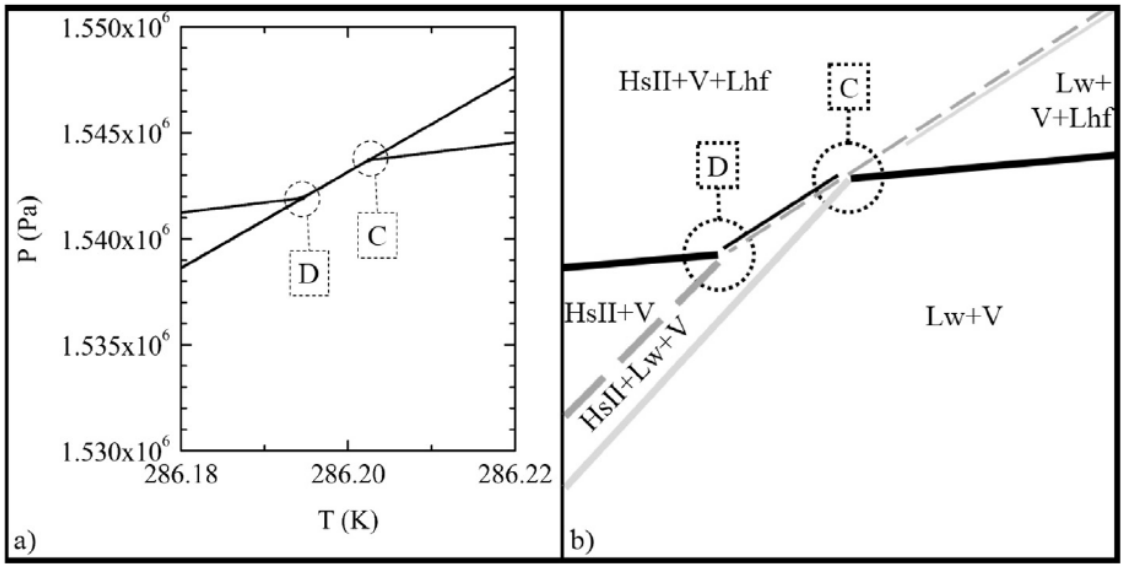

Figure 5.6: Highlight β from P.T phase diagram for the system [H2O, C1, C3] with the global mole composition of [0.40, 0.30, 0.30] in the region of intersection between the boundary lines for the condensation of V and for hydrate formation. The boundary lines represent condition of incipient phase for Hydrate in structure sII (HsII - continuous light gray line), water rich liquid (Lw - dashed dark gray line), and hydrate forming components rich liquid (Lhf - continuous black line). All the regions in this range present vapor phase (V) in equilibrium.

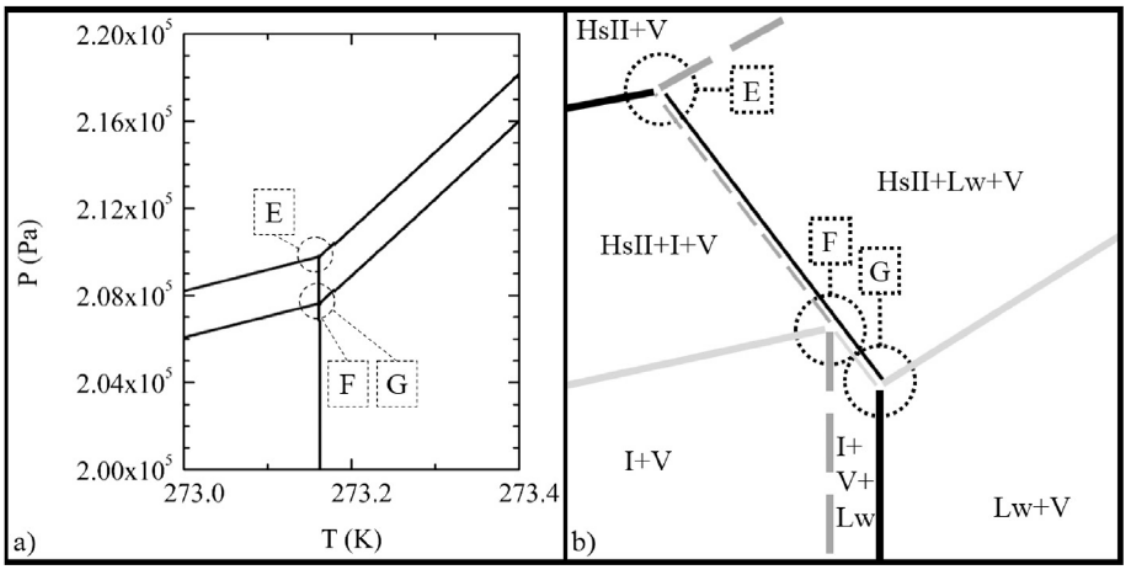

Figure 5.7: Highlight γ from P.T phase diagram of the system [H2O, C1, C3] with the global mole composition of [0.40, 0.30, 0.30] in the region of intersection between freezing water equilibrium line and hydrate formation line. The boundary lines represent condition of incipient phase for Hydrate in structure sII (HsII - continuous light gray line), water rich liquid (Lw - dashed dark gray line), and Ice (I - continuous black line). All the regions in this range present vapor phase (V) in equilibrium.

5.5 Phase diagram for a mixture of water, ethane and propane

Figures 5.8 to 5.10 show the $P \times T$ phase diagram calculated for the system water/ethane/propane with 3 different mixture compositions: $[0.50, 0.15, 0.35]$, $[0.4, 0.3, 0.3]$ and $[0.990, 0.005, 0.005]$ respectively.

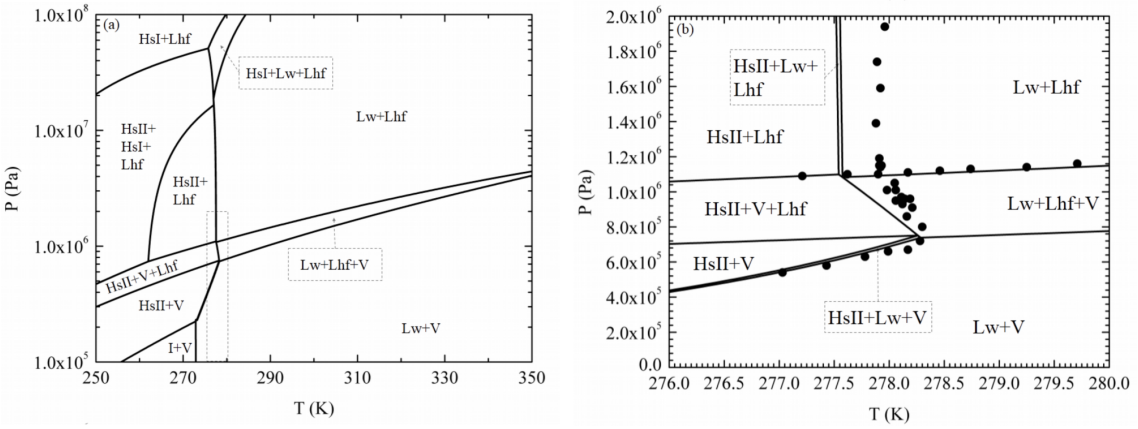

Figure 5.8: Phase diagram for the system water/ethane/propane in the mixture composition of 0.5/0.15/0.35. The regions present Hydrate in structure sI (HsI) and/or sII (HsII), Ice (I), water rich Liquid (Lw), hydrateforming components rich Liquid (Lhf) and/or Vapor (V) phases in equilibrium. Points are experimental data from literature (MOOIJER – VAN DEN HEUVEL, 2004).

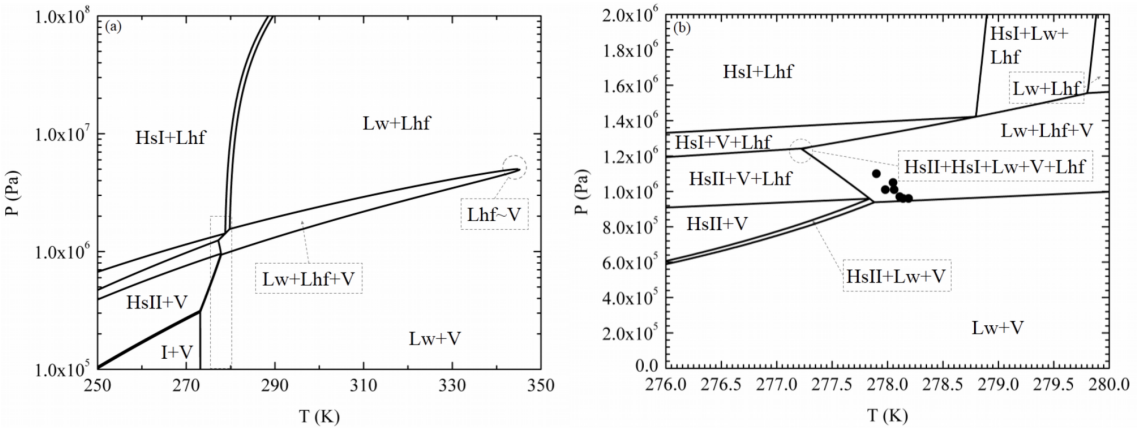

Figure 5.9: Phase diagram for the system water/ethane/propane in the mixture composition of 0.40/0.30/0.30. The regions present Hydrate in structure sI (HsI) and/or sII (HsII), Ice (I), water rich Liquid (Lw), hydrateforming components rich Liquid (Lhf) and/or Vapor (V) phases in equilibrium. Points are univariant experimental data from literature (MOOIJER – VAN DEN HEUVEL, 2004).

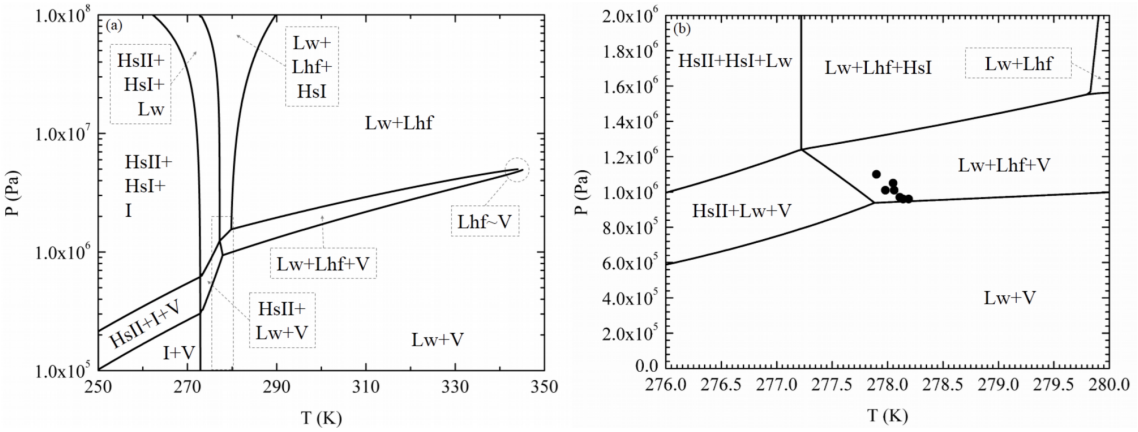

Figure 5.10: Phase diagram for the system water/ethane/propane in the mixture composition of .990/0.005/0.005. The regions present Hydrate in structure sI (HsI) and/or sII (HsII), Ice (I), water rich Liquid (Lw), hydrateforming components rich Liquid (Lhf) and/or Vapor (V) phases in equilibrium. Points are univariant experimental data from literature (MOOIJER – VAN DEN HEUVEL, 2004).

The following different qualitative behavior calculated here are identified: Figures 5.8 and 5.9 show regions of small temperature range corresponding to partial conversion of water into hydrates. In the case presented in Figure 5.9, hydrate structure transition occurs inside the Lhf-V phase envelope, therefore along a univariant line presenting the four phases HsI-HsII-Lhf-V. Also, this phase diagram presents an invariant point in which the 5 phases Lw-HsI-HsII-Lhf-V coexist. In the case presented in Figure 5.8, hydrate structure coexistence occurs at higher pressure conditions. In the case presented in Figure 5.10, due to excess of water in relation to hydrate composition, hydrate formation occurs with consumption of V or Lhf phases, therefore H+I and H+Lw coexistence regions occur. These figures also show reproduction of HsII+Lw+Lhf+V univariant lines independently of system composition, while allowed by mass balance relation. In these calculations, the transition between all different phase equilibrium scenarios is automatically detected. This is observed as, between two successive incipient phase calculations, the solution for the stability variable for a given phase changes between 0 and positive values and, the solution for its phase amount changes between a positive value and zero. This indicates that this phase is present at the condition of the former calculation, and not present at the condition of the latter calculation. As before, the point of connection between segments of the phase boundary presenting different incipient phases, whether they are invariant or not, are calculated from $\beta_1\beta_2-$flash specifications.

5.6 Phase diagram for a mixture of water, carbon dioxide and iso-butane

We generated a $P \times T$ phase diagram generated for the system [water, carbon dioxide, iso-butane] with the global mole composition of [0.40, 0.58, 0.02] (Figure 5.11a). This composition is in a range that corresponds to excess of guest components in relation to water, and in which regions of structural transitions occur.

This diagram presents a complex behavior for a system composed of three components from natural gas as there are many distinct regions in which different phases are in equilibrium. In this diagram, we present our calculations together with experimental data for Lw-H-V equilibrium, which corresponds to the line dividing the gray and white regions in the plot. These measurements however are from some isopleths with dry basis mole fraction of carbon dioxide between 0.96 and 0.971 from literature (SLOAN JR and KOH, 2007).

Figure 5.11b shows the highlight α. It corresponds to the region near which structural transition, and an invariant point occur. In the invariant point, (E), the HsI, HsII, Lhf, V and Lw phases coexist. The segment ED exhibits retrograde behavior, in which HsII dissolves and Lhf will appears upon increase in pressure. Retrograde behavior also occurs in the segment AE, in which HsII dissolves upon increase in pressure, however, with HsI being present. Moreover, in the segment AB, another unusual behavior occurs, in which HsI will dissolve upon reduction in temperature, however with HsII being present.

The physical chemical phase behavior predicted here is rather unintuitive, consider for example a isobaric analysis occurring for the mixture presented in Figure 5.11b at 2.5×10^6 Pa, from 260 to 290 K. Hydrate structure sI is initially present, then is becomes less favored than HsII and disappears, and then it becomes favored again and able to reappear, only to, at slightly higher temperature condition, become less favored and prone to disappear once more. That behavior is represented in the following series of expected transition of stable state for the system following this analysis (HsI + Lhf $\rightarrow$ HsI + Lhf + V $\rightarrow$ HsII + Lhf + V $\rightarrow$ HsII + V $\rightarrow$ HsI + HsII + V $\rightarrow$ HsII + V + Lw $\rightarrow$ Lw + V).

Numerically, this means that there are two solutions for the specification of a given phase as being in incipient condition at some pressure or temperature specifications, and these solutions differ on what are the bulk phases that are present. Therefore, the convergence to each of these two real solutions will de-

pend on the reference phase that is imposed, or if the stability analysis methodology chooses the reference phase automatically, will depend on the initial guesses for these phases amounts and composition.

In the univariant segment BE, 95% of the values of relative absolute deviation for pressure in bubble-point-like and dew-point-like calculations belong to the interval $(2 \times 10^6, 7 \times 10^4)$.

Regarding the predictions in the conditions at which there is no available experimental data, we believe they are sound, according to the capabilities of the individual thermodynamic models that were used because we generate the diagrams using thermodynamic models that are consistent with each other.

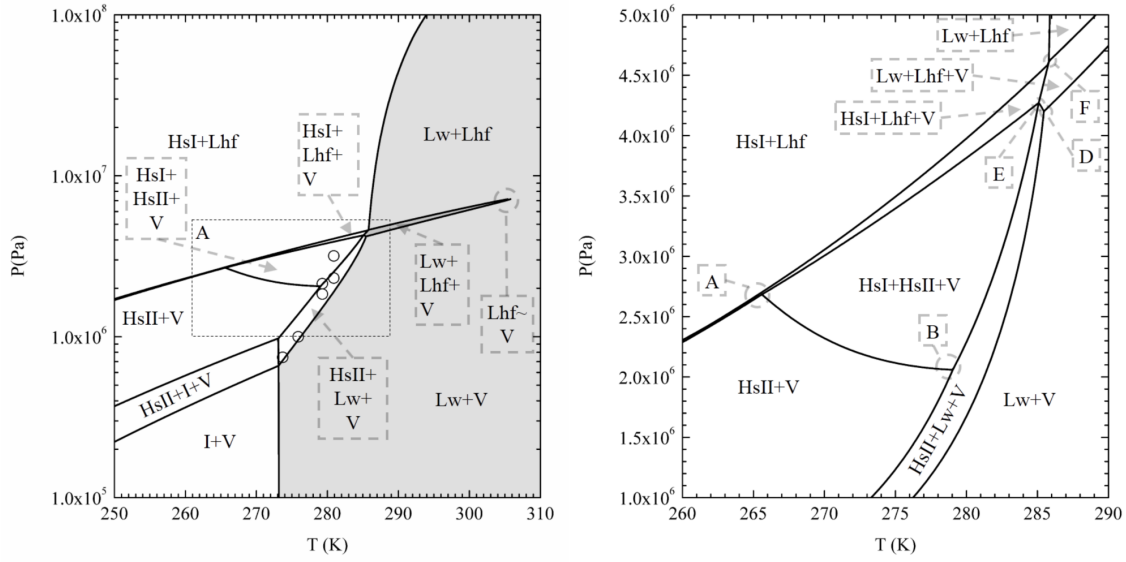

Figure 5.11: Phase diagram for the system [H2O, CO2, iC4] with the global mole composition of [0.40, 0.58, 0.02] dry basis mole fraction of carbon dioxide = 0.967. The regions present Ice (I), Hydrate in structure sII (HsII) and in structure sI (HsI), water rich liquid (Lw), hydrate forming components rich liquid (Lhf) and/or Vapor (V) phases in equilibrium. Experimental data is for isopleths of xdry(CO2) between 0.960 and 0.971 from literature (SLOAN JR and KOH, 2007). Highlight α in the region of structural transition. The regions present Hydrate in structure sII (HsII), and in structure sI, water rich Liquid (Lw), and/or Vapor (V) phases in equilibrium.

Chapter 6

A natural pressure shift

Since the publication of the original van der Waals and Platteeuw model (vdW&P), more recent experimental data show (i) variations of hydrate volume with temperature and pressure for a given guest type (BALLARD, 2004; HIRAI *et al.*, 2000a,b; TSE, 1987), (ii) variation of cage radii with changing hydrate volume (BALLARD, 2004), (iii) different hydrate volume at a given temperature and pressure for different types of guests (HWANG *et al.*, 1993; IKEDA *et al.*, 2000). These phenomena are commonly labeled as hydrate compressibility and cage deformation. Volumetric information, such as this, is of great importance for phase equilibrium and energy balances at high pressure, as made evident by considering the Poynting correction, or the rigorous expressions for isothermal derivatives of the chemical potential with respect to pressure for pure substances,

$$\left(\frac{\partial \mu}{\partial P}\right)_T = \overline{V} \tag{6.1}$$

and for molar enthalpy

$$\left(\frac{\partial \overline{H}}{\partial P}\right)_T = \overline{V} - T\left(\frac{\partial \overline{V}}{\partial T}\right) \tag{6.2}$$

They relate variations in chemical potential (μ) or molar enthalpy $\overline{H}$ with respect to pressure P at constant temperature T to the molar volume equation of state $\overline{V}(T, P)$.

In fact, such information is also considerably important for the modeling of mixtures even at low pressure. As the affinity of guests to cages is strongly dependent on cage radii, the affinities in mixed hydrate should be significantly

different from those in single hydrate.

From the aforementioned experimental observations, we see that the molar volume of the empty lattice (V^{EL}) which corresponds to the ratio between hydrate volume and number of water molecules (Eq. 6.3) depends on the mole fraction of guest components in the hydrate associated with occupancy Θ_{ij}. We can also recognize a relation between the cage radii and the molar volume of the hydrate phase. Consequently, this affects the Langmuir coefficients C_{ij}, which dictate the occupancy. These relations show an interdependence between the variables that describe the hydrate. Finally the occupancy directly affects the chemical potential of water in the hydrate, influencing phase equilibrium conditions even at low pressure as represented in Eq. (6.4).

$$\overline{V}^{\mathrm{EL}} = \frac{V^{\mathrm{H}}}{N_{\mathrm{w}}} \tag{6.3}$$

where V^{H} is the hydrate phase volume and N_{w} is the number of water molecules in the lattice.

$$\underbrace{\overline{V}^{\mathrm{EL}}\left(\Theta_{ij}\right) \rightarrow R_j\left(\overline{V}^{\mathrm{EL}}\right) \rightarrow C_{ij}\left(R_j\right) \rightarrow \Theta_{ij}\left(C_{ij}\right)}_{\text{interdependent}} \rightarrow \Delta\mu_{\mathrm{w}}^{\mathrm{H-EL}} \tag{6.4}$$

These advancements in experimental measurements pose new challenges to modeling and opportunities for model enhancements. Experimental observation of type (i) are usually directly used in correlations for actual hydrate volume as function of T and P (KLAUDA and SANDLER, 2000) or into parameterization or validation of crystal models for the empty lattice (BELOSLUDOV *et al.*, 1991; INERBAEV *et al.*, 2006). This, in turn, affects Poynting integrals in phase equilibrium calculations. Observations of type (ii) are usually also used in correlations (BALLARD and SLOAN JR., 2002), thus propagating type (i) observations into the calculation of Langmuir coefficients and strongly affecting calculation of occupancy in the classical vdW&P derived properties expressions and into particular empirical modifications of the model. Moreover, observations of type (iii) are usually considered by means of using discrete standard volume parameter and ad hoc mixing rules of guest (HWANG *et al.*, 1993). Derived properties expressions may receive ad hoc corrections to the expressions from the standard vdW&P model, which is said ideal with respect to its premises. These corrections intend to compensate for noticeable deviations between ideality and reality. The activity coefficients, at their turn, depend on empirical expressions for volume difference as functions of temperature, pressure and guest

composition (BALLARD, 2004). We have analyzed current modifications of the vdW&P model and noticed that they show a thermodynamic inconsistency in phase equilibrium calculations when including observation of type (ii) or (iii). The inconsistency can be made evident performing a Clapeyron equation based test: in the $P \times T$ diagram, a univariant phase equilibrium curve must intercept the curve of null phase transition volume difference at its maximum temperature (see Section 6.4). This inconsistency happens because the phenomena in observations of type (ii) and (iii) invalidate the constant cage radii premise, premise, a premise on which all expressions for derived properties in the original vdW&P model are based, and current modifications make use of those same expressions.

Our contribution here is in developing an extension of the vdW&P model to contemplate compressible hydrate with cage distortion. Our extension differs from previous works because here, we include the information of volume dependent cage radii at the partition function level and then we carry out the mathematical procedure to obtain expressions for derived properties considering this dependency. In summary, by having varying radii with lattice volume, and varying lattice volume with temperature and pressure, we calculate that there arises a pressure shift between the hydrate and the empty lattice isochoric reference at the same temperature. That pressure shift is responsible for varying actual hydrate volume for standard temperature and pressure for different guest types. Our calculations of pressure shift and volume can be explained in the steps presented in Figure 6.1.

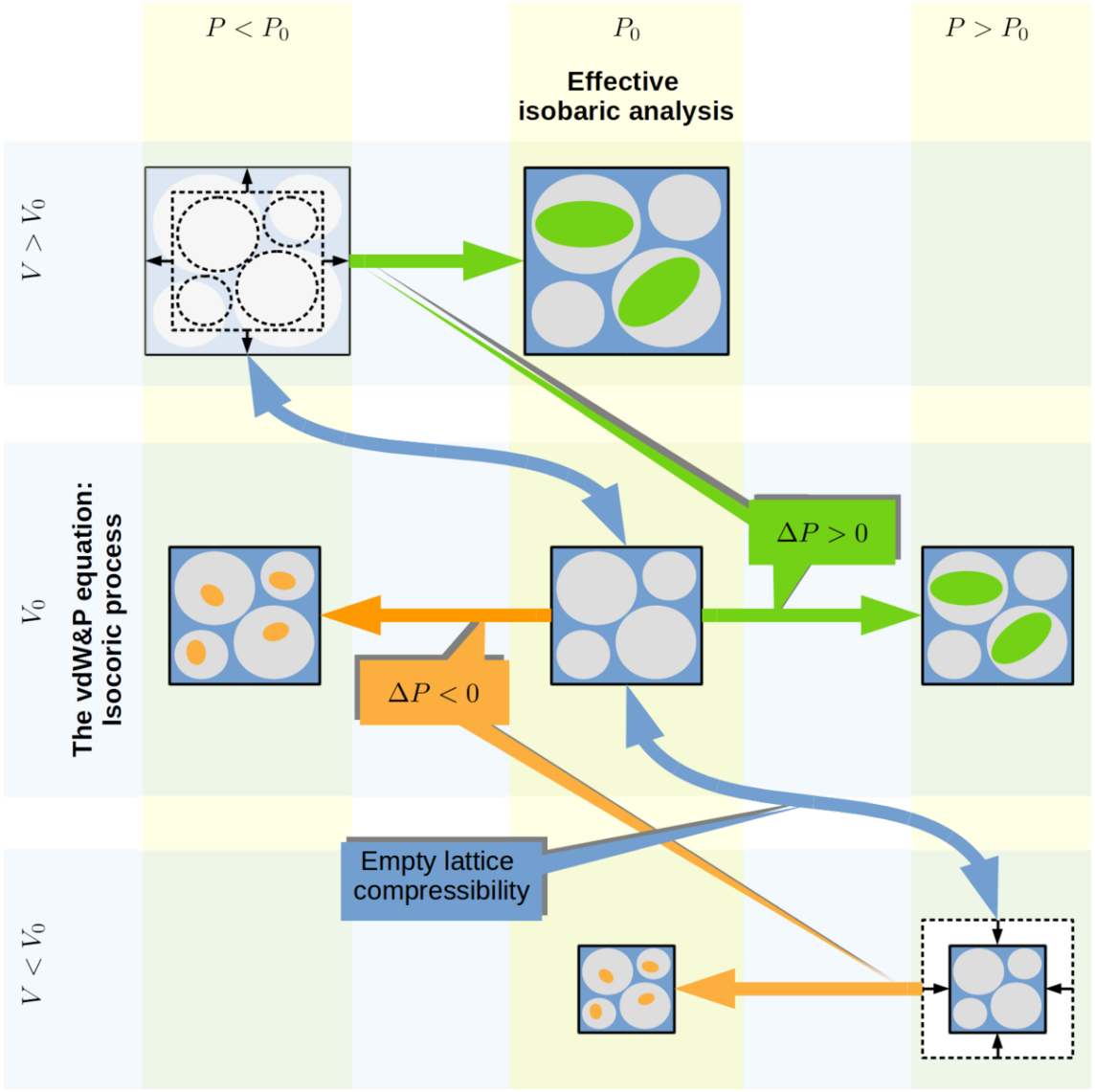

Figure 6.1: Representation of the pressure shift model featuring volume difference for hydrates of different guests at a same pressure P_0. The blue square and gray circles represent the hydrate lattice and its cages, respectively. The green particles represent a component of large molecular size, which increases the hydrate lattice volume (V) with respect to the reference empty lattice volume (V_0), because of a positive pressure shift ($\Delta P^{\mathrm{H-EL}}$). Conversely, the orange particles represent components of small molecular size, which reduce the hydrate lattice volume, because of a negative pressure shift.

From one sole standard empty lattice having volume V_0 at pressure P_0 (blue square for the lattice with gray circles for the cages), consider first the enclathration of guest molecules of type 1 (green ellipsis), which has a big molecular dimension so they will fit tightly in the larger cages. In that process, the hydrate has volume equal to that of the isochoric reference lattice, by definition. However we can calculate a pressure difference ΔP, which for this kind of guest is positive. Now, in order to calculate the volume that this hydrate would show at standard

pressure P_0 we would need to consider the process of enclathration from isochoric empty lattice reference at $P \approx P_0 - |\Delta P|$, therefore $P < P_0$. The volume of the empty lattice at a slightly lower pressure should then be slightly larger than V_0 (dashed lines and black arrows represent volume changes), depending on the empty lattice compressibility in the pressure range under consideration. We then can conclude that the volume of hydrate of guest component of type 1 at P_0 is larger than V_0 , the reference lattice at that same P_0.

With that reasoning, analogously for a guest component of type 2, which has a lower molecular dimension such that it fits loosely in the cages and calculations show to have $\Delta P < 0$, we conclude that the hydrate volume at P_0 is smaller that the reference lattice at that same P_0.

Note that there are competing effects between tightness and looseness of each species and each cage. Also, the pressure shift value is dependent on the reference lattice pressure, so the actual implementation requires an iterative scheme which is detailed in Section 6.7. We now present the derivation of our model extension (Section 6.3), an algorithm for the actual application of the model (Section 6.7) and then present results of our model for a few sample components showing a number of phenomena captured by our model (Chapter 7). The cell theory for hydrates summary is illustrated in Figure (6.2) using methane hydrate parameters.

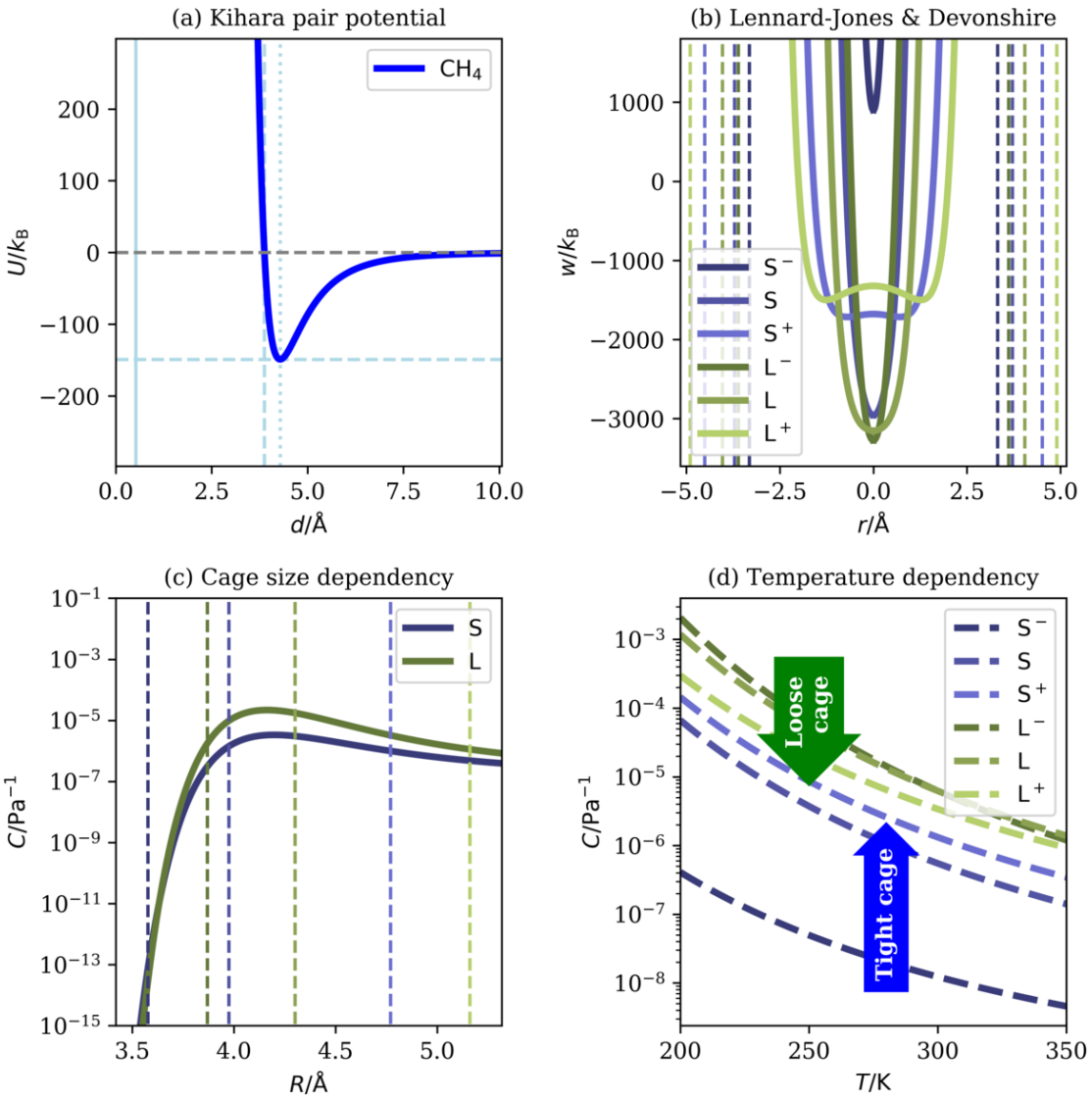

Figure 6.2: Cell theory potentials based on the Kihara intermolecular potential: (a) pair potential energy (U) for the methane-water interaction as function of intermolecular center-of-mass distance (d), (b) cage potential (w) for a methane molecule in small (shades of blue) and large (shades of green) cages of s^{II} hydrate structure with small perturbations (+, -) as function of radial coordinate (r), (c) Langmuir coefficients (C) for small (blue) and large (green) cages versus of the correspondent cage radius (R), and (d) Langmuir coefficients for small (shades of blue) and large (shades of green) cages versus temperature (T) for several small perturbations (+, -) of the cage radius around the standard value.

A pair interaction potential depends on a distance between a guest molecule and a water molecule d and energy interaction parameters. While the cage potential depends on the radial coordinate of a guest inside an assumed spherical cage, the interaction parameters, in addition the coordination number of water molecules per cage, and the cage radius. Finally, the Langmuir coefficients depend only on the actual cages radii and temperature.

The pair potential (Figure 6.2a) shows an attractive, a repulsive and a forbidden region regarding the distance between a guest molecule a the cage boundary. The cage potential (Figure 6.2b) shows either a single minimum at the center of the cage or two minima slightly offset depending on the molecular parameters, coordination number and cage radius. Obviously the radial coordinate in the classical spherical coordinate system does not actually take negative values, so the intention of left half of the plot is to highlight the symmetry of the spherical cage. Finally the Langmuir coefficient at constant temperature show a maximum with respect to cage radius (Figure 6.2c). For a cage whose radius is large, relative to the molecule size, the molecule fits loosely into the cage, then attractive interaction predominates; Thus, for a slightly smaller cage radius, the cage potential energy decreases and the Langmuir coefficients increases. This may happen up to a point where the cage is small enough so that the molecule fits tightly. For a even smaller cage radius, repulsive interaction predominates, cage potential energy increases and Langmuir coefficients decrease. Plotting Langmuir coefficients as function of temperature for small perturbations of the cage radius (Figures 6.2d) shows that increasing the radius for a cage in which the guest molecule fits tightly will make it too small, and the curve of Langmuir coefficient versus temperature is shifted down, (blue curves). On the other hand, increasing the radius for a cage in which the guest component molecule fits loosely will increase the predominance of attractive force and the curve of Langmuir coefficient versus temperature is shifted up (green curves).

In summary, it is shown that a guest component of large molecular size will distort the lattice increasing the hydrate volume, with respect to the reference empty lattice. And our model explains this phenomenon results from the pressure shift caused by the adsorption, and that this pressure shift can be calculated using the vdW&P partition function. Furthermore our model shows that a guest component of small molecular size will also distort the lattice, making the hydrate volume smaller, instead. This contrasts with an assumption used in previous literature (HANDA and TSE, 1986; ZELE *et al.*, 1999) that the smallest molecules would cause no distortion.

6.1 Geometry relation between cages radii and lattice molar volume

Here we relate the cage radii to the lattice molar volume, to support that R_j depends on both the extensive volume of the lattice and on the number of

water molecules, which are independent variables in the semi-grand-canonical partition function. Here, by taking into consideration varying cage radius under the approximation of Lennard-Jones and Devonshire, we intend to represent isotropic cage deformations. Consider a unit cell with N_0 molecules and edge length a_0, therefore with volume a_0^3. Figure 6.3 shows that a is function of the lattice molar volume and, therefore, in the calculations to be performed, it is a function of both lattice volume at constant mole number and function of mole number at constant lattice volume.

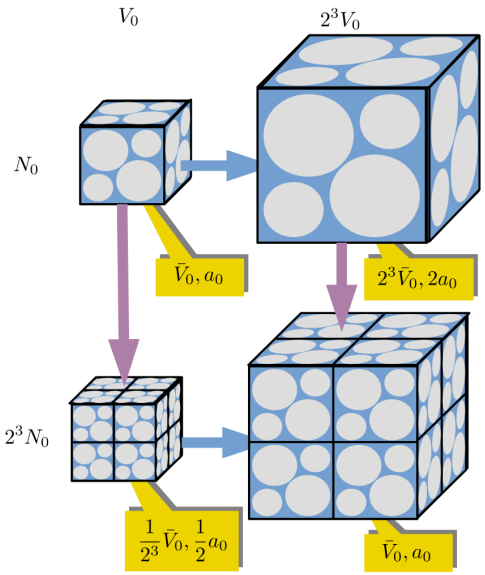

Figure 6.3: Geometric relation between lattice edge length (a), number of molecules (N), extensive volume (V) and molar volume ($\overline{V}$). The unit cell edge parameter varies when varying either the total number of molecules in the phase (purple arrows) or the total volume of the phase (blue arrows) while holding the other constant. It is kept constant when varying both the total number of molecules and total volume while holding constant the molar volume of the phase.

Note that increasing the mole number, which is obtained by multiple of unit cells mole number, holding constant extensive volume, results in smaller molar volume and smaller unit cell edges so that more unit cells fit in the same volume. Alternatively increasing volume while holding constant N_w, which is done expanding one unit cell, results larger molar volume and larger edge length. Only when increasing both extensive and mole number one can keep constant molar volume and thus edge length.

There is evidence of variation of the radius of each cage type with the unit cell lattice parameters from molecular simulations (BALLARD, 2004). Now, we proceed to relate unit cell edge with cages radii according to the following geometrical relations:

1. The unit cell is a basic unit from which the macroscopic phase is described by means of simple replication. The unit cell has constant number of molecules (N_w^{uc}) and its specific volume (V^{uc}/N_w^{uc}) is equal to the macroscopic lattice molar volume $\overline{V}^{EL}$.

$$\frac{V}{N_w} = \frac{V^{uc}}{N_w^{uc}} \tag{6.5}$$

$$d\left(\frac{V}{N_w}\right) = \frac{1}{N_w^{uc}}\, dV^{uc} \tag{6.6}$$

2. Considering a cubic unit cell with variable edge length a^{uc}

$$V^{uc} = a^{uc\,3} \tag{6.7}$$

$$dV^{uc} = 3a^{uc\,2}\, da^{uc} \tag{6.8}$$

3. The cage radii is experimentally correlated to the unit cell edge, we here consider the simplest case, apart from the trivial constant radius case, of it being proportional to the edge length.

$$R_j = a^{uc}\, f_{a^{uc}}^{R_j} \tag{6.9}$$

$$dR_j = f_{a^{uc}}^{R_j} da^{uc} \tag{6.10}$$

4. We calculate the proportionally factor from a measurement of R_{j0} and a_0^{uc} for every cage type at a standard condition.

$$f^{R_j} = \frac{R_{j0}}{a_0^{uc}} \tag{6.11}$$

This variable dependency scheme finally leads to

$$\frac{\partial C_j}{\partial\left(\frac{V}{N_w}\right)} = \frac{\partial C_j}{\partial R_j}\frac{\partial R_j}{\partial a^{uc}}\frac{\partial a^{uc}}{\partial V^{uc}}\frac{\partial V^{uc}}{\partial\left(\frac{V}{N_w}\right)} \tag{6.12}$$

We therefore have related the Langmuir coefficients with lattice molar volume which we use in our calculations.

The relation presented in Figure 6.3 and in Eq. 6.5 to 6.11 support attaining to any empirical relation between R_j and a^{uc} from measurement or molecular simulations, e.g. linear, quadratic..., and relate these variables to hydrate molar volume by changing Eq. 6.9 and 6.10.

6.2 Volumetric properties for the empty lattice

We make a note here that the upper limit pressure in the Poynting integral, which is the independent variable describing $\Delta\mu_{\mathrm{w}}^{\mathrm{EL-PW}}$ in the left hand side of Eq. 6.36 must consistently match P^{EL} from Eq. 3.9 throughout derivation and implementation. It is important to point this out because our model shows that the pressure associated with the empty lattice P^{EL} in thermodynamic properties and phase equilibrium calculations is different than the actual hydrate pressure, which in turn is the system pressure, while the literature currently relies on $P \Rightarrow P^{H} = P^{EL}$.

We now proceed to deal with an expression for $\overline{V}^{\mathrm{EL}}$ as function of temperature and pressure in order to couple it to Eq. 6.36. Although literature has shown possible theoretical models for an empty lattice volume (BELOSLUDOV *et al.*, 2002), we start with a simple correlation. We use an empirical expression to relate pressure and temperature to the volume of the empty lattice, as a pure water crystalline phase. The logic for this expression is the assumptions of constant isothermal compressibility (k) and a parabolic behavior for the edge length isobaric expansion, that is

$$V^{\mathrm{EL}} = \tag{6.13}$$

$$\left(\frac{a_0^{\mathrm{uc}}}{\text{Å}} + \alpha_1\left(\frac{T}{\mathrm{K}}\right) + \alpha_2\left(\frac{T}{\mathrm{K}}\right)^2\right)^3 \frac{10^{-30} N_{\mathrm{A}}}{N_{\mathrm{w}}^{uc}} \tag{6.14}$$

$$\exp\left(-k\left(\frac{P}{\mathrm{Pa}} - \frac{P_0}{\mathrm{Pa}}\right)\right) \tag{6.15}$$

where N_{A} is the Avogadro number, a_0^{uc} is the unit cell edge length parameter corresponding to $P = P_0$ and $T = T_0 = 0$ K. The standard pressure (P_0) of this correlation needs not be the same as P_0 in the expression for chemical potential ($\Delta\mu_{\mathrm{w}}^{\mathrm{EL-Pw}}$, Eq. 6.36).

This expression allows one to relate pressure and volume of the empty lattice. However, experimental data is only available for actual clathrates. Recalling that the hydrate modeled with the vdW&P model has volume V^{H} equal to the empty lattice reference V^{EL} but not the same pressure, the correlation for V^{EL} can be regressed from crystallography measurements and correlations for the hydrate volume V^{H} by taking into consideration the pressure shift calculation. We show a preliminary method for this regression in Section 6.6.

6.3 Thermodynamic properties for compressible hydrates

We now perform the symbolic calculations to obtain derived properties taking the dependency of q_{ij} with V/N_w into consideration. The expressions for N_{ij}, and therefore Θ_{ij}, are the same as before, however the expression for pressure and chemical potential, which are based on partial derivatives with respect to V and N_w, respectively, will both get an extra contribution when considering R dependent on V/N_w.

6.3.1 Hydrate pressure

We can calculate the hydrate pressure in the thermodynamic state described by T, V, N_w and λ_j. Pressure is related to the partition function according to

$$P^H = -k_B T \left(\frac{\partial \frac{\Psi}{k_B T}}{\partial V} \right)_{T, N_w, \underline{\lambda}} \tag{6.16}$$

Applying this operation and using Eq. 3.1 and 3.4 we obtain

$$P^H = \frac{\partial - A^{EL}}{\partial V^{EL}} - k_B T \sum_j \left[\nu_j N_w \frac{\partial \ln\left(1 - \sum_i \left[\Theta_{ij}\right]\right)}{\partial V^H} \right] \tag{6.17}$$

where the empty lattice term corresponds to the pure water empty lattice phase pressure in the condition of V, N_w and T 3.9. We then define the difference in pressure between hydrate having $\boldsymbol{\lambda}$ activity of guests and the empty lattice at the same V, Nw and T condition by ΔP^{H-EL}, which we refer to as the pressure shift.

Applying the product rule and recalling Eq. (6.3) we obtain the final expression for the pressure shift as

$$\Delta P^{H-EL} = P^H - P^{EL} = k_B T \left(\sum_j \left[\nu_j \sum_i \left[\Theta_{ij} \left(\frac{\partial \ln\left(C_{ij}\right)}{\partial \overline{V}^{EL}} \right)_T \right] \right] \right) \tag{6.18}$$

Note that in the case of considering that the Langmuir coefficient itself does not vary with the lattice molar volume, a common simplification in current literature, the pressure shift contribution vanishes and the pressure in the empty

lattice is equal to the actual hydrate pressure. The applicable form of this expression depends on either a partition function for the enclathrated molecules (Eq. 3.11) or an empirical expression for Langmuir coefficients fitted to either rigorous model results (PARRISH and PRAUSNITZ, 1972) or to phase equilibrium data.

Also note that in case the R_j were not related to V/N_w through our geometry considerations, as would be the case of a hydrate capable of some kind of interstitial compressibility while keeping cages size constant, which is at best a rough approximation for small compressibility, then the partial derivative of R_j with respect to V/N_w, would vanish, and therefore that of C_{ij} with respect to $\overline{V}$ would also vanish, despite our fundamental consideration of $C_{ij}\left(R_j\right)$ and, finally, $\Delta P^{\mathrm{H-EL}}$ would vanish naturally, as a limit case. This case is referred to in the results and discussion section as the "Interstitial" model.

In the general case, one can say that the lattice does “see” the guest component molecules, so much that (a) the pressure of the phase significantly increases or decreases with the adsorption extent at constant volume or alternatively (b) the volume does vary in function of occupancy at a constant pressure analysis. The pressure shift expression can also be understood as

$$\Delta P^{\mathrm{H-EL}} = \sum_j \nu_j \left(\sum_i \left[\left(\Theta_{ij}\right) P_{ij}^{\mathrm{cage}} \left(\frac{\partial V_j^{\mathrm{cage}}}{\partial \overline{V}} \right) \right] \right) \tag{6.19}$$

if we have P_{ij}^{c} defined as

$$P_{ij}^{\mathrm{cage}} = k_{\mathrm{B}} T \left(\frac{\partial \ln\left(q_{ij}\right)}{\partial V_j^{\mathrm{cage}}} \right)_T = k_{\mathrm{B}} T \left(\frac{\partial \ln\left(C_{ij}\right)}{\partial V_j^{\mathrm{cage}}} \right)_T \tag{6.20}$$

where, from the Lennard-Jones and Devonshire cell theory,

$$V_j^{\mathrm{cage}} = \frac{4}{3}\pi R_j^3 \tag{6.21}$$

The cage pressures in Eq. 6.20 carry the interpretation of pressure of the probe enclathrated guest subsystem under the external field of a cage of type j. From that, the pressure shift is reconstructed weighting each cage pressure with its occupancy and relative differential contribution of that cage volume to the phase volume. That is, what matters in this modeling is not how cage and total volume add up, but how variations in each cage are related to total variation, as in Section 6.1. This definition of a pressure from the partition function of parti-

cles under an external field is usual in the confined fluids literature (BARBOSA *et al.*, 2016).

Note, however, that there is always a cage pressure, but there will only exist a pressure shift if we do consider, in our modeling, a relation between the cage volume and the phase molar volume, and it is only noticeable if occupancy in those cages are noticeable.

For phase equilibrium calculations, it should be clear that the hydrate pressure is equal to every other bulk phase pressure, as it is the thermodynamic property conjugated to the hydrate volume.

6.3.2 Chemical potential of the host component

The chemical potential of water is related to the partition function according to Eq. B.23. Note here that, because Langmuir coefficients depend on molar volume, there will be a term for the derivatives of Langmuir coefficients with mole numbers in accordance with Figure 6.3. We take that into account via chain rule and product rule. Then, a contribution arises, which is equivalent to the pressure shift contribution $\Delta P^{\mathrm{H-EL}}$.

$$\Delta\mu_{\mathrm{w}}^{\mathrm{H-EL}} = k_{\mathrm{B}}T\left(\sum_{j}\left[\nu_j \ln\left(1-\sum_{i}\left[\Theta_{ij}\right]\right)\right]\right) + \Delta P^{H-EL}\left(\frac{V}{N_{\mathrm{w}}}\right) \tag{6.22}$$

This expression allows us to calculate chemical potential of water in the hydrate relative to the empty lattice condition. In order to perform phase equilibrium calculations, we need to model the chemical potential of the empty lattice relative to a practical reference state: pure liquid water, conventional ice, or pure ideal gas.

Now, consider the case where the cages radii (R_j) were considered as depending on $\overline{V}^{\mathrm{EL}}$ through our geometry consideration, while the actual lattice volume was considered independent of pressure. In this case, we are in a consistent limit case where our model, despite calculating a pressure shift, yields the same results for chemical potential as the standard model. This happens because the new contribution in the $\Delta\mu^{\mathrm{H-EL}}$ expression ($\overline{V}^{\mathrm{EL}}\ \Delta P^{\mathrm{H-EL}}$) cancels out with the new contribution in $\Delta\mu^{\mathrm{EL-Pw}}$. The new contribution in $\Delta\mu^{\mathrm{EL-Pw}}$ is that the Poynting integral in the current model is calculated using for the upper limit $P^{\mathrm{EL}} = P^{\mathrm{H}} - \Delta P^{\mathrm{H-EL}}$, while in the standard model it was $P^{\mathrm{EL}} = P^{\mathrm{H}}$. Therefore the new contribution is difference between the Poynting integral in the new

model and in the old model, which is due to the difference in the upper limit of integration. In the case of a constant $\overline{V}$, this difference is simply ($\overline{V}^{\mathrm{EL}}\ \Delta P^{\mathrm{H-EL}}$).

$$\int_{P^{\mathrm{EL}}}^{P^{\mathrm{H}}=P^{\mathrm{EL}}+\Delta P^{\mathrm{H-EL}}} \left[\frac{\overline{V}^{\mathrm{EL}}(T)}{RT}\right] dP = \frac{\overline{V}^{\mathrm{EL}}}{RT}\Delta P^{\mathrm{H-EL}} \tag{6.23}$$

The contribution of Θ_{ij} will be the same in both cases, as it is depending on R_j, which depends on $\overline{V}^{\mathrm{EL}}$, and this is constant and the same in both cases. This case is referred to in the results and discussion section as the "Limit Case" modeling.

6.4 The Clapeyron equation

Previous works have considered dependency of R with $\overline{V}$ in the Langmuir coefficients calculations, while not considering the pressure shift in $\Delta\mu^{\mathrm{H-EL}}$ or $\Delta\mu^{\mathrm{EL-PW}}$ expressions. Here, we show this leads to an inconsistency noticeable in phase equilibrium calculations. According to the multicomponent and multiphase expression for the Clapeyron equation for univariant equilibrium,

$$\frac{dP}{dT} = \frac{|\Delta\overline{H}^{uni}|}{T|\Delta\overline{V}^{uni}|} \tag{6.24}$$

where the right hand side of Eq. 6.24 represents the ratio of determinants shown from the Gibbs-Duhem relation in TESTER and MODELL (1997b).

$$\frac{|\Delta\overline{H}^{uni}|}{T|\Delta\overline{V}^{uni}|} = \frac{\begin{vmatrix} -\overline{H}^{H}/T^2 & x_w^H & x_g^H \\ -\overline{H}^{L}/T^2 & x_w^L & x_g^L \\ -\overline{H}^{V}/T^2 & x_w^V & x_g^V \end{vmatrix}}{\begin{vmatrix} -\overline{V}^{H}/T & x_w^H & x_g^H \\ -\overline{V}^{L}/T & x_w^L & x_g^L \\ -\overline{V}^{V}/T & x_w^V & x_g^V \end{vmatrix}} \tag{6.25}$$

Considering the common approximation of $x_{\mathrm{w}}^V = 0$ and $x_{\mathrm{g}}^L = 0$, it simplifies to

$$\Delta\overline{V}^{uni} = \overline{V}^{H} - \overline{V}^{L}x_w^H - \overline{V}^{V}x_g^H \tag{6.26}$$

and

$$\Delta\overline{H}^{uni} = \overline{H}^{H} - \overline{H}^{L}x_w^H - \overline{H}^{V}x_g^H \tag{6.27}$$

which are the variations in volume and enthalpy, respectively, on the dissociation of 1 mol of hydrate into Pw and V.

As the slope (dP/dT) is equal to the ratio between $|\Delta H^{uni}|$ and $T\ |\Delta \overline{V}^{uni}|$, when $|\Delta \overline{V}^{uni}|$ vanishes, the phase equilibrium curve has vertical slope.

Here, we show the application of this test to the phase equilibrium diagram of hydrate of a pseudo component based on ethane, as illustrated in Figure 6.4.

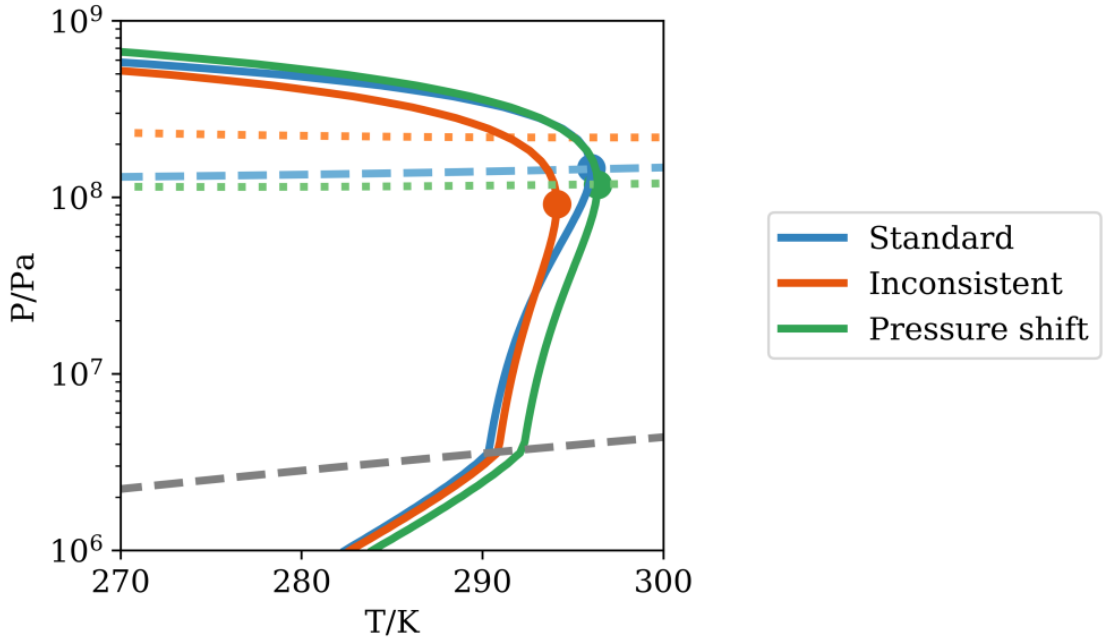

Figure 6.4: Consistency test with the Clapeyron equation. The continuous lines are univariant three phase equilibrium lines between hydrate, liquid water and a fluid phase rich in the guest component. The colors blue, orange and greed correspond to the models Standard, Inconsistent and Pressure shift, respectively. The circles in these curves mark the value for which the slope is vertical. The corresponding dashed lines are the loci where the presented volume difference $|\Delta \overline{V}^{uni}|$ is null. The gray line and point represent the gas-liquid transition curve and critical point, respectively, for the fluid phase rich in the guest component.

The dotted curves are the contour level for $|\Delta \overline{V}^{uni}| = 0$. The blue curve represents the standard model, which does meet this Clapeyron equation criteria. A model with lattice volume dependent Langmuir coefficients, shown in orange, lacks this consistency if the derived properties equations are not revised. Finally, the green curve results from the model proposed here. In conclusion, the inclusion of volume dependent Langmuir coefficients achieves sensitivity of the phase equilibrium behavior regarding the model parameters at high pressure, and the revision of expressions ensures the model passes the Clapeyron equation consistency test and achieves sensitivity of the phase equilibrium behavior

regarding the model parameters also at low pressure.

6.5 Dissociation enthalpy

We note that our modification influences the enthalpy calculations previously presented by a few works (AVLONITIS, 2005; JÄGER *et al.*, 2016; MEDEIROS *et al.*, 2018). These values appear in the Clapeyron equation test numerator, therefore they are related to the equilibrium curve slope, and they are also important in energy balances in general. Internal energy is related to the partition function according to

$$U^{\mathrm{H}} = -k_{\mathrm{B}}T^2 \left(\frac{\partial \frac{\Psi}{k_{\mathrm{B}}T}}{\partial T} \right)_{V,N,\underline{\lambda}} \tag{6.28}$$

where, as in the pressure calculation, a contribution from the empty lattice partition (Q^{EL}) function arises, and it leads to the internal energy of the empty lattice (U^{EL}) at given T, V, N_{w}.

The internal energy of the hydrate can therefore be expressed relatively to the internal energy of the empty lattice at a same T, V, N_{w} by

$$\frac{U^{\mathrm{H}} - U^{\mathrm{EL}} - \sum_i N_i \overline{U}^{\mathrm{PIG}}}{N_{\mathrm{w}} k_{\mathrm{B}} T^2} = \sum_i \left[\sum_j \left[\nu_j \Theta_{ij} \left(\frac{\partial \ln \left(TC_{ij} \right)}{\partial T} \right) \right] \right] \tag{6.29}$$

From that, we can derive enthalpy as

$$H^{\mathrm{H}} = U^{\mathrm{H}} + P^{\mathrm{H}} V^{\mathrm{H}} \tag{6.30}$$

$$H^{\mathrm{EL}} = U^{\mathrm{EL}} + P^{\mathrm{EL}} V^{\mathrm{EL}} \tag{6.31}$$

$$V = V^{\mathrm{H}} = V^{\mathrm{EL}} \tag{6.32}$$

and

$$P^{\mathrm{PIG}} V^{\mathrm{PIG}} = k_{\mathrm{B}} T \tag{6.33}$$

Therefore

$$\frac{H^{\mathrm{H}} - H^{\mathrm{EL}} - \sum N_i \overline{H}^{\mathrm{PIG}}}{N_{\mathrm{w}}} = +\overline{V}^{\mathrm{EL}} \Delta P^{\mathrm{H-EL}} - k_{\mathrm{B}} T \frac{\sum_i N_i}{N_{\mathrm{w}}} + k_{\mathrm{B}} T^2 \sum_i \left[\sum_j \left[\nu_j \Theta_{ij} \left(\frac{\partial \ln \left(T\, C_{ij} \right)}{\partial T} \right) \right] \right] \quad (6.34)$$

This expression represents the enthalpy of adsorption of N_i molecules of guest component on an empty lattice, from an ideal gas phase, per molecule of water, which we name $\Delta H^{\mathrm{H-EL-IG}}$.

In order to find an application for that expression, we combine it with residual gas enthalpy at T, P, N_i, ($\Delta H^{\mathrm{G-PIG}}$) and enthalpy of transformation for the lattice at T,P^{EL},N_{w} into stable pure liquid water at T, P, N_{w} ($\Delta H^{\mathrm{EL-PW}}$), resulting in an expression for the enthalpy of dissociation ($\Delta H^{\mathrm{G+PW-H}}$). This combination is done weighting the terms with the composition into

$$\frac{\Delta H^{\mathrm{G+PW-H}}}{N_{\mathrm{w}}} = - \frac{\Delta H^{\mathrm{H-EL-IG}}}{N_{\mathrm{w}}} + \sum_i \left[x_i \Delta H^{\mathrm{G-PIG}} \right] + x_{\mathrm{w}} \Delta H^{\mathrm{EL-PW}} \quad (6.35)$$

This is analogue to the expression presented in MEDEIROS *et al.* (2018), but noting, now, that $\Delta H^{\mathrm{EL-PW}}$ represents a difference in enthalpy of an empty lattice at P^{EL} and a stable pure liquid water at P, and that $\Delta H^{\mathrm{H-EL-IG}}$ includes a pressure shift contribution ($\overline{V}^{\mathrm{EL}} \Delta P^{\mathrm{H-EL}}$).

The contribution of $\Delta H^{\mathrm{EL-PW}}$ can be expressed relatively to a standard condition at T_0 and P_0 as

$$\Delta H^{\mathrm{EL-PW}} = \Delta H_{00}^{\mathrm{EL-PW}} + \int_{T_0}^{T} \Delta C_{P_0}^{\mathrm{EL-PW}} dT + \int_{P_0}^{P^{\mathrm{EL}}} \left[\overline{V}^{\mathrm{EL}}(T) - T \left(\frac{\partial \overline{V}}{\partial T} \right)_N \right] dP \quad (6.36)$$

As we noted in the expression for the chemical potential of water, in the limiting case of constant lattice volume, our model yields the same results as the standard model also for enthalpy calculations. If $\overline{V}^{\mathrm{EL}}$ is constant with respect to T and P, then the pressure shift contribution in the expression for $\Delta H^{\mathrm{H-EL-IG}}$ is equal to the factor removed from the volume integral for enthalpy in the

expression for the $\Delta H^{\mathrm{EL-PW}}$, as shown:

$$\frac{1}{R\,T}\int_{P^{\mathrm{EL}}}^{P^{\mathrm{H}}=P^{\mathrm{EL}}+\Delta P^{\mathrm{H-EL}}}\left[\overline{V}^{\mathrm{EL}}(T)-T\left(\frac{\partial\overline{V}}{\partial T}\right)_{N}\right]dP=\frac{\overline{V}^{\mathrm{EL}}}{RT}\Delta P^{\mathrm{H-EL}} \tag{6.37}$$

6.6 Parameterization

The reference condition for the properties of the empty lattice, with respect to liquid water is taken as 273.15 K (0 °C) and 1.01325×10^5 Pa (1 atm), the values for the properties ($\Delta\mu^{\mathrm{EL-Pw}}_{\mathrm{w},T_0,P_0}$, $\Delta\overline{H}^{\mathrm{EL-Pw}}_{\mathrm{w},T_0,P_0}$ and $\Delta \mathrm{C}_{\mathrm{P}\,\mathrm{w},T_0,P_0}^{\mathrm{EL-Pw}}$) were based on those of PARRISH and PRAUSNITZ (1972) and HOLDER *et al.* (1988), while the volume correlation is based on crystal data of KLAPPROTH *et al.* (2003) and SHPAKOV *et al.* (1998). The parameters for the Lennard-Jones and Devonshire cage of Kihara potential were based on PARRISH and PRAUSNITZ (1972). Here, we consider the radii dependence on $\overline{V}^{\mathrm{EL}}$ making the R_j proportional to the lattice edge parameter (cubic unit cell parameter) a_0, using the radii from Parrish and Prausnitz as our R_0, i. e. R at T_0 and P_0.

A more detailed justification and the values used are described in detail in the Appendix C.

6.7 Pressure shift solution algorithm

We have stated that our model has, intrinsically, an interdependence loop in the variables Θ_{ij}, $\overline{V}^{\mathrm{EL}}$ R_j, $\Delta P^{\mathrm{H-EL}}$, P^{H} and P^{EL}. For that reason, it requires an iterative method for convergence of equilibrium properties at a given condition. In a simplest case, given a value for the empty lattice pressure P^{EL} and fugacities of all guest components, the calculation is straightforward:

Function `calcPShift`(T, P^{EL}, $\hat{f}_i$)**:**
  Calculate $\overline{V}^{EL}$ from T, P^{EL};
  Calculate R_j from $\overline{V}^{EL}$;
  Calculate C_{ij} from T, R_j;
  Calculate Θ_{ij} from $C_{kj}, \hat{f}_k$;
  Calculate $\left(\partial C_{ij}/\partial\overline{V}^{\mathrm{EL}}\right)_T$ from T, R_j;
  Calculate $\Delta P^{\mathrm{H-EL}}$ from $T, \Theta_{ij}, \left(\partial C_{ij}/\partial\overline{V}^{\mathrm{EL}}\right)_T$;
return $\Delta P^{\mathrm{H-EL}}$

First, the pressure shift $\Delta P^{\mathrm{H-EL}} + P^{\mathrm{EL}}$ is calculated using

`calcPShift`$(T, P^{EL}, \hat{f}_i)$, then the hydrate pressure is calculated from $P^{H} = \Delta P^{H-EL} + P^{EL}$.

However, for direct specification of P^{H}, an implicit solution method is required (convergePEL). We developed the following successive substitution algorithm to converge the pressure shift and obtain thermodynamic properties of the hydrate.

Function `convergePEL`$(T,\ P^{H},\ \hat{f}_i)$**:**
  guess: $\Delta P^{H-EL} = 0$
  do
    Calculate $P^{EL} = P^{H} - \Delta P^{H-EL}$
    Update $\Delta P^{H-EL} = \text{calcPShift}(T, P^{EL}, \hat{f}_k)$
    Calculate RES $= \left(\left[\Delta P^{H-EL}\right]^{k+1} - \left[\Delta P^{H-EL}\right]^{k} \right) / P^{H}$
  loop while abs (RES) $> 1 \times 10^{-9}$;
return P^{EL}

The algorithm convergence analysis for three basis cases of pure methane, ethane and carbon dioxide at T_0 and P_0 are shown in Figure 6.5.

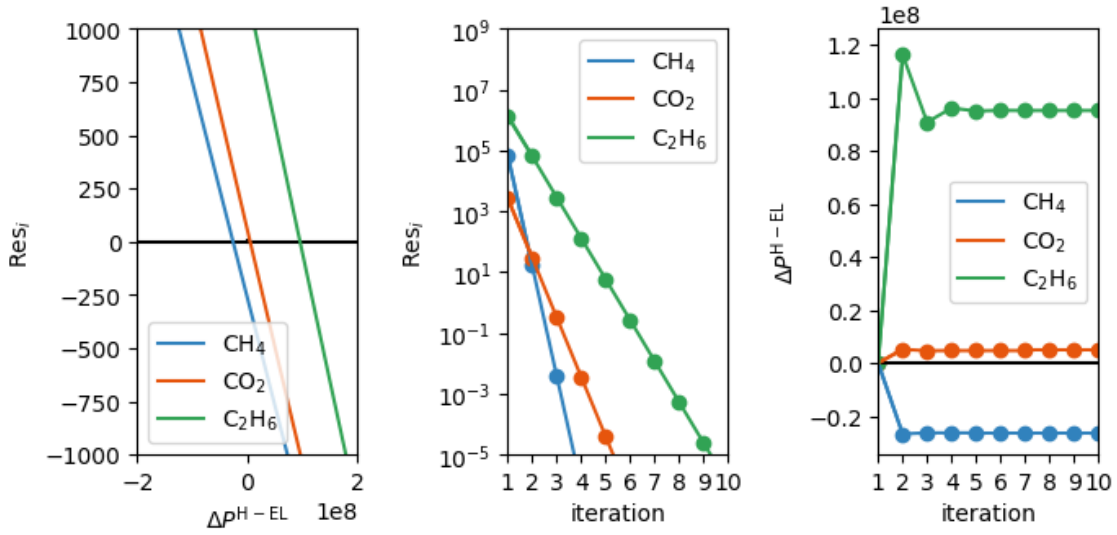

Figure 6.5: Analysis of the pressure shift algorithm for given hydrate pressure: pressure shift variable (ΔP^{H-EL}), residue (RES) and iteration for methane, ethane and carbon dioxide single hydrates at the reference temperature T_0 and reference pressure P_0. The values were sampled for each iteration and are connected by straight lines for the visualization of trends.

These examples show that the residue is approximately linear with respect to the variable ΔP^{H-EL}, and that convergence is fast showing that the successive substitution algorithm is sufficiently robust in this condition. The residue drops

by a few orders of magnitude each iteration and the oscillation in the variable around the solution value is quite small.

In the case where we wanted to perform calculations given the empty lattice pressure, while associating fugacities of guest components with the system pressure the unkwnown a priori, we used a slightly different successive substitution algorithm (convergePH), as follows.

Function `convergePH`(T, P^{EL}, EOS)**:**
  guess: $\Delta P^{\mathrm{H-EL}} = 0$
  do
    Calculate $P^{\mathrm{H}} = P^{\mathrm{EL}} + \Delta P^{\mathrm{H-EL}}$
    Calculate $\hat{f}_g$ from the EOS using $P = P^H$ and $T = T$
    Update $\Delta P^{\mathrm{H-EL}} = \mathrm{calcPShift}(T, P^{\mathrm{EL}}, \hat{f}_g)$
    Calculate $\mathrm{RES} = \left(\left[\Delta P^{\mathrm{H-EL}}\right]^{k+1} - \left[\Delta P^{\mathrm{H-EL}}\right]^{k} \right) / P^{\mathrm{H}}$
  loop while $\mathrm{abs}\,(\mathrm{RES}) > 1 \times 10^{-9}$;
return P^{H}

That was required for calculations of phase equilibrium using either the ideal gas law or the equation of state of Peng and Robinson, in regions of high pressure where it was observed that more than one root of P^{EL} existed for a given P^{H}.

In this algorithm, a step control is required to prevent the hydrate pressure P^{H} from being negative, which does not characterize a physically meaningful phase equilibrium solution, and can cause problems in the calculations of fugacity coefficients in the equation of state for the fluid phase and in the residue used in this algorithm.

Chapter 7

Results and discussion of the pressure shift model

Here we present results from using our model to hydrates of three components: methane, ethane and CO_2. We discuss the behavior captured by the model and the variation of that behavior from guest to guest (different guest dependent parameters).

All calculations of thermodynamic properties and phase equilibrium presented in this chapter were performed in the IPython environment for interactive computing (PÉREZ and GRANGER, 2007), using the SciPy ecosystem of open-source software for mathematics, science, and engineering to handle data arrays (NumPy, OLIPHANT, 2006), estabilished numerical methods (SciPy, JONES *et al.*, 2001), and plots for both interactive data visualization and publication (Matplotlib, HUNTER, 2007).

7.1 Lattice volume, cages radii and Langmuir coefficients.

The lattice volume $\overline{V}^{\mathrm{EL}}$ decreases as the lattice pressure P^{EL} increases, according to the constant compressibility correlation used. As the volume decreases, also does the cage radii according to the proportionality criteria used. The behavior of Langmuir coefficients with respect to changes in radii depends on the relative size of the guest molecule and the cage. We present calculations of $\overline{V}^{\mathrm{EL}}$, R_j and C_{ij} for probe molecules of methane, ethane and carbon dioxide at constant T, along a range of P^{EL} in Figure 7.1.

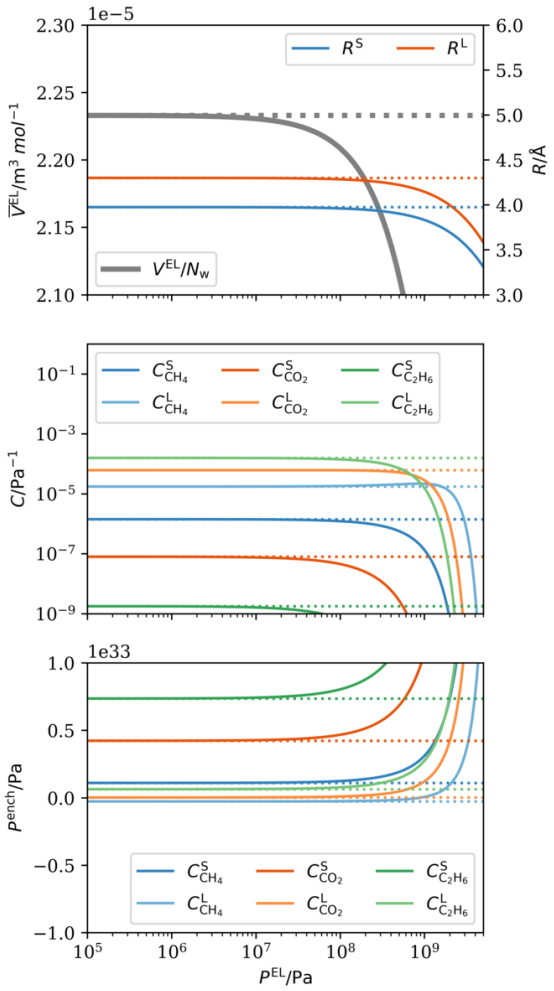

Figure 7.1: Lattice molar volume ($\overline{V}^{EL}$) and cage radii (R_j) (a) for small and large cages, Langmuir coefficients (C_{ij}) for several guest components (b) and cage pressure (P_{ij}^{cage}) (c). All calculated and plotted as function of empty lattice pressure (P^{EL}).

This analysis shows how, in our model, the Langmuir coefficients are indirectly and naturally a function of the lattice pressure. The dashed lines represent constant $\overline{V}^{EL}$, R_j and therefore constant C_{ij} in order to grant some perspective on the variations between the standard (constant volume and cages radii) and compressible (varying volume and cages radii) models. From that, we see that the current correlation for molar lattice volume describe significant compression for condition of pressure above 1×10^8 Pa. Langmuir coefficients calculations show that methane molecules fits tightly in the small cages, so affinity decreases when the cage size decreases, becoming too small to accommodate methane molecules near 1×10^9 Pa. In the same manner, both small and large cages are relatively small regarding CO_2 and ethane. On the other hand, the methane molecule fits loosely in the large cage, so it is better adjusted above 1×10^8 Pa as the cage

shrinks, and the C_{ij} increase.

7.2 Predictions of guest dependent lattice volume

We performed calculations of pressure shift for methane, carbon dioxide and ethane at T_0 and P_0. For each component, we obtain different values of $\Delta P^{\mathrm{H-EL}}$ and, therefore, different lattice volume for the same hydrate pressure. In the following calculations, for each component, we varied the parameters a_i, σ_i and ϵ_i in a range, one at a time, while keeping the other two parameters constant. We plot both the resulting pressure shift and lattice volume versus those parameters to investigate the sensitivities of the model. We also calculated theoretical cage occupancy of the probe molecules to draw insight.

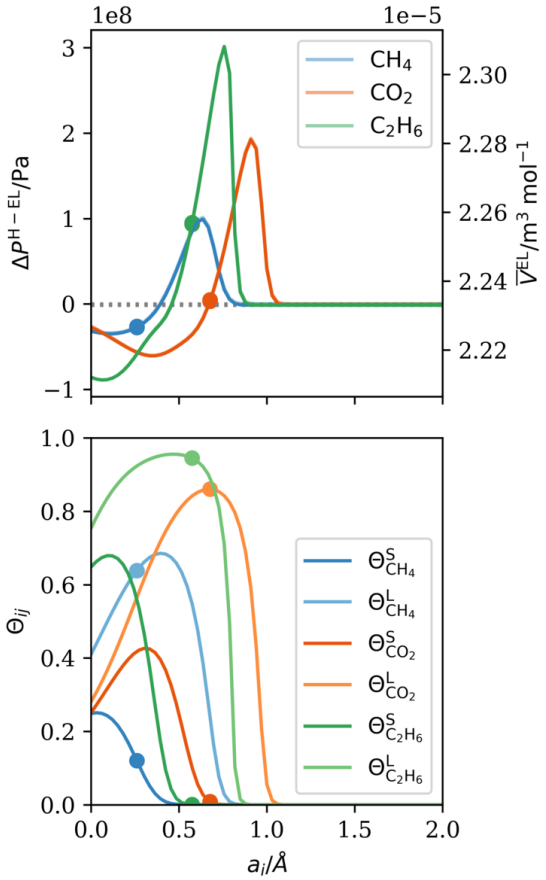

Figure 7.2: Pressure shift ($\Delta P^{\mathrm{H-EL}}$), lattice molar volume ($\overline{V}^{\mathrm{EL}}$) and occupancy Θ_{ij} of a single hydrate of a probe guest versus the hard-core size (a_i) cage potential parameter, holding the other cage potential parameters constant. The points are the standard values for the parameters used in this work for methane, carbon dioxide and ethane.

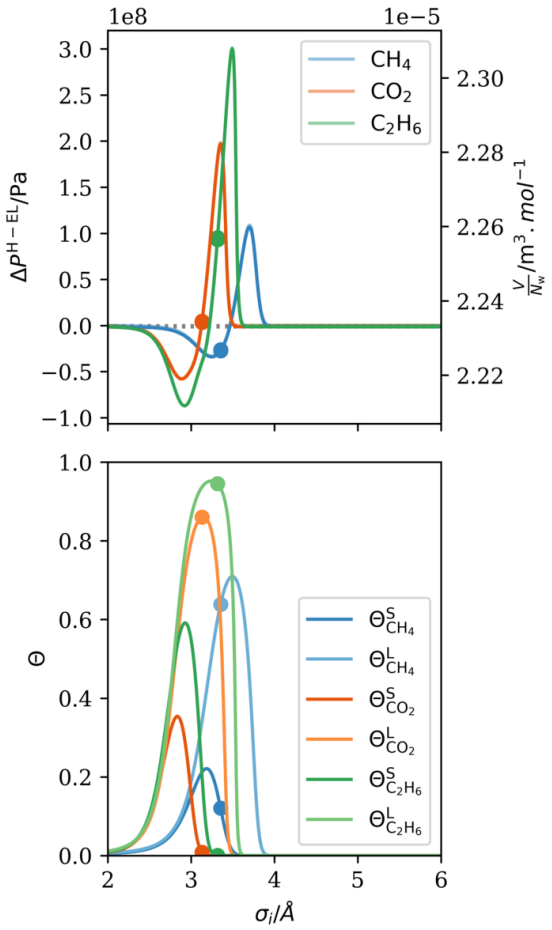

Figure 7.3: Pressure shift ($\Delta P^{\mathrm{H-EL}}$), lattice molar volume ($\overline{V}^{\mathrm{EL}}$) and occupancy Θ_{ij} of a single hydrate of a probe guest versus the soft-core size cage potential parameter, holding the other cage potential parameters constant. The points are the standard values for the parameters used in this work for methane, carbon dioxide and ethane.

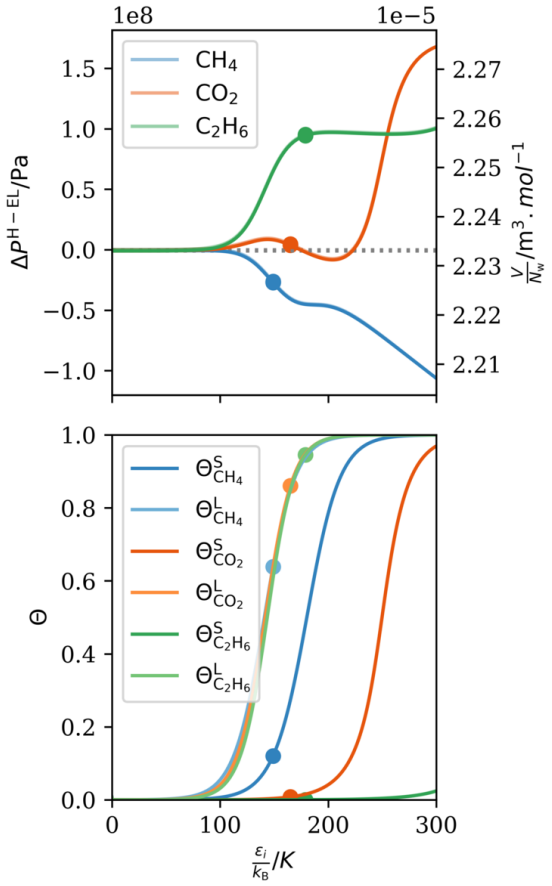

Figure 7.4: Pressure shift, lattice molar volume and occupancy of probe molecule hydrates versus the the energy cage potential parameter, holding the other cage potential parameters constant. The points are the standard values for the parameters used in this work for methane, carbon dioxide and ethane.

In Figures 7.2, 7.3 and 7.4, the pressure shift and molar volume plots versus cage potential parameters overlap. That happens because at constant T, the molar lattice volume is expressed as

$$\bar{V}^{\mathrm{EL}}\left(P^{\mathrm{EL}}\right) = \bar{V}_0^{\mathrm{EL}} e^{-k\left(P^{\mathrm{EL}}-P_0\right)} \tag{7.1}$$

In this section, we are doing calculations at $P^{\mathrm{H}} = P_0$, therefore $P^{\mathrm{EL}} = P_0 - \Delta P^{\mathrm{H-EL}}$, consequently

$$\bar{V}^{\mathrm{EL}}\left(P^{\mathrm{EL}}\right) = \bar{V}_0^{\mathrm{EL}} e^{-k\left(-\Delta P^{\mathrm{EL}}-P_0\right)} \tag{7.2}$$

where k is the compressibility of the lattice from the correlation for the lattice molar volume.

As k has order of magnitude of 1×10^{-10} Pa^{-1} and $\Delta P^{\mathrm{H-EL}}$ has order of

magnitude of 1×10^8 Pa, these calculations are done well inside the range of validity of the approximation $e^x = 1 - x$.

Therefore, in these series of calculations, $\overline{V}^{\mathrm{EL}}$ is approximately described by

$$\bar{V}^{\mathrm{EL}}\left(P^{\mathrm{EL}}\right) = \bar{V}_0^{\mathrm{EL}}\left(1 - k\Delta P^{\mathrm{EL}-P_0}\right) \tag{7.3}$$

If $\overline{V}^{\mathrm{EL}}$ is a linear function of $\Delta P^{\mathrm{H}-\mathrm{EL}}$, their plots versus parameter values differ solely by a vertical axis offset and a multiplicative factor changing scale. Then, in those plots, the two series overlap and it becomes a matter of reading $\Delta P^{\mathrm{EL}-P_0}$ in the left axis and $\bar{V}$ in the right axis, in such a way, the horizontal reference line marks a pressure difference of zero on the left axis and the standard lattice volume (V_0) at $P^{\mathrm{EL}} = P_0$ on the right axis.

Regarding the hardcore parameter of the Kihara potential (a_i), in 7.2, note that for large values the molecules will fit more tightly. Then $\Delta P^{\mathrm{EL}-\mathrm{H}}$ becomes increasingly positive, because it is proportional to the derivatives of Langmuir coefficients with respect to radii, and in a tight cage an increase in R_j diminishes repulsive interactions, therefore increasing C_{ij}. However, when the cages become much smaller, occupancy drops sharply, therefore also does the ΔP and $\overline{V}^{\mathrm{EL}}$ since the contributions in the pressure shift expression are weighted by the occupancies.

For small values of a_i, the cage is loose enough and derivatives of Langmuir coefficients with respect to radii are now negative. Furthermore, for a_i tending to zero, the influence of σ_i dominates the behavior.

The analysis of small and large values of σ_i is mostly analogous to the analysis of a_i. The difference is that, for σ_i tending to zero, there will be no interaction energy at all and both occupancy and the pressure shift drop to zero.

For both a_i and σ_i, it can be seen that, for one desired value of occupancy in a given cage, two values of the parameter (while keeping the other constant) may seem plausible, however one may be discarded for yielding a significantly different value for the occupancy in the other cage. Also, each value is located in opposing sides regarding the stationary occupancy point, which means that they are related to different domains of sign for the derivatives of C_{ij} with respect to R_j. As a result, each will have opposing contribution to $\Delta P^{\mathrm{H}-\mathrm{EL}}$ for the cage under analysis, and as a consequence, parameter values lower than the stationary point contribute to negative pressure shift and lower than standard molar volume, while parameter values higher than the stationary point contribute to

positive pressure shift and lattice molar volume higher than the reference condition lattice molar volume.

Note that, for methane, at the standard parameter value, the pressure shift is negative because the loose cage effect dominates. Then, as both cages become small, relatively to increasing molecular size parameters, the pressure shift becomes positive.

Finally, increasing ϵ_i always increases attractive interaction, so it will increase Langmuir coefficients and therefore occupancies. Changes to ϵ_i change the magnitude of both C_{ij} and $\left(\partial C_{ij}/\partial \overline{V}^{\mathrm{EL}}\right)_T$. The pressure shift is a result of competing effects of Θ_{ij} and $\left(\partial C_{ij}/\partial \overline{V}^{\mathrm{EL}}\right)_T$ for each cage. Consequently, a steep filling or emptying in C_{ij} is usually reproduced in the $\Delta P^{\mathrm{H-EL}}$ and, if small and large cages have opposing effects, as is the case for these calculations for methane, it can be the case that either one of them dominates the behavior or that they balance each other.

7.3 Disambiguation of parameters for large guests

Let us consider a clathrate of one single type of cage or, similarly, a s^{I} hydrate of a component that is known to occupy only one type of cage. According to the standard model, this component could, at first, have any of two values of σ_i that yield the same C_{ij} and, therefore, the same occupancy, the same $\Delta\mu_{\mathrm{w}}^{\mathrm{H-EL}}$ and, ultimately, the same equilibrium pressure. In this manner, measurements of occupancy or phase equilibrium would not suffice to disambiguate these possible values for σ_i.

In the pressure shift model, however, we predict different $\Delta P^{\mathrm{H-EL}}$ and therefore different $\overline{V}^{\mathrm{EL}}$, either higher or lower than the standard condition molar volume $\overline{V}_0^{\mathrm{EL}}$ from the correlation with $P^{\mathrm{EL}} = P_0$.

Consider as an illustrating case, a hydrate of a given guest component having a structure where only enclathration in one type of cage is possible. Calculations of the Langmuir coefficients and of the pressure shift were made for a case as these (Figure 7.5). These calculations were performed using the parameters of ethane in large cages of s^{I} hydrates, while Langmuir coefficients for the guest component in the small cages was set to zero.

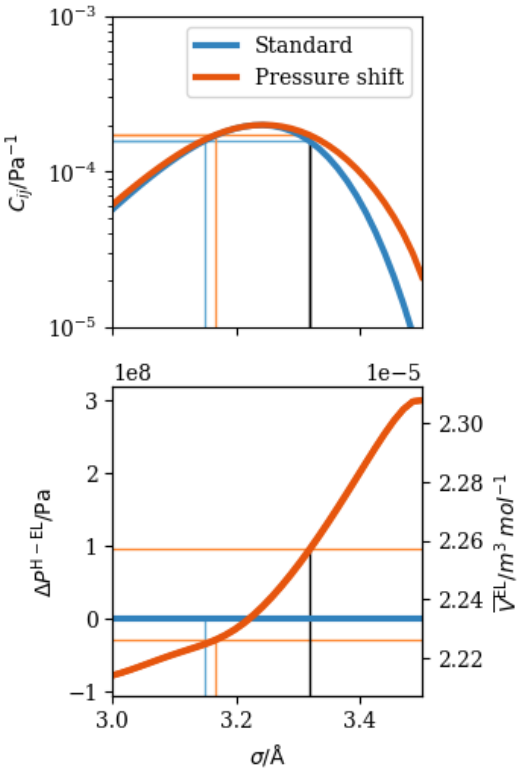

Figure 7.5: Disambiguation of molecular size parameters with the pressure shift model at the standard temperature and pressure. The blue solid lines show calculations for the standard model, while the orange solid lines show calculations for the Pressure shift model for (a) Langmuir coefficients C_{ij} and (b) Pressure shift $\Delta P^{\mathrm{H-EL}}$and lattice molar Volume $\overline{V}^{\mathrm{EL}}$, both as function of the soft-core Kihara parameter σ_i.

In the standard vdW&P model, given a constant value for cage radius, it is not possible to disambiguate between two values of σ_i that generate the same Langmuir coefficient because they also generate the same pressure $P^{\mathrm{EL}} = P^{\mathrm{H}}$ and there is no additional information (Figure 7.5a).

On the other hand, in the pressure shift model the two values of σ_i that generate the same Langmuir coefficient will result in different molar lattice volume and cage radius at the same pressure P_0, either lower or higher than $\overline{V}_0^{\mathrm{EL}}$ due to different results for $\Delta P^{\mathrm{H-EL}}$ (Figure 7.5b).

This means that a measurement of $\overline{V}^{\mathrm{EL}}$ can disambiguate the parameterization of σ_i. In addition, the difference in molar volume varies with temperature and pressure, thus influences the phase equilibrium curve at conditions of higher temperature or pressure, as seen in the next section.

7.4 Phase equilibrium

In this section, we compare the hydrate - liquid water - gas univariant phase equilibrium and thermodynamic properties along this phase equilibrium curve. We present results for six modeling strategies, as illustrated in Figure 7.6. They differ from one to another by combining assumptions in different manners, thus considering some phenomena and neglecting others. All of these calculations were performed using the Peng-Robinson equation of state for the guest component fluid phase.

The goal, at the current stage of development of this work, is not to determine which model is closer to the experimental data, but rather to determine the influence of each version on the null $\Delta\overline{V}^{\text{uni}}$ line, the phase equilibrium curve at both low and high pressure and thermodynamic consistency according to the Clapeyron equation. This serves as an important insight for any posterior attempt at the parameterization of the new model for an optimal fit to multi-component experimental data.

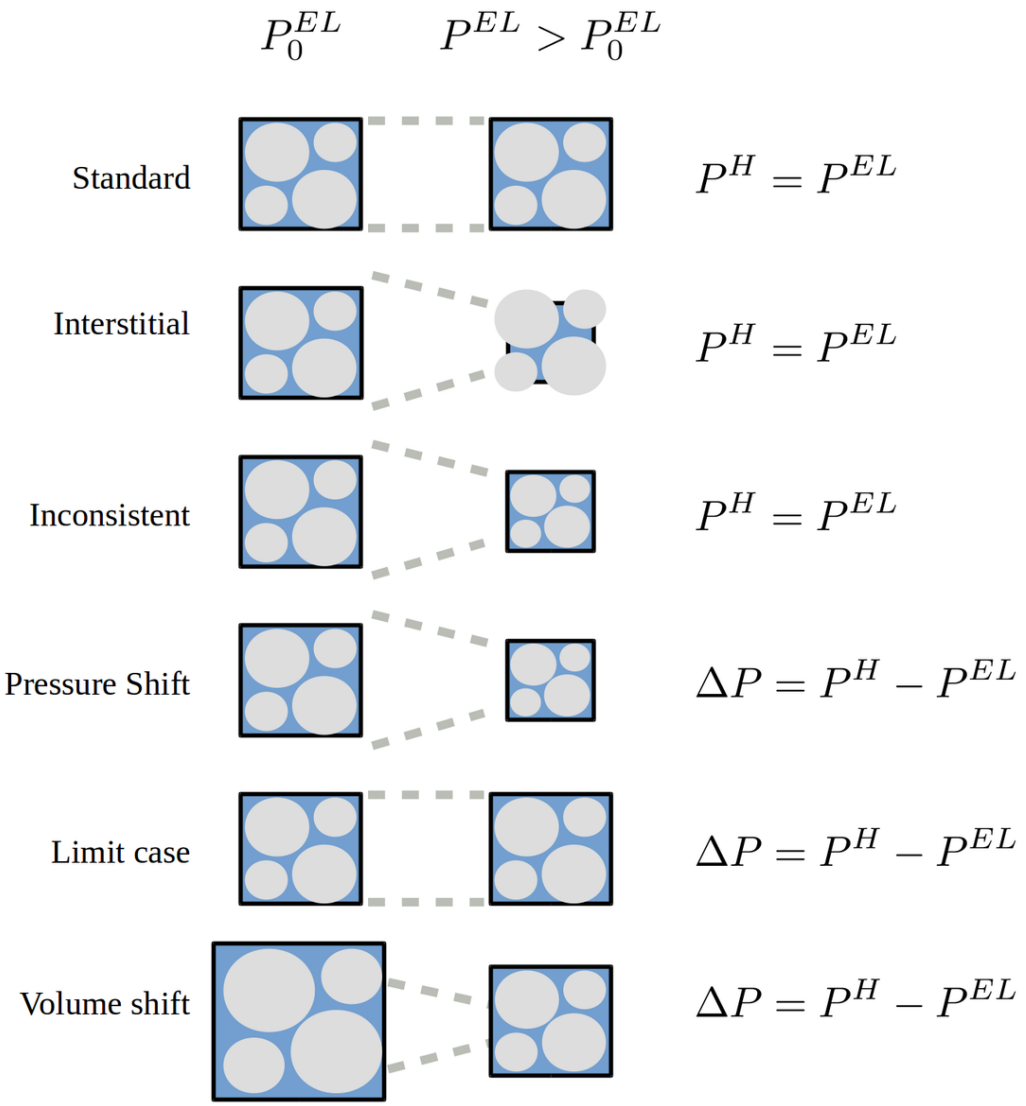

Figure 7.6: Comparison of different lattice behavior modeled in literature (Standard, Interstitial and Inconsistent) and proposed here (Pressure shift, Limit case, Volume shift). In the Standard van der Waals and Platteuw model, there is no change in the lattice volume. In the Interstitial compressibility model, lattice volume changes, but the radii of cages remains constant. In the Inconsistent compressibility models, lattice volume and cages radii change, but derived properties based on isochoric hypothesis are used, therefore the modeling is inconsistent. In the Pressure shift model proposed here, new expressions for derived properties are taken from the partition function and a difference in hydrate and lattice pressure is calculated. In the Limit Case model, the pressure shift expressions are used with an incompressible lattice, and yields the same results as the standard model. In the Volume shift model, a preliminary regression method is used to change the lattice volume at the reference pressure, to match the standard model hydrate volume for a system at that pressure.

The standard modeling approach is the vdW&P model assuming constant cage radii and, independently, constant molar volume (MCKOY and

SINANOĞLU, 1963; PARRISH and PRAUSNITZ, 1972; VAN DER WAALS and PLATTEEUW, 1959).

The modeling approach we call interstitial assumes possible variations of volume with lattice pressure, but neglecting variations of cage radius. This affects Poynting integrals, while cage radii remains constant, therefore not affecting Langmuir coefficients nor resulting in pressure shift contributions (KLAUDA and SANDLER, 2000; MEDEIROS *et al.*, 2018).

The modeling approach we labeled as inconsistent refers to a family of models that use Langmuir coefficients dependent on molar volume, without revising the expressions for derived properties (BALLARD and SLOAN JR., 2002; HSIEH *et al.*, 2012). Molar volume varies with temperature and pressure, also does cage radii, but as the $\Delta P^{\mathrm{H-EL}}$ contribution is not acknowledged, the hydrate pressure P^{H} is assumed equal to the reference lattice pressure P^{EL}. They are labeled inconsistent for failing to pass the Clapeyron equation test.

The pressure shift model is the approach proposed here, in which revising the expressions for derived properties, we showed a difference between the pressure of actual clathrate and empty lattice having the same volume, and this yielded new contributions in the expressions for several thermodynamic properties, as shown before.

The limit case model, as mentioned in the derivation section, refers to limit case calculations performed here. In this case, the cages radii R_j physically depend on $\overline{V}^{\mathrm{EL}}$ and the pressure shift expressions are considered but, at the same time, a model for the empty lattice itself is chosen so that the lattice volume is constant with respect to the lattice pressure.

At last, the volume shift corresponds to the pressure shift model with a simple adjustment for the cubic unit cell edge parameter a_0 in the lattice molar volume correlation such that the lattice molar volume $\overline{V}^{\mathrm{EL}}$ at the reference condition (T_0 and $P^{\mathrm{EL}} = P_0^{\mathrm{H}} - \Delta P^{\mathrm{H-EL}}(T_0, P_0)$) approximately corresponds to the experimental hydrate volume at T_0 and P_0. This strategy is a preliminary fit for qualitative purpose: we shift the cubic unit cell edge parameter a in the model for the empty lattice in order to have that, at $P^{\mathrm{H}} = P_0$ and $P^{\mathrm{EL}} = P_0 - \Delta P_0$, the resulting molar volume is equal to the molar volume given by the original correlation of MEDEIROS *et al.* (2018) parameterized with hydrate data as function of hydrate pressure.

$$\bar{V}^{\mathrm{EL}}\left(a_0^{\mathrm{EL}}, P = P^{\mathrm{EL}}\right) = \bar{V}^{\mathrm{H}}\left(a_0^{\mathrm{H}}, P = P_0\right) \tag{7.4}$$

We perform the same shifting strategy for the radii, finding new $R_{j,0}$ parameter so that when P^{H} is P_0, the calculated R_j matches the original $R_{j,0}$, which are supported by crystallography experimental data or fitted for optimal Langmuir coefficients calculations in the cell theory. We have developed a minor iterative scheme for that preliminary shift.

The parameters in the volume shifted model are useful as initial estimates or references for the setup of search limits in a parameter regression to generate an optimized pressure shift model for applications.

In Figures 7.7 to 7.12 we show the phase equilibrium curve $\left(P^{\mathrm{H,Pw,V}} \times T\right)$ and the curve of null volume difference $\left(P^{\Delta\overline{V}^{\mathrm{uni}}=0} \times T\right)$ in phase equilibrium diagrams for all 6 models for each of methane, ethane and carbon dioxide, respectively. In addition, we plot thermodynamic properties $\Delta\overline{V}^{\mathrm{uni}}$, $\Delta\overline{H}^{\mathrm{uni}}$, $\Delta P^{\mathrm{H-EL}}$ and Θ_{ij} along the equilibrium points of the phase equilibrium curve.

In these figures, the volume shift model for all three components corresponds to the pressure shift modeling with reference cages radii and unit cell parameters shifted to represent methane hydrate original calculations. Therefore, the calculations are based on adjusting three of the parameters of the model based on data for methane hydrates, and of predictive nature for other components.

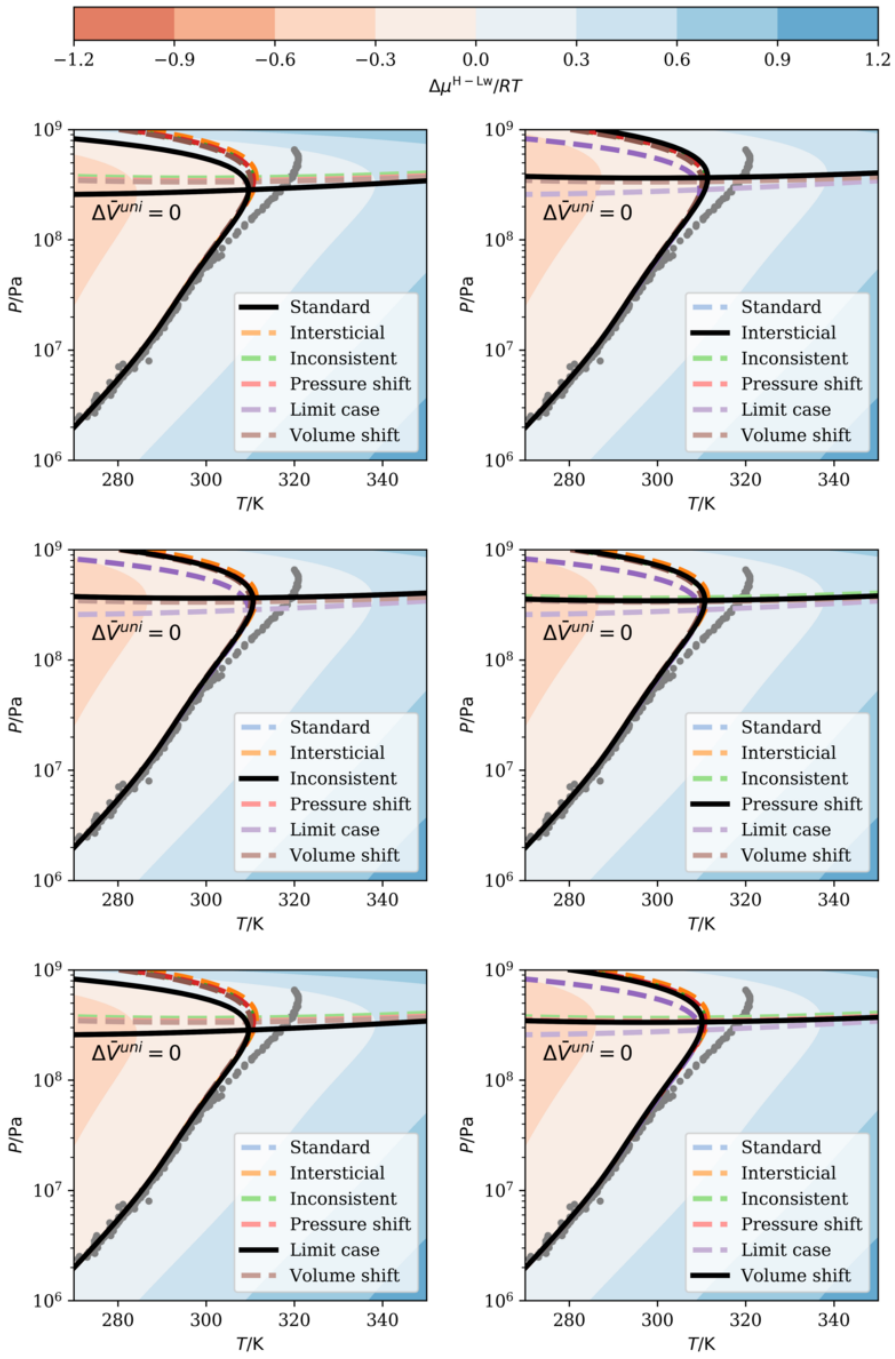

Figure 7.7: Phase equilibrium behavior of methane hydrates for the 6 models under analysis. In each subfigure (a-f) the phase equilibrium curve and the curve of null dissociation volume difference for one of the models is stressed as a continuous black line, and the color scale changed to match the chemical potential difference between hydrate and liquid water for that model. While the curves for the other models are depicted as dashed and in different colors. The gray points are experimental data from NIST in (KROENLEIN *et al.*, 2015)

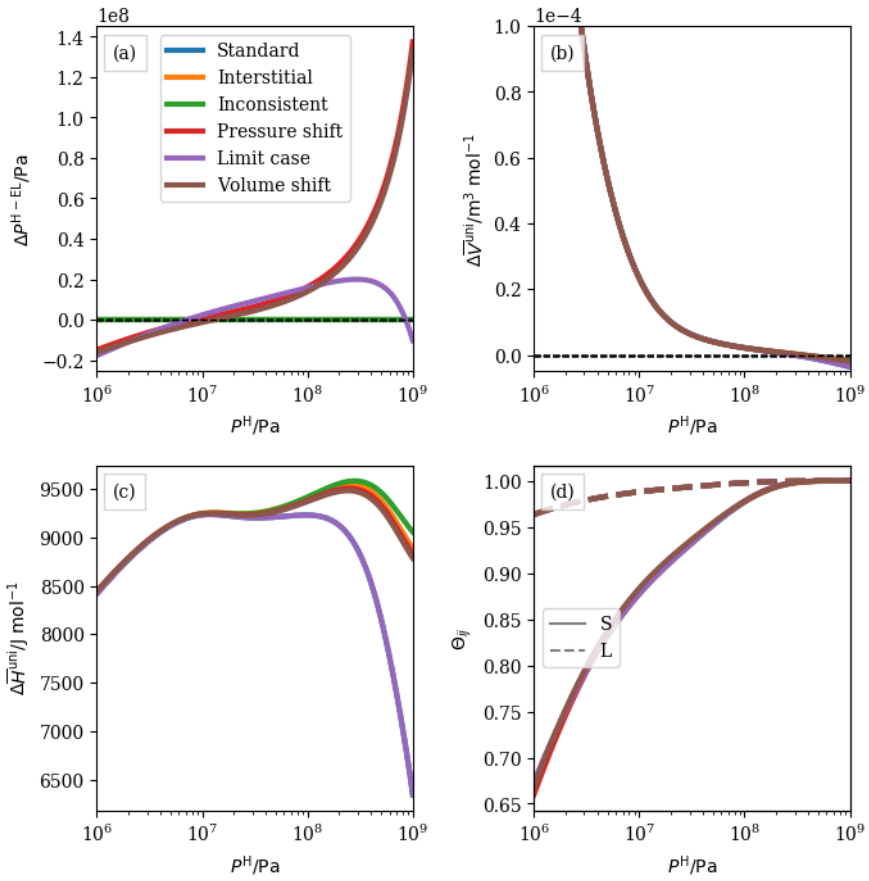

Figure 7.8: Thermodynamics properties of methane hydrates for the 6 models under analysis. Pressure shift (a), dissociation volume change (b), occupancy (b) for the small cages (continous lines) and large cages (dashed lines) and dissociation enthalpy change (d).

For methane (Figure 7.7 and 7.8), the influence of the modifications is noticeable at high pressure conditions. The standard and the limit case yield exactly the same results for phase equilibrium on these numerical evaluations, even though finite pressure shift values are calculate as shown in Figure (7.8b). In the limiting case model, one can see that $\Delta P^{\mathrm{H-EL}}$ at first, increases as the pressure increases (Figure 7.8b), and at sufficiently high pressure it decreases. This occurs because as the molar volume is constant, the pressure shift is function of T only, and following the phase equilibrium line, after the maximum temperature, an increase in pressure leads to a lower temperature, while for other cases the effect of temperature change is overshadowed but a much more prominent pressure dependency.

For ethane and carbon dioxide (Figures 7.9 to 7.12), there are either cusps or discontinuities corresponding to liquid-vapor transition in all plots. The discontinuities happen for $\Delta\overline{V}^{\mathrm{uni}}$ and $\Delta\overline{H}^{\mathrm{uni}}$ because of the guest component fluid

phase, which brings a contribution to the overall differences.

For Θ_{ij} and $\Delta P^{\mathrm{H-EL}}$, we obtain cusps because, as the slope of the phase equilibrium curve is given by

$$\left(\frac{\partial P^{\mathrm{H,Pw,V}}}{\partial T}\right) = \frac{\Delta \overline{H}^{\mathrm{uni}}}{\left(T\ \Delta \overline{V}^{\mathrm{uni}}\right)} \tag{7.5}$$

it means that a discontinuity in the right hand side ratio is equivalent to a discontinuity in the left hand side derivative and, consequently, the slope before and after the fluid phase transition is suddenly different.

The curves for Θ_{ij} and for $\Delta P^{\mathrm{H-EL}}$ as function of P and T along the phase equilibrium loci were calculated individually from each point in the phase equilibrium curve, but the curves for theses properties must exactly correspond to the integration of

$$\left(\frac{\partial \Theta}{\partial P}\right)_{uni} = \left(\frac{\partial \Theta}{\partial T}\right)_{P} \left(\frac{\partial T}{\partial P}\right)_{uni} \tag{7.6}$$

and of

$$\left(\frac{\partial \Delta P}{\partial P}\right)_{uni} = \left(\frac{\partial \Delta P}{\partial T}\right)_{P} \left(\frac{\partial T}{\partial P}\right)_{uni} \tag{7.7}$$

respectively.

This shows how the cusp in the phase equilibrium curve is propagated to the plots of Θ_{ij} and $\Delta P^{\mathrm{H-EL}}$ versus P^{H}.

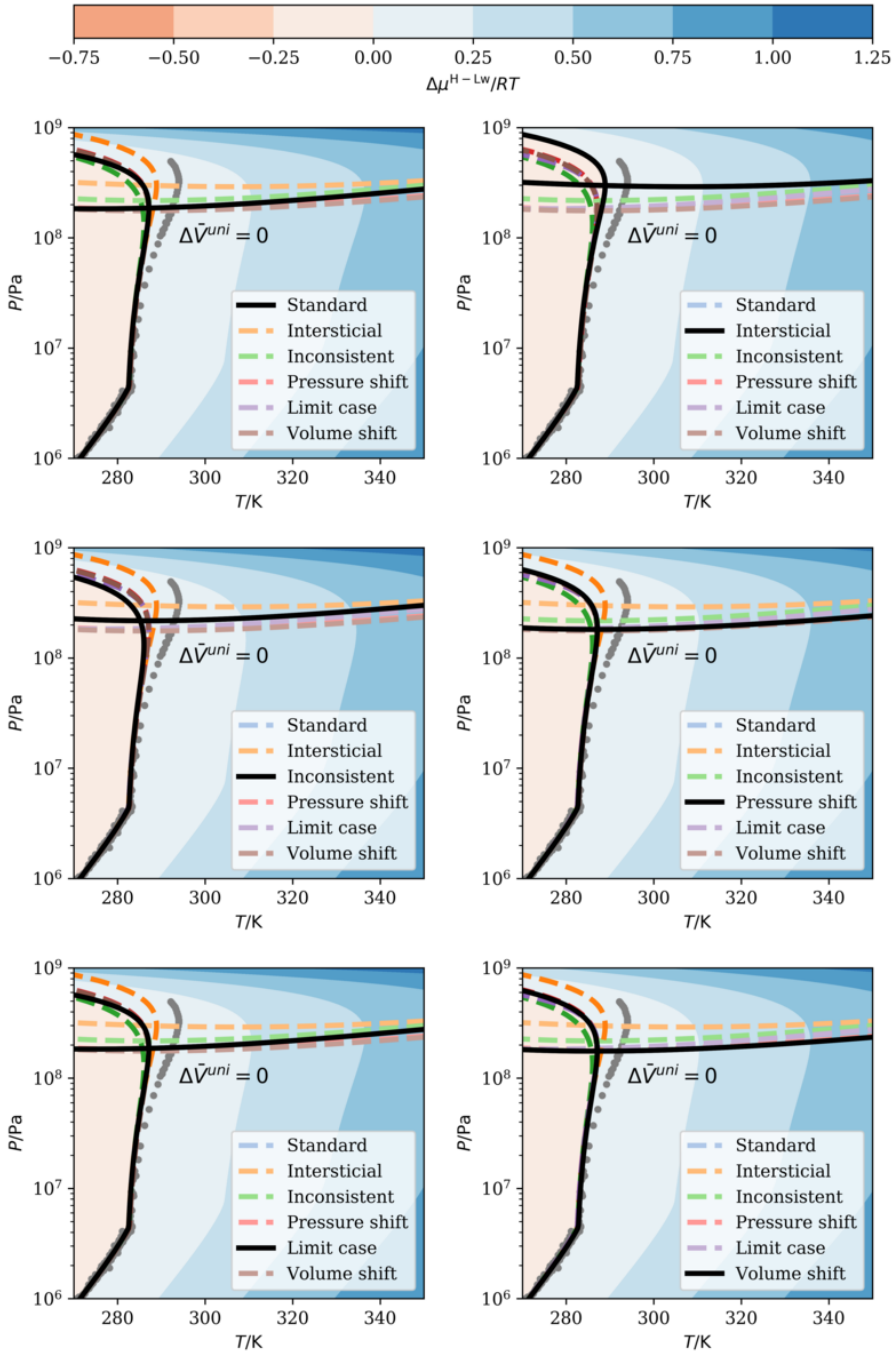

Figure 7.9: Phase equilibrium behavior of carbon dioxide hydrates for the 6 models under analysis. In each subfigure (a-f) the phase equilibrium curve and the curve of null dissociation volume difference for one of the models is stressed as a continuous black line, and the color scale changed to match the chemical potential difference between hydrate and liquid water for that model. While the curves for the other models are depicted as dashed and in different colors. The gray points are experimental data from NIST in (KROENLEIN *et al.*, 2015)

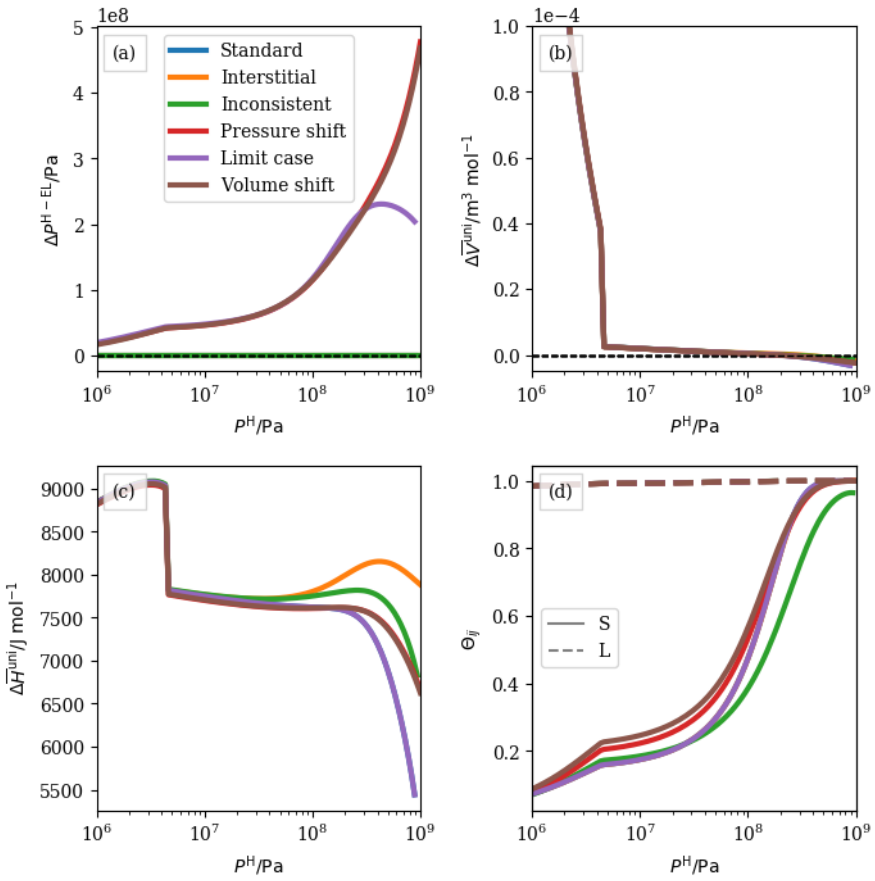

Figure 7.10: Thermodynamics properties of carbon dioxide hydrates for the 6 models under analysis. Pressure shift (a), dissociation volume change (b), occupancy (b) for the small cages (continous lines) and large cages (dashed lines) and dissociation enthalpy change (d).

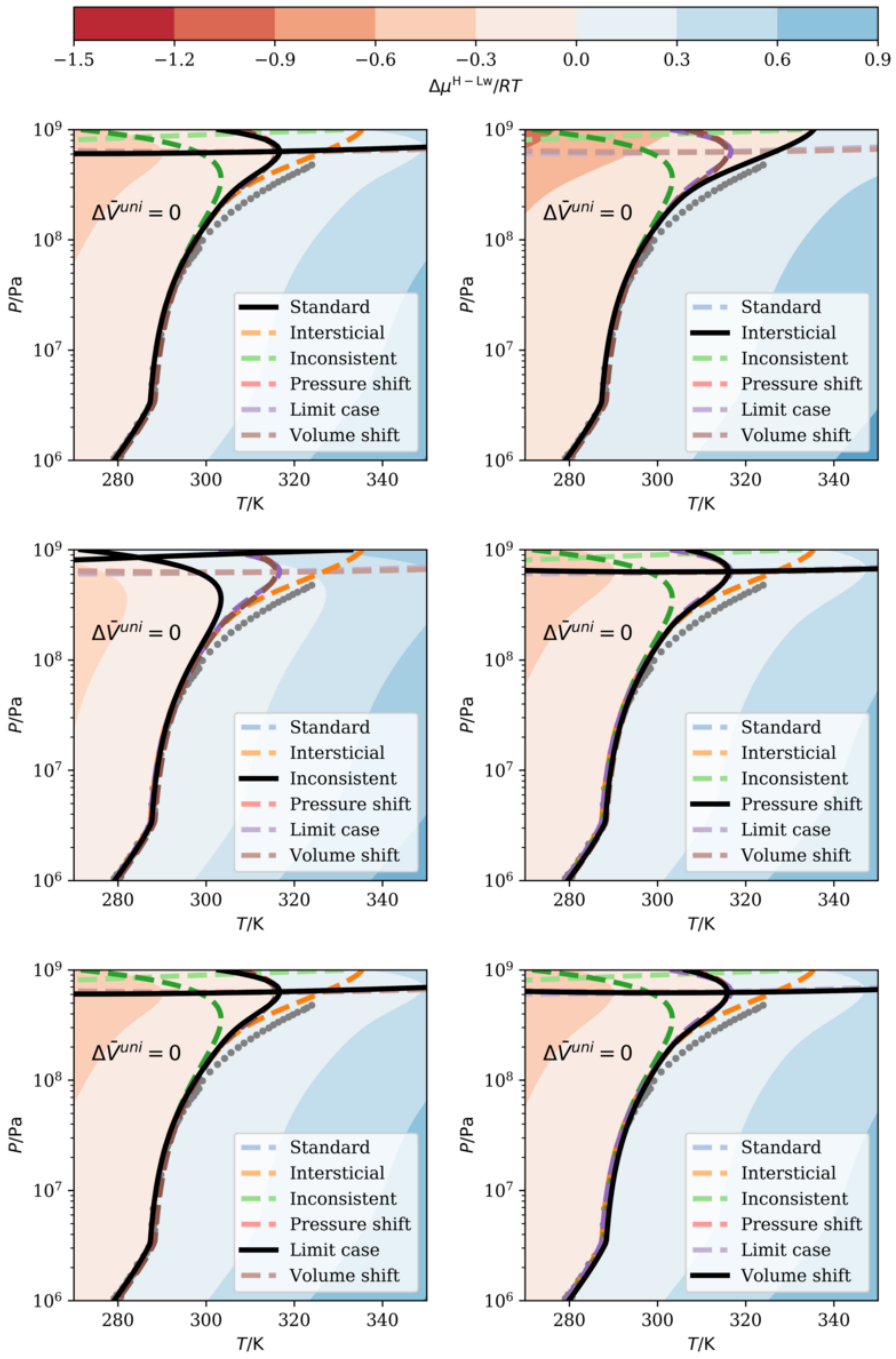

Figure 7.11: Phase equilibrium behavior of ethane hydrates for the 6 models under analysis. In each subfigure (a-f) the phase equilibrium curve and the curve of null dissociation volume difference for one of the models is stressed as a continuous black line, and the color scale changed to match the chemical potential difference between hydrate and liquid water for that model. While the curves for the other models are depicted as dashed and in different colors. The gray points are experimental data from NIST in (KROENLEIN *et al.*, 2015)

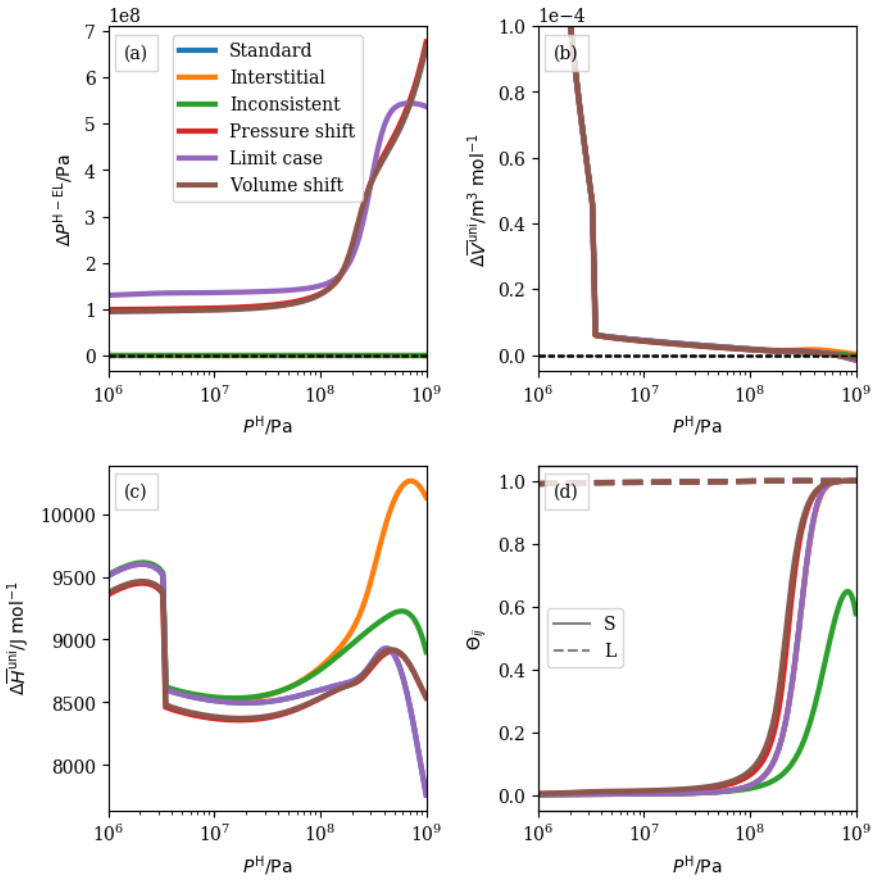

Figure 7.12: Thermodynamics properties of ethane hydrates for the 6 models under analysis. Pressure shift (a), dissociation volume change (b), occupancy (b) for the small cages (continous lines) and large cages (dashed lines) and dissociation enthalpy change (d).

Note that, for ethane (Figure 7.11 and 7.12), above 1×10^8 Pa, all models predict filling of the small cages, but the inconsistent model is the only one to predict these cages becoming empty at pressure condition between 1×10^8 Pa and 1×10^9 Pa due to cage compressibility. The pressure shift model predicts that the phase is compressed to a lower extent, because of the reciprocal influence of the guest towards the cage being taken into consideration trough the revised expressions. Additionally, the Clapeyron equation inconsistency is much clearer in this third case because calculated $\Delta P^{\mathrm{H-EL}}$ values for ethane are, in general, larger than for the other components.

Now, we examine the influence of the ambiguous values for σ_i discussed before in the phase equilibrium behavior along a range of temperature and pressure, considering the standard model and the pressure shift model, each with its own pair of ambiguous σ_i. As before, the following calculations neglect occupation of the small cage in order to provide insight into the potential for disam-

biguation of the model in systems with this characteristics (e. g. hidroquinone clathrates, which have only 1 type of cage).

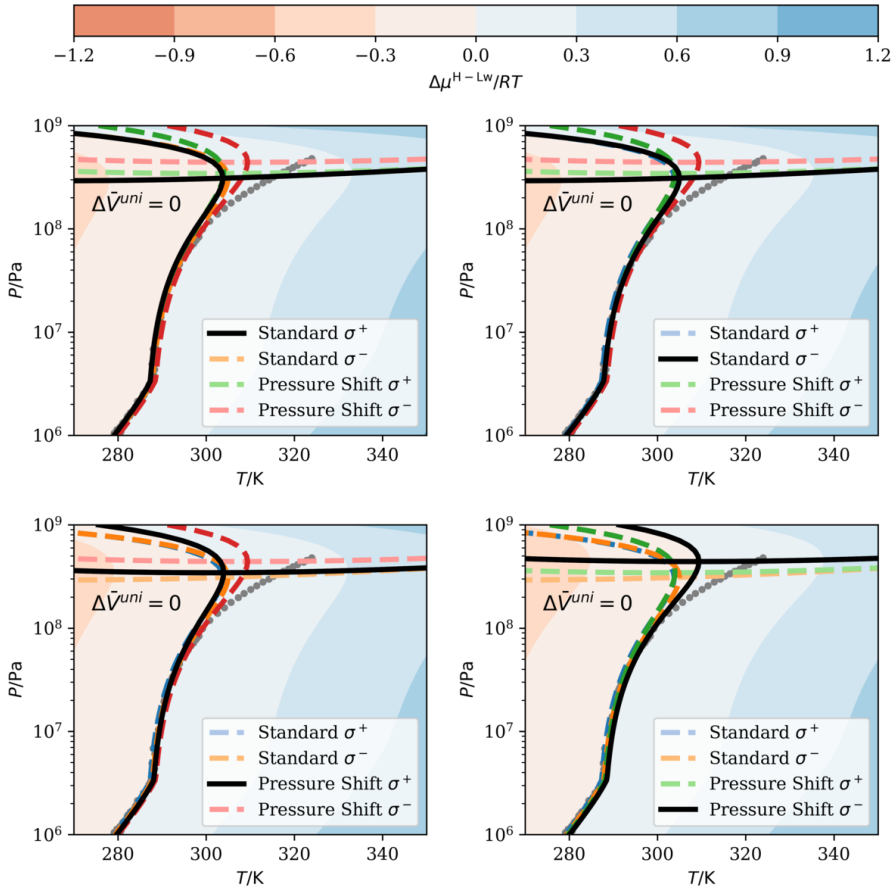

Figure 7.13: Phase equilibrium behavior of a hydrates with a single type of cage for the pressure shift and standard models and different values of σ_i that generate the same values for Langmuir coefficient at P_0.

In the standard model the results with either value of σ_i are almost indistinguishable because the Langmuir coefficients are equal for both parameter values at T_0 and, at higher temperature conditions in the range studied here, differ only slightly. On the other hand, in the pressure shift model, at higher temperature and pressure, the volume varies and, therefore, also the Langmuir coefficients. And this variation is different for either values of σ_i, consequently, the phase equilibrium curve is noticeably different for each σ_i value at higher temperature and pressure.

7.5 Swelling of the hydrate lattice

By means of performing calculations of pressure shift and molar volume of several single guest hydrates, we observed the swelling phenomena depicted in Figure 7.14. This phenomenon is characterized by an increase in the molar volume of the lattice $\overline{V}^{\mathrm{EL}}$, i. e., the ratio between extensive volume of the hydrate V^{H} and the number of molecules of water in that volume N_{w}, (Figure 7.14b) that happens when the bulk and hydrate pressure are increased and the fugacity of guests is also increased accordingly to an equation of state for the gas phase.

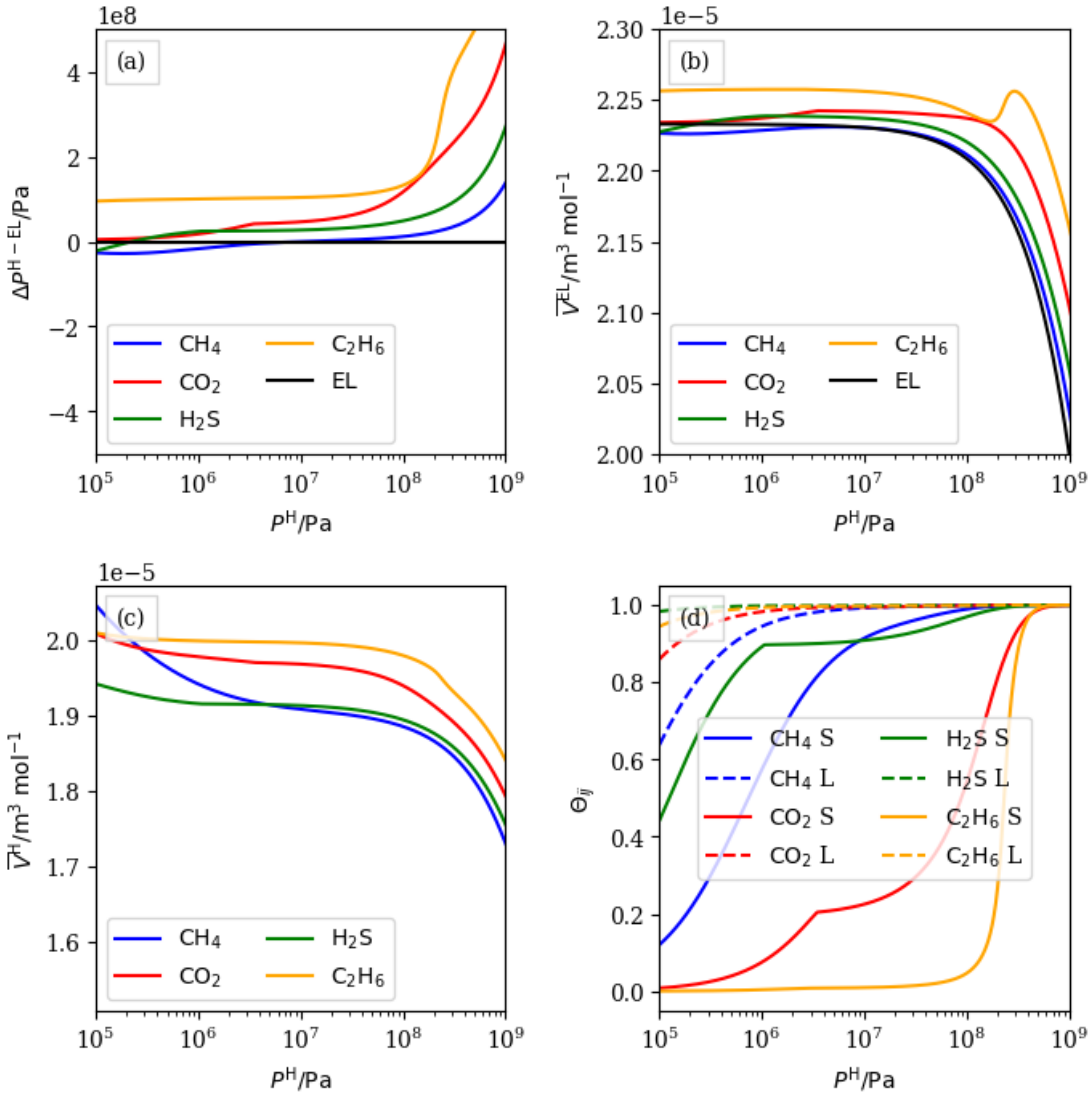

Figure 7.14: Swelling of hydrates at high pressure conditions using the proposed pressure shift model.

The swelling phenomenon was observed in the calculations for all of methane, ethane, carbon dioxide and hydrogen sulfide performed here. For

each case, the swelling occurs in a different range of pressure, depending on the relative size of the cages and guest molecules.

The reason for the swelling is that when the fugacity is increased, it favors the adsorption of more guest molecules on to the lattice, increasing the occupancy (7.14d) and depending on the relative size of the cages and guest molecules, this will either increase or reduce the pressure shift according to Equation (B.70).

We concluded that the swelling phenomenon occurs whenever the pressure shift, be it either positive or negative, increases steeply with an increase in the pressure of the system, causing the lattice pressure to decrease while the hydrate and bulk pressure increase and consequently causing the volume to increase, according to the following reasoning.

Mathematically, the swelling phenomenon occurs whenever

$$\left(\frac{\partial \bar{V}}{\partial P}\right)_T > 0 \tag{7.8}$$

where

$$P = P^{\mathrm{H}} = P^{\mathrm{EL}} + \Delta P^{\mathrm{H-EL}} \tag{7.9}$$

therefore

$$\left(\frac{\partial \bar{V}}{\partial P}\right)_T = \left(\frac{\partial \bar{V}}{\partial P^{\mathrm{EL}}}\right)_T \left(\frac{\partial P^{\mathrm{EL}}}{\partial P}\right)_T = \left(\frac{\partial \bar{V}}{\partial P^{\mathrm{EL}}}\right)_T \left(1 - \left(\frac{\partial \Delta P^{\mathrm{H-EL}}}{\partial P}\right)_T\right) > 0 \tag{7.10}$$

As $\left(\partial \overline{V}/\partial P^{\mathrm{EL}}\right)_T$ is necessarily negative for isotropic mechanically stable materials, in accordance with our correlation with constant positive compressibility, it follows that

$$\left(\frac{\partial \Delta P^{\mathrm{H-EL}}}{\partial P^{\mathrm{EL}}}\right)_T > 1 \tag{7.11}$$

That is, when the value of the slope of the pressure shift versus hydrate pressure (7.14a) is larger than 1, the swelling phenomenon occurs in the plot of $\overline{V}^{\mathrm{EL}}$ versus P^{H}.

In addition, we confirmed that there is no violation, regarding the actual

hydrate, of the positive volume compressibility thermodynamic principle assumed for the empty lattice, because the overall molar volume of the hydrate, as given by

$$V^{\mathrm{H}} / \left(N_{\mathrm{w}} + \sum_{i} (N_i) \right) \tag{7.12}$$

remains decreasing with increasing hydrate pressure (7.14c). The behavior captured by our model is equivalent to that observed experimentally for hidroquinone clathrate with up to triple cage occupation by hydrogen molecules (ROZSA and STROBEL, 2014).

7.6 Iso-structural phase equilibrium

More investigations on the model capabilities showed possible iso-structural phase equilibrium. The molar volume of the lattice versus hydrate pressure shows a region where, for a given pressure, one, three or five molar volume solutions exist. Figure 7.15 shows this behavior for hydrates with structure s^{I}, with a value for the lattice compressibility ten times larger than that used for the previous calculations, and fugacity of guest component given by the ideal gas equation of state.

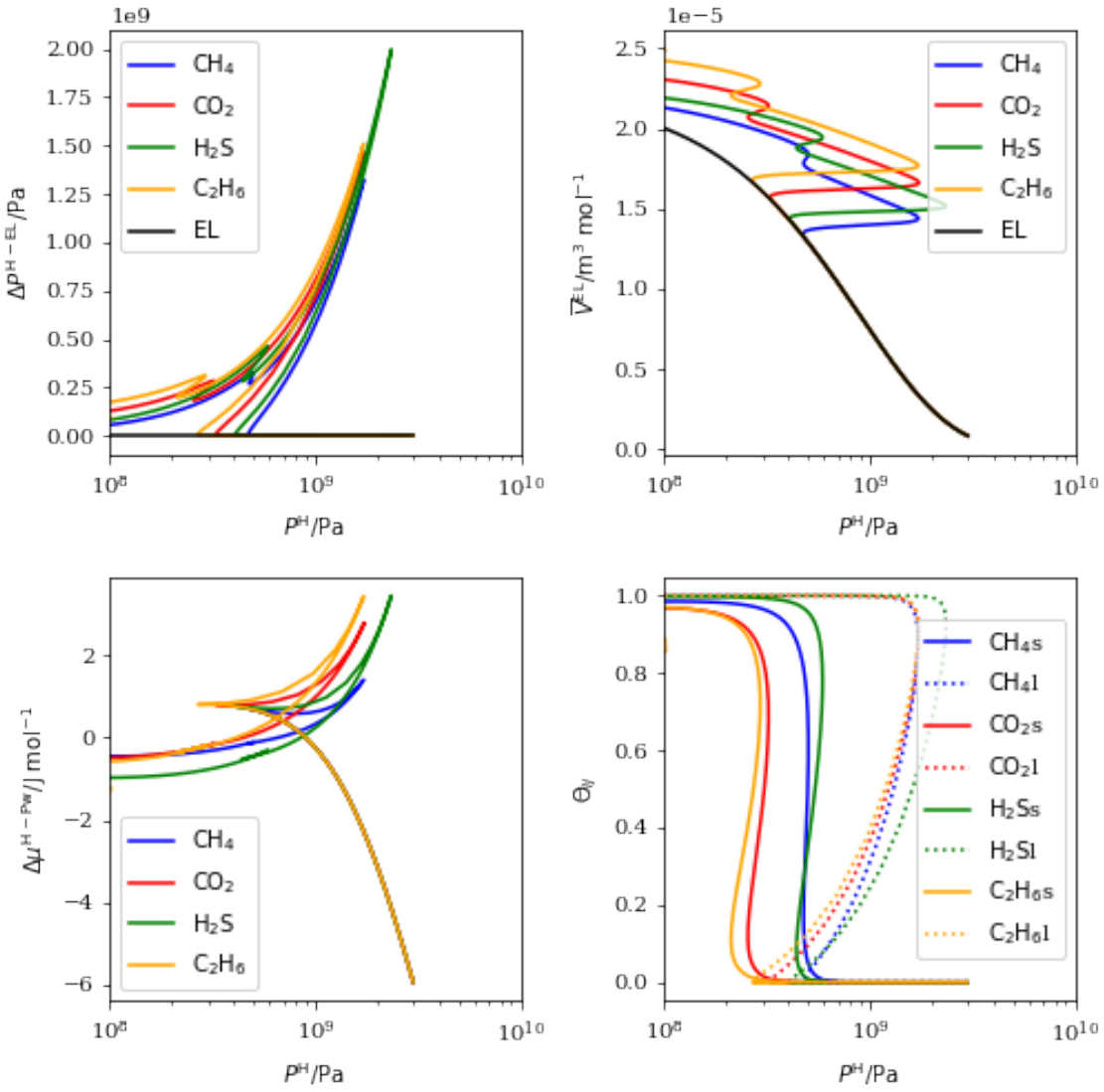

Figure 7.15: Prediction of iso-structural phase equilibria for hydrates. Calculations of pressure shift, lattice molar volume, chemical potential difference for water between hydrate and liquid states, occupancy of small and large cages, all calculated and plotted versus system pressure. Calculations for single guest hydrates of methane, carbon dioxide, hydrogen sulfide, ethane, and the reference empty lattice. Calculations show up to five roots for some properties at some ranges of given system pressure.

Figure 7.16 shows the region of metastable iso-structural phase equilibrium for carbon dioxide hydrates: Figure 7.16b shows there are three solutions for latttice volume for a value of hydrate pressure in a range. Figure 7.16c shows that for two of them the chemical potential of water is the same. The plot of chemical potential difference between hydrate and pure liquid water shows a swallowtail behavior similar to cubic equations of state: when following chemical potential as function of pressure for low and high solutions of molar volume, at constant temperature, there is one pressure where the chemical potential for

both conditions is the same, which characterizes a phase equilibrium. This phase equilibrium is at least metastable regarding these two hydrate phases, but not necessarily a stable equilibrium state regarding other possible phases. As shown in Figure 7.16d, this structural change is associated with a sudden change in the occupancy of the small cages (full red line), the vertical lines mark the pressure and pair of properties resulting in equal chemical potential. The molar volume after the transition is such that the small cages are too small to accommodate guest molecules. The dashed lines represent calculations of properties when occupancy of small cages is not allowed, it can be noted that after the transition the calculations for the pressure shift model match the calculations with restriction on the small cages.

Nevertheless, this result, qualitatively corroborates with results for methane hydrates from HIRAI *et al.* (2000b) in which the molar volume after the transition is such that the small cages are too small to accommodate the guest molecules and from LAFOND *et al.* (2015). Finally, as this depends on lattice and guest parameters, the phenomenon may be observed for clathrate of other structures, other lattice component and other single or mixed guest components at moderate pressures.

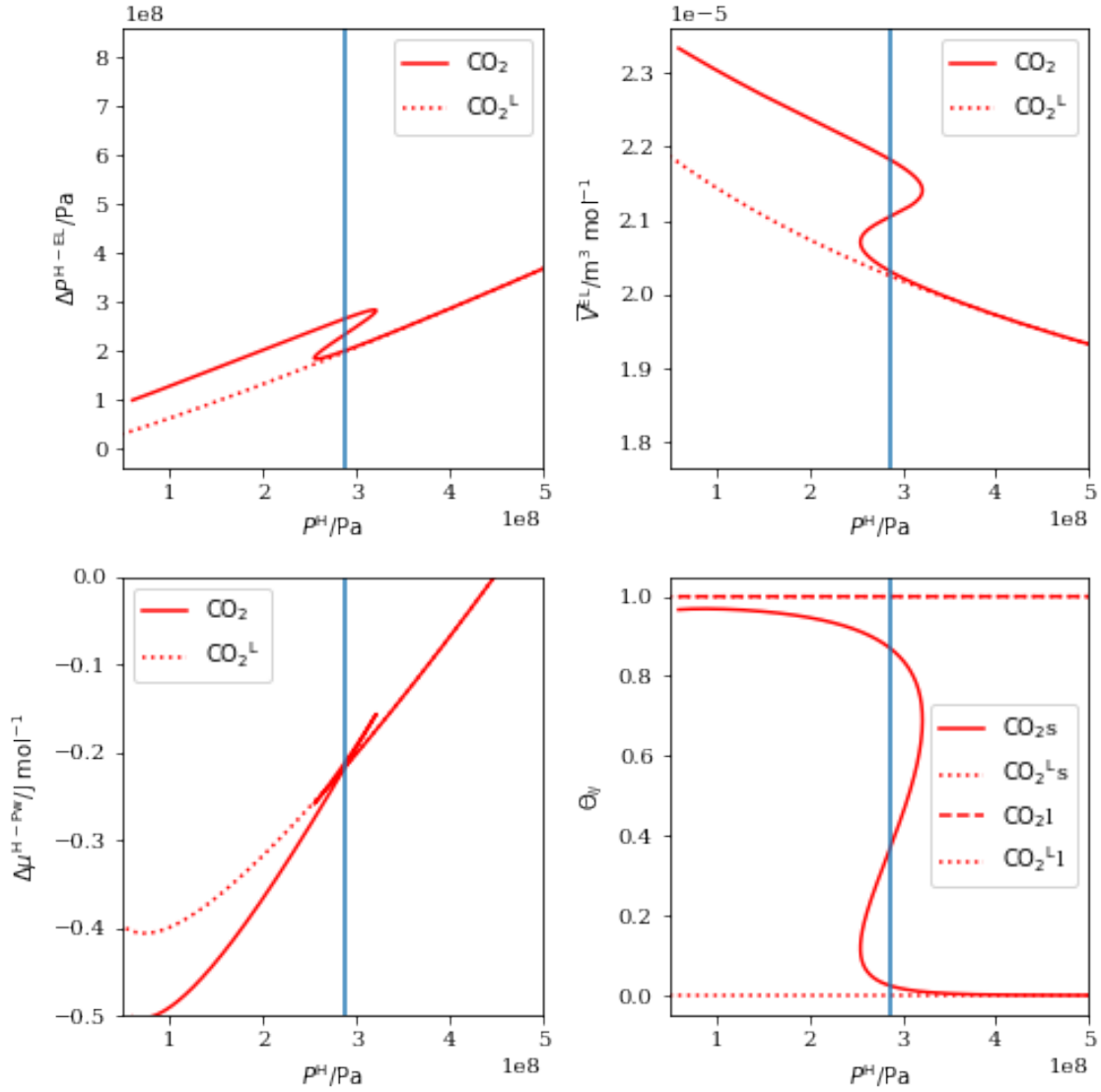

Figure 7.16: Detailing iso-structural phase equilibria for a Carbon dioxide hydrate. The blue vertical line connects states with the same chemical potential difference for water (c) at a given system pressure, with different lattice pressure (a) lattice molar volume (b) and cages occupancy (d).

Finally, this behavior of the model indicates that a critical temperature should exist for this iso-structural phase transition, as the lattice molar volume and occupancy of the two phases in equilibrium tend to the same values. This behavior is shown in Figure 7.17, the calculations are qualitative, for a hydrate of carbon dioxide with lattice compressibility of 100 times the experimental methane hydrate compressibility (Appendix C).

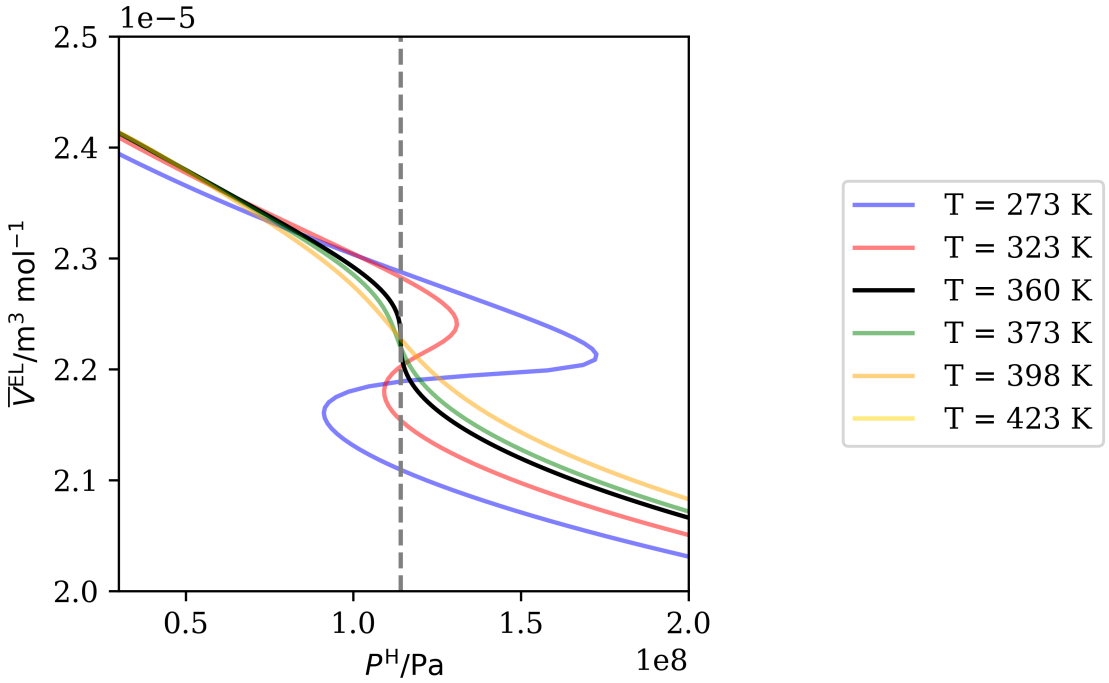

Figure 7.17: Critical behavior of the iso-structural phase equilibria. Lattice molar volume versus hydrate pressure calculated at various temperatures indicates the existence of a critical temperature for this iso-structural phase transition.

The critical behavior shown in 7.17 is analogous to the critical behavior of pure substances in liquid-vapor equilibrium as shown by cubic equations of state in the P versus $\overline{V}$ plane. In the classical fluid phase equilibria scenario, two pure fluid phases coexist along a univariant phase equilibria line of P versus T, up to a critical point where the molar volume of both phases tend to the same value, the critical volume. Analogously, in this scenario, three phases might coexist: a gas or non polar liquid phase poor in water, and two hydrate phases with a given structure and an different molar lattice volume and occupancy, assuming such temperature and pressure region that the hydrate phases are more stable, relative to a liquid water or ice phase. Then these three phases, in a two component mixture, might coexist along a univariant phase equilibria line of P versus T, up to a critical point where the lattice molar volume and occupancy of both hydrate phases tend to the same values. For temperature conditions higher than that, only one solution for lattice molar volume and occupoancy exist for a given structure, at given system pressure. Then, as pressure increases, the occupancy of the hydrate phase decreases smoothly, because the structure compressibility effect and consequent reduction of the Langmuir coefficients overcome the effect of increasing fugacity, that can be analyzed from the gas/non polar liquid phase.

Current calculations are of qualitative nature, they indicate that simulations

for different parameter sets should help investigate which systems (host/guest) might present a critical transition in a range of temperature and pressure that could be observed experimentally.

7.7 Final remarks

In conclusion, our model is capable of solving a thermodynamic inconsistency observed in phase equilibrium calculations and tested using a multicomponent and multiphase Clapeyron equation. The model was capable of predicting different hydrate volume depending on the guest components involved at a same pressure. The model was also capable of predicting both the phenomena of swelling of the lattice and of iso-structural phase equilibrium with sudden change in composition and molar volume. We stress that our model extension does not use any extra parameter other than those of the standard clathrate modeling framework.

Chapter 8

Conclusions

This work studied the thermodynamics of hydrates with two emphasis, first the rigorous modeling based on the original van der Waals and Platteeuw model, where we have proposed an extension for compressible clathrates, and second, the development of a phase equilibria algorithm with special design for hydrate systems.

Regarding the thermodynamic model, our extension of the van der Waals and Platteuw model consists in obtaining derived properties thermodynamically consistent with density dependent cage radii. Our model extension accomplishes four achievements. First, it fixes a common inconsistency in the state of the art in modeling compressible clathrates, which is made evident by a analysis of phase equilibrium calculation with the Clapeyron equation. Second, it naturally shows different volume for clathrates of different guests for the same structure at the same temperature and pressure. Third, we have observed the swelling phenomena, where the lattice molar volume increases when the system pressure increases and adsorption of guest components is favored. And fourth, we have observed a iso-structural equilibrium, so far in a meta-stable region, for methane hydrate with sudden variation on volume and on the occupation of the small cages. We stress that our model extension does not use any extra parameter other than those of the standard clathrate modeling framework.

Perspectives for the research on the modeling of compressible clathrates include:

- Further investigate the swelling phenomena, determination of systems where it is more likely to occur and measure.
- Further investigate the isostructural equilibrium phenomena, calculations

of isostructural equilibrium in stable condition, determination of systems where it is more likely to occur and measure.

- Performing calculations for mixed hydrate systems to investigate the phase equilibrium behavior.
- Performing parameter regression for the whole set of parameters of the clathrate modeling framework with a variety of data and discuss the capability of the model of reducing parameter correlation, and the performance of the pressure shift modification on mixtures and high pressure regions.

Regarding the multiphase flash algorithm study, the proposed flash algorithm allows the generation of complex behavior phase diagrams, including single and mixed hydrates retrograde dissociation, hydrate structures coexistence, invariant points, thermodynamic inhibitor induced freezing point depression, low water content gas sublimation line. The proposed improvements in the algorithm contributes to both algorithm speed and robustness: The proposed Newton-Raphson loop works on an equation system with less than half the size of the originally used equation system. The residue equations whose solution by numerical methods originally showed problems are now solved analytically. Management in appearance/disappearance of phases based on the Gibbs phase rule prevents occurrence of singular equation system for phase amounts calculations. Multi reference K-values allow the handling of phases which exclude certain components. The special approach proposed to hydrate phase fugacities updating in the successive substitution method provided a generalization of the algorithm, allowing the generation of shadow phase solution for the hydrate phases, consistent with the theory in which the algorithm is relied, when calculations outside formation region are performed, and allowing the use of hydrates as reference phases.

Perspectives for the research on phase equilibrium algorithms for hydrate systems include

- Extension of the algorithm framework for isochoric (TVN) and isoenthalpic (HVN) specifications, for direct application in processes or experiments involving rigid vessels and hindered heat transfer.
- Extension of the algorithm to reactive systems, in special for aqueous phases that contain weak acids and bases that may be present in the non-polar fluid phase in molecular form, and salt mixtures from which many crystal combinations may form.

Bibliography

AVLONITIS, D., 2005, "An investigation of gas hydrates formation energetics", *AIChE journal*, v. 51, n. 4, pp. 1258–1273.

BALLARD, A. L., 2004, *A Non-Ideal Hydrate Solid Solution Model For A Multi-Phase Equilibria Program*. Ph.D. Thesis, Colorado School of Mines.

BALLARD, A. L., SLOAN JR., E. D., 2004, "The next generation of hydrate prediction", *Fluid Phase Equilibria*, v. 218, n. 1 (apr), pp. 15–31.

BALLARD, A. L., SLOAN JR., E. D., 2002, "The next generation of hydrate prediction: I. Hydrate standard states and incorporation of spectroscopy", *Fluid Phase Equilibria*, v. 194-197 (mar), pp. 371–383.

BARBOSA, G. D., TRAVALLONI, L., CASTIER, M., et al., 2016, "Extending an equation of state to confined fluids with basis on molecular simulations", *Chemical Engineering Science*, v. 153, pp. 212–220.

BELOSLUDOV, V. R., INERBAEV, T. M., SUBBOTIN, O. S., et al., 2002, "Thermal expansion and lattice distortion of clathrate hydrates of cubic structures I and II", *Journal of Supramolecular Chemistry*, v. 2, n. 4-5, pp. 453–458.

BELOSLUDOV, V., LAVRENTIEV, M. Y., DYADIN, Y. A., 1991, "Theory of clathrates", *Journal of inclusion phenomena and molecular recognition in chemistry*, v. 10, n. 4, pp. 399–422.

BISHNOI, P. R., GUPTA, A. K., ENGLEZOS, P., et al., 1989, "Multiphase equilibrium flash calculations for systems containing gas hydrates", *Fluid Phase Equilibria*, v. 53, pp. 97–104.

GUPTA, A. K., RAJ BISHNOI, P., KALOGERAKIS, N., 1991, "A method for the simultaneous phase equilibria and stability calculations for multiphase reacting and non-reacting systems", *Fluid Phase Equilibria*, v. 63, n. 1-2 (jan), pp. 65–89. ISSN: 03783812.

HANDA, Y. P., TSE, J. S., 1986, "Thermodynamic properties of empty lattices of structure I and structure II clathrate hydrates", *The Journal of Physical Chemistry*, v. 90, n. 22 (oct), pp. 5917–5921.

HILBERT, R., TÖDHEIDE, K., FRANCK, E., 1981, "PVT Data for Water in the Ranges 20 to 600° C and 100 to 4000 bar", *Berichte der Bunsengesellschaft für physikalische Chemie*, v. 85, n. 9, pp. 636–643.

HIRAI, H., HASEGAWA, M., YAGI, T., et al., 2000a, "Methane hydrate, amoeba or a sponge made of water molecules", *Chemical Physics Letters*, v. 325, n. 5-6 (aug), pp. 490–498.

HIRAI, H., KONDO, T., HASEGAWA, M., et al., 2000b, "Methane Hydrate Behavior under High Pressure", *The Journal of Physical Chemistry B*, v. 104, n. 7 (feb), pp. 1429–1433.

HOLDER, G., ZETTS, S., PRADHAN, N., 1988, "Phase behavior in systems containing clathrate hydrates: a review", *Reviews in chemical engineering*, v. 5, n. 1-4, pp. 1–70.

HSIEH, M.-K., TING, W.-Y., CHEN, Y.-P., et al., 2012, "Explicit pressure dependence of the Langmuir adsorption constant in the van der Waals–Platteeuw model for the equilibrium conditions of clathrate hydrates", *Fluid Phase Equilibria*, v. 325, pp. 80–89.

HUNTER, J. D., 2007, "Matplotlib: A 2D graphics environment", *Computing In Science & Engineering*, v. 9, n. 3, pp. 90–95.

HWANG, M.-J., HOLDER, G. D., ZELE, S. R., 1993, "Lattice distortion by guest molecules in gas-hydrates", *Fluid Phase Equilibria*, v. 83, pp. 437–444.

IKEDA, T., MAE, S., YAMAMURO, O., et al., 2000, "Distortion of host lattice in clathrate hydrate as a function of guest molecule and temperature", *The Journal of Physical Chemistry A*, v. 104, n. 46, pp. 10623–10630.

INERBAEV, T. M., BELOSLUDOV, V. R., BELOSLUDOV, R. V., et al., 2006, "Dynamics and equation of state of hydrogen clathrate hydrate as a function of cage occupation", *Computational Materials Science*, v. 36, n. 1-2, pp. 229–233.

JÄGER, A., VINŠ, V., SPAN, R., et al., 2016, "Model for gas hydrates applied to CCS systems part III. Results and implementation in TREND 2.0", *Fluid Phase Equilibria*, v. 429, pp. 55–66.

JOHN, V., PAPADOPOULOS, K., HOLDER, G., 1985, "A generalized model for predicting equilibrium conditions for gas hydrates", *AIChE Journal*, v. 31, n. 2, pp. 252–259.

JONES, E., OLIPHANT, T., PETERSON, P., et al., 2001. "SciPy: Open source scientific tools for Python". Availablet: <http://www.scipy.org/>. [Online; accessed 2018].

KLAPPROTH, A., GORESHNIK, E., STAYKOVA, D., et al., 2003, "Structural studies of gas hydrates", *Canadian journal of physics*, v. 81, n. 1-2, pp. 503–518.

KLAUDA, J. B., SANDLER, S. I., 2000, "A fugacity model for gas hydrate phase equilibria", *Industrial & engineering chemistry research*, v. 39, n. 9, pp. 3377–3386.

KROENLEIN, K., MUZNY, DIKY, C., , K. A., et al., 2015. "Clathrate Hydrate Physical Property Database". Availablet: <http://gashydrates.nist.gov/HydrateViewer/>.

LAFOND, P. G., GRIM, R. G., SUM, A. K., 2015, "Clathrate hydrate equilibrium modeling: Do self-consistent cell models provide unique equilibrium solutions?" *Canadian Journal of Chemistry*, v. 93, n. 8 (aug), pp. 826–830.

LEE, S.-Y., HOLDER, G. D., 2002, "Model for gas hydrate equilibria using a variable reference chemical potential: Part 1", *AIChE Journal*, v. 48, n. 1, pp. 161–167.

LENNARD-JONES, J. E., DEVONSHIRE, A., 1937, "Critical phenomena in gases-I", *Proc. R. Soc. Lond. A*, v. 163, n. 912, pp. 53–70.

Lide, D. R. (Ed.), 2005, *CRC handbook of chemistry and physics: a ready-reference book of chemical and physical data*. 86. ed ed. Boca Raton, CRC Press. ISBN: 978-0-8493-0486-6. OCLC: 179976746.

MCKOY, V., SINANOĞLU, O., 1963, "Theory of dissociation pressures of some gas hydrates", *The journal of chemical physics*, v. 38, n. 12, pp. 2946–2956.

MEDEIROS, F. D. A., SEGTOVICH, I. S. V., BARRETO JR., A. G., et al., 2018, "Heat of dissociation from Statistical Thermodynamics: Using calorimetric data to estimate gas hydrate parameters", *The Journal of Chemical Thermodynamics*, v. 117, pp. 164–179.

MICHELSEN, M. L., 1982, "The isothermal flash problem. Part I. Stability", *Fluid phase equilibria*, v. 9, n. 1, pp. 1–19.

MOOIJER – VAN DEN HEUVEL, M. M., 2004, *Phase Behaviour and Structural Aspects of Ternary Clathrate Hydrate Systems The Role of Additives*. Ph.D. Thesis, TU Delft.

NG, H.-J., ROBINSON, D. B., 1980, "A Method for Predicting the Equilibrium Gas Phase Water Content in Gas-Hydrate Equilibrium", *Industrial & Engineering Chemistry Fundamentals*, v. 19, n. 1 (feb), pp. 33–36.

NG, H.-J., ROBINSON, D. B., 1977, "The prediction of hydrate formation in condensed systems", *AIChE Journal*, v. 23, n. 4 (jul), pp. 477–482.

O'CONNELL, J. P., HAILE, J. M., 2005, *Thermodynamics: fundamentals for applications*. Cambridge University Press.

OLIPHANT, T. E., 2006, *A guide to NumPy*, v. 1. Trelgol Publishing USA.

PARRISH, W. R., PRAUSNITZ, J. M., 1972, "Dissociation Pressures of Gas Hydrates Formed by Gas Mixtures", *Industrial & Engineering Chemistry Process Design and Development*, v. 11, n. 1 (jan), pp. 26–35.

PÉREZ, F., GRANGER, B. E., 2007, "IPython: a System for Interactive Scientific Computing", *Computing in Science and Engineering*, v. 9, n. 3 (may), pp. 21–29. ISSN: 1521-9615.

PRATT, R. M., BALLARD, A. L., SLOAN JR, E., 2001, "Beware of singularities when calculating clathrate hydrate cell potentials!" *AIChE journal*, v. 47, n. 8, pp. 1897–1898.

RACHFORD JR., H. H., RICE, J. D., 1952, "Procedure for use of electronic digital computers in calculating flash vaporization hydrocarbon equilibrium", *Journal of Petroleum Technology*, v. 4, n. 10, pp. 19–3.

REID, R. C., PRAUSNITZ, J. M., POLING, B. E., 1987, *The properties of gases and liquids*. McGraw Hill Book Co., New York, NY.

ROZSA, V. F., STROBEL, T. A., 2014, "Triple Guest Occupancy and Negative Compressibility in Hydrogen-Loaded β-Hydroquinone Clathrate", *The Journal of Physical Chemistry Letters*, v. 5, n. 11, pp. 1880–1884. PMID: 26273868.

SEGTOVICH, I. S. V., MEDEIROS, F. DE A., , et al., 2018, "A natural pressure shift in extending the van der Waals and Platteeuw model to compressible clathrates". In: *XI Iberoamerican conference on phase equilibria and fluid properties for process design*, October.

SEGTOVICH, I. S. V., BARRETO JR., A. G., TAVARES, F. W., 2016a, "Simultaneous multiphase flash and stability analysis calculations including hydrates", *Fluid Phase Equilibria*, v. 413 (apr), pp. 196–208.

SEGTOVICH, I. S. V., BARRETO JR., A. G., TAVARES, F. W., 2016b, "Phase diagrams for hydrates beyond incipient condition — Complex behavior in methane/propane and carbon dioxide/iso-butane hydrates", *Fluid Phase Equilibria*, v. 426 (oct), pp. 75–82.

SHPAKOV, V., TSE, J., TULK, C., et al., 1998, "Elastic moduli calculation and instability in structure I methane clathrate hydrate", *Chemical Physics Letters*, v. 282, n. 2, pp. 107–114.

SLOAN JR, E. D., KOH, C., 2007, *Clathrate hydrates of natural gases*. CRC press.

SLOAN JR., E. D., KHOURY, F. M., KOBAYASHI, R., 1976, "Water Content of Methane Gas in Equilibrium with Hydrates", *Industrial & Engineering Chemistry Fundamentals*, v. 15, n. 4 (nov), pp. 318–323.

TESTER, J. W., MODELL, M., 1997a, *Thermodynamics and Its Applications, 3rd*. Prentice Hall, Inc., New Jersey, USA.

TESTER, J. W., MODELL, M., 1997b, *Thermodynamics and its applications*. Prentice-Hall international series in the physical and chemical engineering sciences. 3rd ed ed. Upper Saddle River, N.J, Prentice Hall PTR. ISBN: 978-0-13-915356-3.

TSE, J., 1987, "Thermal expansion of the clathrate hydrates of ethylene oxide and tetrahydrofuran", *Le Journal de Physique Colloques*, v. 48, n. C1, pp. C1–543.

VAN DER WAALS, J. H., PLATTEEUW, J. C., 1959, "Clathrate solutions", *Advances in chemical physics*, pp. 1–57.

WARRIER, P., KHAN, M. N., SRIVASTAVA, V., et al., 2016, "Overview: Nucleation of clathrate hydrates", *The Journal of Chemical Physics*, v. 145, n. 21, pp. 211705.

WILCOX, W. I., CARSON, D., KATZ, D., 1941, "Natural gas hydrates", *Industrial & Engineering Chemistry*, v. 33, n. 5, pp. 662–665.

ZELE, S., LEE, S.-Y., HOLDER, G., 1999, "A theory of lattice distortion in gas hydrates", *The Journal of Physical Chemistry B*, v. 103, n. 46, pp. 10250–10257.

ZHOU, M., WANG, K., MEN, Z., et al., 2014, "Pressure-induced isostructural phase transition of a metal–organic framework Co2(4, 4′-bpy)3(NO3)4·xH2O", *CrystEngComm*, v. 16, n. 20, pp. 4084–4087.

Appendix A

Derivation of the equations used in the multiphase flash algorithm

This appendix presents detailed derivation of the equations used in the algorithm. These are: multiphase Rachford-Rice equations, equations for updating the composition, equations for updating the hydrate guests fugacity, and equations for calculating the stability variables. We propose the use of multi-reference in the derivation of these equations. The first three groups, when applied to assumed present phases, K-values are the basis of our equilibrium calculations, while the fourth group, together with the second and third groups applied to not present phases are the basis of our stability analysis.

A.1 Gibbs energy minimization

The value of the composition and relative amount of each phase in the state of equilibrium at specified temperature T, pressure P, and total amount of each component N_i^c, corresponds to the global minimum in Gibbs energy, for a number n_c of components and of n_f phases.

Assuming each phase in internal equilibrium, their individual thermodynamic properties, as volume and chemical potential of each component, can be calculated from these phases given value of composition. The independent variables for the optimization problem, in the multiphase scope, are the amount $n_{i,j}$ of each component in each phase but in a reference phase (REF), of which, component amounts $n_{i,REF}$ depends on the other phases component amounts according to mass balance relations (Eq. A.1).

Let c enumerate all components from 1 to n_c, let f enumerate all phases from 1 to n_f, and let $f_{\neq REF}$ enumerate all phases in f, excluding the reference phase REF.

$$n_{i,REF} = N_i^c - \sum_{j \text{ in } f_{\neq REF}} \left(n_{i,j}\right) \quad \texttt{for } i \texttt{ in } c \tag{A.1}$$

Total Gibbs energy can be expressed with respect to the independent variables, after explicitation of chemical potential of each component in the reference phase and substitution of the amount of each component in the reference phase with the mass balance relations (Eq. A.1):

$$G = \sum_{i \text{ in } c} \left(N_i^c \mu_{i,REF}\right) + \sum_{i \text{ in } c} \left(\sum_{j \text{ in } f_{\neq REF}} \left(n_{i,j} \left(\mu_{i,j} - \mu_{i,REF}\right)\right) \right) \tag{A.2}$$

In which $n_{i,j}$ are the total amount, in moles, and $\mu_{i,j}$ are the chemical potential of index i component in index j phase, and N_i^c are the total amounts of index i component in the system, which is a constant in flash calculations.

All remaining relevant dependent variables for mass balance in the multiphase scope are defined in the following equations (Eq. A.3 to A.9):

Total amount of components N_j^f in index phase are defined by:

$$N_j^f = \sum_{i \text{ in } c} \left(n_{i,j}\right) \tag{A.3}$$

Mole fraction $x_{i,j}$ of index i component in index j phase are defined by:

$$x_{i,j} = \frac{n_{i,j}}{N_j^f} \tag{A.4}$$

Hence restricted to:

$$\sum_{i \text{ in } c} \left(x_{i,j}\right) = 1 \quad \texttt{for } j \texttt{ in } f \tag{A.5}$$

Total amount of components N^S in the system is defined by:

$$N^S = \sum_{i \text{ in } c} \left(N_i^c\right) \tag{A.6}$$

Relative amount β_j of index j phase in the system is defined, for non-null N^{S}, by:

$$\beta_j = \frac{N_j^{\mathrm{f}}}{N^{\mathrm{S}}} \tag{A.7}$$

Therefore can be rewritten as

$$\beta_j = \sum_{i \text{ in } c} \left(\frac{n_{i,j}}{N^{\mathrm{S}}} \right) \tag{A.8}$$

Hence restricted to

$$\sum_{j \text{ in } f} (\beta_j) = 1 \tag{A.9}$$

Overall molar fraction z_i of index i component is defined by:

$$z_i = \frac{N_i^{\mathrm{c}}}{N^{\mathrm{S}}} \tag{A.10}$$

The minimization problem is physically restricted to non-negative relative amounts of phases (β_j).

$$\beta_j = \sum_{i \text{ in } c} \left(\frac{n_{i,j}}{N^{\mathrm{S}}} \right) \geq 0 \text{ for } j \text{ in } f_{\neq REF} \tag{A.11}$$

This inequality restriction can be converted to an equation restriction in the independent variables, using the method of slack variables (ς), as follows:

$$\varsigma_j^2 - \sum_{i \text{ in } c} \left(\frac{n_{i,j}}{N^{\mathrm{S}}} \right) = 0 \text{ for } j \text{ in } f_{\neq REF} \tag{A.12}$$

And then, the restricted minimization problem is converted in a unrestricted minimization problem using Lagrange method. By doing so, it becomes possible to identify the minimum in Gibbs energy, if it is located in the boundary of the domain of the independent variables established by the restriction, as stationary points of the Lagrangian objective function Λ^{G}.

$$\Lambda^{\mathrm{G}} = G + \sum_{j \text{ in } f_{\neq REF}} \left(\lambda_j \left(\varsigma_j^2 - \sum_{i \text{ in } c} \left(\frac{n_{i,j}}{N^{\mathrm{S}}} \right) \right) \right) \tag{A.13}$$

In which λ_j are the Lagrange multiplier. Also, the reference phase is, by definition, present at equilibrium, so the restriction need not be applied for that phase as well.

A.2 Stationary point calculation

The resolution of the minimization problem is pursued using the first order optimization criteria, i.e. that the partial derivative of the objective function (Λ^{G}) with respect to each independent variable in $[\varsigma, \lambda, n]$ is zero, which leads to a stationary point.

First, equating to zero the partial derivatives of Λ^{G} with respect to each Lagrangian multiplier λ_j restates the equality restriction previously imposed:

$$\left(\frac{\partial \Lambda^{\mathrm{G}}}{\partial \lambda_j}\right)_{\varsigma, n, \lambda_{\neq j}} = \varsigma_j^2 - \sum_{i \text{ in } c} \left(\frac{n_{i,j}}{N^{\mathrm{S}}}\right) = 0 \text{ for } j \text{ in } f_{\neq REF} \tag{A.14}$$

$$\varsigma_j = \sqrt{\beta_j} \text{ for } j \text{ in } f_{\neq REF} \tag{A.15}$$

Second, equating to zero the partial derivatives of Λ^{G} with respect to each slack variable ς_j yields a set of nonlinear residue equations that will be recalled later.

$$\left(\frac{\partial \Lambda^{\mathrm{G}}}{\partial \varsigma_j}\right)_{\varsigma_{\neq j}, n, \lambda} = 2\varsigma_j \lambda_j = 0 \text{ for } j \text{ in } f_{\neq REF} \tag{A.16}$$

$$\varsigma_j \lambda_j = 0 \text{ for } j \text{ in } f_{\neq REF} \tag{A.17}$$

Third, equating to zero the partial derivatives of Λ^{G} with respect to component amounts $n_{i,j}$ yields the definition of the so called stability variable θ_j:

$$\left(\frac{\partial \Lambda^{\mathrm{G}}}{\partial n_{i,j}}\right)_{\varsigma, n_{\neq i,j}, \lambda} = \left(\frac{\partial G}{\partial n_{i,j}}\right)_{n_{\neq i,j}} - \frac{\lambda_j}{N^{\mathrm{S}}} = 0 \tag{A.18}$$

for i in c, for j in $f_{\neq REF}$

$$\left(\frac{\partial G}{\partial n_{i,j}}\right)_{n_{\neq i,j}} = \frac{\lambda_j}{N^S} \tag{A.19}$$
$\texttt{for } i \texttt{ in } c, \quad \texttt{for } j \texttt{ in } f_{\neq REF}$

Expansion of the left hand term in Eq. (A.18), based on Eq. (A.2), and requiring application of product rule as the amount of an index i component in an index j phase will affect every index k component in the phase.

$$\left(\frac{\partial G}{\partial n_{i,j}}\right)_{n_{\neq i,j}} = \left(\mu_{i,j} - \mu_{i,REF}\right) + \sum_{k \text{ in } c} \left(n_{k,j} \left(\frac{\partial \mu_{k,j}}{\partial n_{i,j}}\right)_{T,P,n_{\neq i,j}} \right) \tag{A.20}$$
$\texttt{for } i \texttt{ in } c, \quad \texttt{for } j \texttt{ in } f_{\neq REF}$

Ultimately, the second term in the right hand side of this equation is zero, according to Gibbs-Duhem relation. So, at last, Equation (A.18) yields:

$$\left(\mu_{i,j} - \mu_{i,REF}\right) = \frac{\lambda_j}{N^S} \tag{A.21}$$
$\texttt{for } i \texttt{ in } c, \quad \texttt{for } j \texttt{ in } f_{\neq REF}$

From this result, the stability variable, θ_j, is defined:

$$\theta_j = \frac{\lambda_j}{N^S RT} \quad \texttt{for } j \texttt{ in } f_{\neq REF} \tag{A.22}$$

And consequently:

$$\theta_j = \frac{\left(\mu_{i,j} - \mu_{i,REF}\right)}{RT} \quad \texttt{for } j \texttt{ in } f_{\neq REF} \tag{A.23}$$

It should be noted that this variable corresponds to a dimensionless stationary point tangent plane distance (TPD^{SP}).

Invoking the definition of fugacity ratios from chemical potential differences, the stability variable can also be expressed as:

$$\theta_j = \ln\left(\frac{\hat{f}_{i,j}}{\hat{f}_{i,REF}}\right) \quad \texttt{for } i \texttt{ in } c, \quad \texttt{for } j \texttt{ in } f_{\neq REF} \tag{A.24}$$

Equation (A.16) may, finally, be expressed, for non-negative β_j, as:

$$Res_j^S = \beta_j \theta_j = 0 \texttt{ for } j \texttt{ in } f_{\neq REF} \tag{A.25}$$

Eq. (A.26) constitutes a set of non-linear residue equations that will be used directly in the development of the algorithm. Some aspects regarding this set of equations should be stressed: In case θ_j is equal to zero, equality of chemical potential applies, index j is in equilibrium with the remaining phases in the system, and β_j may be positive, corresponding to a present at equilibrium phase, or also equal to zero, corresponding to an incipient condition phase.

In case an index j phase is not present at equilibrium, the corresponding stability variable θ_j will be greater than zero and the composition of this phase will correspond to a shadow phase.

A.3 Generalized RachfordRice equation

In this section, a set of equation similar to those from Rachford and Rice method, however, generalized to include both present at equilibrium and shadow phases. It may be worthy to remember that the equations that will be obtained in this section are not additional equations required for closure of degrees of freedom, but rather alternative equations developed from the previous equilibrium and stability equations, using relations from mass balance and from molar fraction complementarity to allow the splitting of the system of equations in two blocks of resolution.

Similarly to Rachford-Rice approach, we define K-values (distribution coefficients) $K_{i,j}$ to represent relative affinity of a component between two phases. However, we propose the definition of multi-reference K-values, that is, calculated with a different reference phase for each component, which is assumed present and must not exclude the regarded component.

$$K_{i,j} = \frac{\phi_{i,ref(i)}}{\phi_{i,j}} \tag{A.26}$$

So that $K_{i,j}$ will be zero for index j phases excluding index i component, and, otherwise, always lower than 1.

While fugacity coefficients are expressed as:

$$\phi_{i,j} = \frac{\hat{f}_{i,j}}{x_{i,j}P} \tag{A.27}$$

Using Equations (A.25), (A.27) and (A.28) for an index j phase and a reference phase for all components assumed present.

$$\theta_{ref(i)} = 0 \texttt{ for } i \texttt{ in } c \tag{A.28}$$

$$x_{i,j} = x_{i,ref(i)} K_{i,j} e^{\theta_j} \tag{A.29}$$

From this, it is possible to obtain explicit expressions for molar fraction as functions of different variables. The intensive form of the multiphase mass balance is expressed, having explicit the mass balance reference phase *REF* being used for the dependent relative amount definition, as:

$$z_i = \sum_{j \texttt{ in } f_{\neq REF}} (\beta_j x_{i,j}) + \left(1 - \sum_{j \texttt{ in } f_{\neq REF}} (\beta_j)\right) x_{i,REF} \texttt{ for } i \texttt{ in } c \tag{A.30}$$

In which index j counts only assumed present phases.

Substituting Eq. (A.29) in Eq. (A.30), and imposing that the Res^S equations are met, the summation can be expressed only in terms of assumed present phases and then stability variables in the summation vanishes.

$$z_i = x_{i,ref(i)} \left(\sum_{j \texttt{ in } f_{\neq REF}} (\beta_j K_{i,j}) + \left(1 - \sum_{j \texttt{ in } f_{\neq REF}} (\beta_j)\right) K_{i,REF} \right) \texttt{ for } i \texttt{ in } c \tag{A.31}$$

From which we get:

$$x_{i,ref(i)} = \frac{z_i}{K_{i,REF} + \sum_{l \texttt{ in } f_{\neq REF}} (\beta_l (K_{i,l} - K_{i,REF}))} \texttt{ for } i \texttt{ in } c \texttt{ for } j \texttt{ in } f \tag{A.32}$$

Also, fugacity can be expressed as function of the variables used in this

section, in the same way developed for molar fractions.

$$\hat{f}_{i,j} = \frac{z_i K_{i,j} e^{\theta_j}}{K_{i,REF} + \sum_{l \text{ in } f_{\neq REF}} \left(\beta_l \left(K_{i,l} - K_{i,REF}\right)\right)} \phi_{i,j} P \text{ for } i \text{ in } c \text{ for } j \text{ in } f \tag{A.33}$$

From Eq. (A.32) a set of non-linear residue equations will, be derived as follows:

Subtracting Eq. (A.5) for an index j phase and for the reference phase being used for the dependent relative amount definition, in combination with Eq. (A.29), we get:

$$\sum_{i \text{ in } c} \left(x_{i,ref(i)} \left(K_{i,j} e^{\theta_j} - K_{i,REF} \right) \right) = 0 \text{ for } j \text{ in } f \tag{A.34}$$

Substituting Eq. (A.32) in Eq. (A.34) we get the generalized Rachford-Rice equation:

$$Res_n^E = \sum_{i \text{ in } c} \left(\frac{z_i \left(K_{i,n} e^{\theta_n} - K_{i,REF} \right)}{K_{i,REF} + \sum_{l \text{ in } f_{\neq REF}} \left(\beta_l \left(K_{i,l} - K_{i,REF}\right)\right)} \right) = 0 \tag{A.35}$$

$$\text{for } i \text{ in } c \text{ for } j \text{ in } f$$

However, for assumed present phases, $\theta_j = 0$, in order to meet Res_j^{S} analytically, therefore, let p contain the indexes for assumed present phases, i. e. phases whose θ variables are equal to zero, then Res_n^{p} is a nonlinear function of β_j only. And for shadow phases, θ_j can be evaluated explicitly. Therefore, we derived, from these, the following two decoupled set of equations:

$$Res_n^{\mathrm{p}} = \sum_{i \text{ in } c} \left(\frac{z_i \left(K_{i,n} - K_{i,REF} \right)}{K_{i,REF} + \sum_{l \text{ in } p} \left(\beta_l \left(K_{i,l} - K_{i,REF}\right)\right)} \right) = 0 \tag{A.36}$$

$$\text{for } i \text{ in } c \text{ for } j \text{ in } f$$

For assumed present phases, and

$$\theta_j = \ln\left(\frac{\sum\limits_{i \text{ in } c}\left[\dfrac{z_i\left(K_{i,REF}\right)}{K_{i,REF} + \sum\limits_{l \text{ in } p}\left[\beta_l\left(K_{i,l} - K_{i,REF}\right)\right]}\right]}{\sum\limits_{i \text{ in } c}\left[\dfrac{z_i\left(K_{i,j}\right)}{K_{i,REF} + \sum\limits_{l \text{ in } p}\left[\beta_l\left(K_{i,l} - K_{i,REF}\right)\right]}\right]}\right) \tag{A.37}$$

For assumed shadow phases. Partial derivatives of Res^{p} with respect to β_j are taken analytically, and those with respect to T or P, are taken analytically in chain rule as function of partial derivatives of $\phi_{i,j}$, which in turn can be taken numerically or analytically depending of the thermodynamic model implementation.

Appendix B

Derivation of the pressure shift model

In this appendix we present the detailed derivation of thermodynamics properties from the semi-grand canonical partition function, taking into consideration the dependence of the partition function for the single enclathrated molecule under an external field with respect to lattice molar volume.

We start by recalling the basic equations composing the hydrate modeling framework, as published in literature, and whose interpretations are discussed in the body of this thesis.

B.1 The semi-grand canonical partition function

The semi-grand canonical partition function, $\Xi^H = \Xi^H\left(T, V^{\mathrm{H}}, N_{\mathrm{w}}, \boldsymbol{\lambda}\right)$, is a function of the number of water molecules, N_{w}, the absolute activity (λ_i) defined for each component (i) in the hydrate phase, the volume of the hydrate phase V^{H} and temperature T as independent variables. It is expressed as

$$\ln(\Xi) = \ln\left(Q^{EL}\right) + \sum_j \left[\nu_j N_{\mathrm{w}} \ln\left(\sum_i \left[q_{ij}\lambda_i\right] + 1\right)\right] \tag{B.1}$$

Where the absolute activity (λ_i) for each component in the hydrate phase is defined from its chemical potential (μ_i).

$$\mu_i = k_{\mathrm{B}} T \ln\left(\lambda_i\right) \tag{B.2}$$

Where the proportionality factor (ν_j) is the ratio between number of cages of each type and the number of water molecules in a hydrate unit cell for a given geometry of the lattice structure.

The hydrate thermodynamic potential Ψ is related to Helmholtz energy A according to

$$(\Psi) = \left(A - \sum_i (N_i \mu_i) \right) = (-k_B T \ln (\Xi)) \tag{B.3}$$

and therefore it can be shown that its differential form, from classical thermodynamics is

$$d\frac{\Psi}{k_B T} = -\frac{U}{k_B T^2} dT - \frac{P}{k_B T} dV + \frac{\mu_w}{k_B T} dN_w - \sum_i [N_i d \ln (\lambda_i)] \tag{B.4}$$

B.2 The empty lattice reference

The empty lattice is described by the canonical partition function, $Q^{EL}(T, V^{EL}, N_w)$, as a function of temperature, volume and number of molecules, being it pure in water. The volume of that describes the empty lattice in this partition function is the same as the hydrate volume. The empty lattice thermodynamic potential is related to Helmholtz energy according to

$$(A) = (-k_B \ T \ \ln (Q)) \tag{B.5}$$

and therefore its differential form, from classical thermodynamics is

$$d\left(\frac{A}{k_B T}\right) = -\frac{U}{k_B T^2} dT - \frac{P}{k_B T} dV + \frac{\mu_w}{k_B T} dN_w \tag{B.6}$$

B.3 Cell theory and Langmuir coefficients

The single molecule canonical partition function under the mean field cage potential, $q_{i,j} = q_{ij}(T, V^H, N_w)$, is a function of temperature, volume and number of molecules of water.

Langmuir coefficients are defined from this partition function and fugacity as

$$q_{ij} \lambda_i = C_{ij} \hat{f}_i \tag{B.7}$$

And we can express q_{ij} from C_{ij}, for convenient symbolic calculations as

$$q_{ij} = k_{\mathrm{B}} T \Phi_i C_{ij} \tag{B.8}$$

With Φ_i representing the configurational integral for internal degrees of freedom (as rotation and vibration) and particle momentum (thermal de Broglie wavelength).

We describe q_{ij} and C_{ij} using the cage potential derived from the Kihara pair interaction potential. The resulting expression for w_{ij} is given by

$$\mathtt{D1} = \frac{a_i}{R_j} \tag{B.9}$$

$$\mathtt{D2} = 1 - \frac{r}{R_j} - \mathtt{D1} \tag{B.10}$$

$$\mathtt{D3} = 1 + \frac{r}{R_j} - \mathtt{D1} \tag{B.11}$$

$$\mathtt{DEL}(i) = \frac{\mathtt{D2}^{-i} - \mathtt{D3}^{-i}}{i} \tag{B.12}$$

$$\mathtt{R1} = \frac{\sigma_i^{12}}{R_j^{11}} \tag{B.13}$$

$$\mathtt{R2} = \frac{\sigma_i^{6}}{R_j^{5}} \tag{B.14}$$

$$\mathtt{S1} = \mathtt{DEL}(10) + \mathtt{D1DEL}(11) \tag{B.15}$$

$$\mathtt{S2} = \mathtt{DEL}(4) + \mathtt{D1DEL}(5) \tag{B.16}$$

$$w_{ij} = \frac{2 Z_j \epsilon_i \left(\mathtt{R1S1} - \mathtt{R2S2}\right)}{r} \tag{B.17}$$

Where a_i, σ_i and ϵ_i are the parameters from the Kihara pair interaction potential of guest component (i) and a water molecule from the lattice. Monospaced symbols represent non physically meaningful quantities used for breaking equations into smaller terms.

And the Langmuir Coefficients are calculated by the free volume integral considering the cage potential according to

$$C_{ij} = \frac{\int_0^{R-a_j} \left[\exp\left(\frac{-w_{ij}}{k_{\mathrm{B}} T}\right) 4\pi r^2\right] \mathrm{d}r}{k_{\mathrm{B}} T} \tag{B.18}$$

Where the dependency of q_{ij} and C_{ij} on V and N_{w} is solely by means of

the cage radii $R = R\left(\overline{V}^{\mathrm{EL}}\right)$ as function of the lattice molar volume

$$\overline{V}^{\mathrm{EL}} = \frac{V^{\mathrm{H}}}{N_{\mathrm{w}}} \tag{B.19}$$

B.4 Derivation of thermodynamic properties from the partition function

We now proceed to obtain derived properties, specifically relations of guest amount, pressure, chemical potential of water, internal energy and enthalpy.

According to Eq. B.4, we can calculate the following derived properties from first derivatives of the partition function:

$$N_i = -\left(\frac{\partial \frac{\Psi}{k_{\mathrm{B}}T}}{\partial \ln\left(\lambda_i\right)}\right)_{T,V^{\mathrm{H}},N_{\mathrm{w}},\lambda_{\neq i}} \tag{B.20}$$

$$P^{\mathrm{H}} = -k_{\mathrm{B}}T\left(\frac{\partial \frac{\Psi}{k_{\mathrm{B}}T}}{\partial V^{\mathrm{H}}}\right)_{T,N_{\mathrm{w}},\underline{\lambda}} \tag{B.21}$$

$$U^{\mathrm{H}} = -k_{\mathrm{B}}T^2\left(\frac{\partial \frac{\Psi}{k_{\mathrm{B}}T}}{\partial T}\right)_{V^{\mathrm{H}},N_{\mathrm{w}},\underline{\lambda}} \tag{B.22}$$

$$\mu_{\mathrm{w}}^{\mathrm{H}} = k_{\mathrm{B}}T\left(\frac{\partial \frac{\Psi}{k_{\mathrm{B}}T}}{\partial N_{\mathrm{w}}}\right)_{T,V^{\mathrm{H}},\underline{\lambda}} \tag{B.23}$$

From these relations, we anticipate that we need to be able to calculate derivatives of the Langmuir coefficients with respect to volume, number of molecules of water and temperature.

The differential form of the Langmuir coefficients with respect to volume and number of water molecules is

$$dC_{ij}(V^{\mathrm{H}}, N_{\mathrm{w}}) = \frac{\partial C_{ij}}{\partial V^{\mathrm{H}}}dV^{\mathrm{H}} + \frac{\partial C_{ij}}{\partial N_{\mathrm{w}}}dN_{\mathrm{w}} \tag{B.24}$$

However, as it is assumed that the Langmuir coefficients can be expressed

solely as function of lattice molar volume this must be equivalent to

$$dC_{ij}\left(\frac{V^{\mathrm{H}}}{N_{\mathrm{w}}}\right)=\frac{\partial C_{ij}}{\partial\left(\frac{V^{\mathrm{H}}}{N_{\mathrm{w}}}\right)}d\left(\frac{V^{\mathrm{H}}}{N_{\mathrm{w}}}\right) \tag{B.25}$$

Where the differential form of the lattice molar volume with respect to Volume and number of water molecules is

$$d\left(\frac{V^{\mathrm{H}}}{N_{\mathrm{w}}}\right)=\frac{\partial\left(\frac{V^{\mathrm{H}}}{N_{\mathrm{w}}}\right)}{\partial V^{\mathrm{H}}}dV^{\mathrm{H}}+\frac{\partial\left(\frac{V^{\mathrm{H}}}{N_{\mathrm{w}}}\right)}{\partial N_{\mathrm{w}}}dN_{\mathrm{w}} \tag{B.26}$$

Therefore, executing the partial derivatives

$$d\left(\frac{V^{\mathrm{H}}}{N_{\mathrm{w}}}\right)=\left(\frac{1}{N_{\mathrm{w}}}\right)dV^{\mathrm{H}}+\left(\frac{-V^{\mathrm{H}}}{N_{\mathrm{w}}^{2}}\right)dN_{\mathrm{w}} \tag{B.27}$$

Using this relation, we show that the differential form of the Langmuir coefficients with respect to independently variable volume and number of moles depending on the partial derivative of the Langmuir coefficients with lattice molar volume takes a simple form for numerical calculations as follows.

$$dC=\frac{\partial C_{ij}}{\partial\overline{V}^{abbel}}\left(\frac{1}{N_{\mathrm{w}}}dV^{\mathrm{H}}+\frac{-V^{\mathrm{H}}}{N_{\mathrm{w}}^{2}}dN_{\mathrm{w}}\right) \tag{B.28}$$

From this, we express the symbolic partial derivatives of Langmuir coefficients with respect to volume

$$\left(\frac{\partial C_{ij}}{\partial V^{\mathrm{H}}}\right)_{T,N_{\mathrm{w}}}=\left(\frac{\partial C_{ij}}{\partial\overline{V}^{\mathrm{EL}}}\right)_{T}\frac{1}{N_{\mathrm{w}}} \tag{B.29}$$

and with respect to number of water molecules

$$\left(\frac{\partial C_{ij}}{\partial N_{\mathrm{w}}}\right)_{T,V^{\mathrm{H}}}=\left(\frac{\partial C_{ij}}{\partial\overline{V}^{\mathrm{EL}}}\right)_{T}\frac{-V^{\mathrm{H}}}{(N_{\mathrm{w}})^{2}} \tag{B.30}$$

both depending on the partial derivative of the Langmuir coefficients with respect only to lattice molar volume.

The derivatives of Langmuir coefficients with respect to lattice molar volume is related to the The derivatives of Langmuir coefficients with respect to

cage radii according to

$$\left(\frac{\partial C_{ij}}{\partial \overline{V}^{\mathrm{EL}}}\right)_T = \left(\frac{\partial C_{ij}}{\partial R_j}\right)_T \left(\frac{\partial R_j}{\partial \overline{V}^{\mathrm{EL}}}\right) \tag{B.31}$$

From Eq. B.8

$$\left(\frac{\partial \ln\left(q_{ij}\right)}{\partial R_j}\right)_T = \frac{1}{C_{ij}} \left(\frac{\partial C_{ij}}{\partial R_j}\right)_T \tag{B.32}$$

We can evaluate $\left(\partial C_{ij}/\partial R_j\right)_T$ from Eq. B.18 using the Leibniz rule for differentiation of integrals

$$\frac{\partial}{\partial x}\int_l^u f(t;x)dt = f(u;x)\left(\frac{\partial u}{\partial x}\right) - f(l;x)\left(\frac{\partial l}{\partial x}\right) + \int_l^u \left(\frac{\partial f}{\partial x}\right)(t;x)dt \tag{B.33}$$

with R_j for x, 0 for l, $R_j - a_i$ for u, and $4\pi r^2 e^{(-w_{ij}/k_{\mathrm{B}}T)}$ for f.

Then

$$\left(\frac{\partial l}{\partial x}\right) = \left(\frac{\partial 0}{\partial R_j}\right) = 0 \tag{B.34}$$

and

$$\left(\frac{\partial u}{\partial x}\right) = \left(\frac{\partial R_j - a_i}{\partial R_j}\right) = 1 \tag{B.35}$$

however w_{ij} at the boundary is undetermined with limit at infinity

$$\lim_{r \to R_j - a_i}\left(w_{ij}\right) \to \infty \tag{B.36}$$

therefore, the exponential factor, in the limit, is zero

$$f(l;x) = \lim_{w_{ij}\to\infty}\left(4\pi r^2 e^{\frac{-w_{ij}}{k_{\mathrm{B}}T}}\right) \to 0 \tag{B.37}$$

finally ,the derivatives in the third contribution are taken symbolically

$$\left(\frac{\partial f(t;x)}{\partial x}\right) = \left(\frac{\partial}{\partial R_j}\right)\left(4\pi r^2 \exp\left(\frac{-w_{ij}(r;R_j)}{T}\right)\right) \tag{B.38}$$
$$= \frac{-4\pi}{T} e^{\left(\frac{-w_{ij}}{k_B T}\right)} \left(\frac{\partial w_{ij}}{\partial R_j}\right) r^2$$

Then

$$\left(\frac{\partial C_{ij}}{\partial R_j}\right) = \frac{\int_0^{R_j} \frac{-4\pi r^2}{k_B\, T} \left(\frac{\partial w_{ij}}{\partial R_j}\right) \exp\left(\frac{-w_{ij}(r)}{k_B\, T}\right) \mathrm{d}r}{k_B\, T} \tag{B.39}$$

And the expression for $\left(\partial w_{ij}/\partial R_j\right)$ is obtained symbolically from the aforementioned expressions for w_{ij}

$$\texttt{dD1dR} = -\frac{a_i}{R_j^2} \tag{B.40}$$
$$\texttt{dD3dR} = 1 - \frac{r}{R_j^2} - \texttt{dD1dR} \tag{B.41}$$
$$\texttt{dDELdR}(i) = \frac{-i\texttt{D2}^{-i-1}\texttt{dD2dR} + i\texttt{D3}^{-i-1}\texttt{dD3dR}}{i} \tag{B.42}$$
$$\texttt{dR1dR} = -11\left(\frac{\sigma_i}{R_j}\right)^{12} \tag{B.43}$$
$$\texttt{dR2dR} = -5\left(\frac{\sigma_i}{R_j}\right)^{-6} \tag{B.44}$$
$$\texttt{dS1dR} = \texttt{dDELdR}(10) + \texttt{dD1dRDEL}(11) + \texttt{D1dDELdR}(11) \tag{B.45}$$
$$\texttt{dS2dR} = \texttt{dDELdR}(4) + \texttt{dD1dRDEL}(5) + \texttt{D1dDELdR}(5) \tag{B.46}$$
$$\left(\partial w_{ij}/\partial R_j\right) = \frac{2Z_j\epsilon_i}{r}\ \left(\texttt{dR1dRS1} - \texttt{dR2dRS2} + \texttt{R1dS1dR} - \texttt{R2dS2dR}\right) \tag{B.47}$$

Regarding derivatives with respect to temperature, from Eq. B.8

$$\left(\frac{\partial \ln\left(q_{ij}\right)}{\partial T}\right)_{R_j} = \frac{1}{C_{ij}\, T}\ \left(\frac{\partial C_{ij}\, T}{\partial T}\right)_{R_j} + \left(\frac{\partial \ln\left(\Phi_i\right)}{\partial T}\right) \tag{B.48}$$

we evaluate again from Eq. B.18 using the Leibniz rule for differentiation of integrals.

In this case, as neither of the limits $R_j - a_i$ and 0 are functions of T at

constant V^{H} and N_{w}.

$$\left(\frac{\partial C_{ij}\ T}{\partial T}\right)_{R_j} = \frac{1}{k_{\mathrm{B}}}\int_0^{R_j-a_i}\left(4\pi r^2 e^{(-w_{ij}/(k_{\mathrm{B}}\ T))}(-w_{ij}/k_{\mathrm{B}})(-1/(T^2))\right)dr \quad \text{(B.49)}$$

We evaluate the free volume integrals for all of C_{ij}, $\left(\partial C_{ij}/\partial R_j\right)_T$ and $\left(\partial C_{ij}\ T/\partial T\right)_{R_j}$ using the Simpson method.

B.5 Number of guest component molecules

From Eq. B.20 one can relate number of guest with the partition function as follows

$$N_i = \left(\frac{\partial\left(\sum_j\left[\nu_j N_{\mathrm{w}}\ln\left(\sum_i\left[q_{ij}\lambda_i\right]+1\right)\right]\right)}{\partial\ln\left(\lambda_i\right)}\right)_{T,V^{\mathrm{H}},N_{\mathrm{w}},\lambda_{\neq i}} \quad \text{(B.50)}$$

Where Q^{EL} is not a function of guest activities λ_i, but each term in the cage type summation is.

$$N_i = \sum_j\left[\left(\frac{\partial\left(\nu_j N_{\mathrm{w}}\ln\left(\sum_i\left[q_{ij}\lambda_i\right]+1\right)\right)}{\partial\ln\left(\lambda_i\right)}\right)_{T,V^{\mathrm{H}},N_{\mathrm{w}},\lambda_{\neq i}}\right] \quad \text{(B.51)}$$

Taking the chain rule on the differentiation of the logarithm function

$$N_i = \sum_j\left[\nu_j N_{\mathrm{w}}\frac{1}{\left(\sum_i\left[q_{ij}\lambda_i\right]+1\right)}\left(\sum_i\left[\left(\frac{\partial q_{ij}\lambda_i}{\partial\ln\left(\lambda_i\right)}\right)_{T,V^{\mathrm{H}},N_{\mathrm{w}},\lambda_{\neq i}}\right]\right)\right] \quad \text{(B.52)}$$

And rearranging the summations

$$N_i = \sum_i\left(\sum_j\left(\nu_j N_{\mathrm{w}}\frac{q_{ij}\lambda_i}{\left(\sum_i\left(q_{ij}\lambda_i\right)+1\right)}\right)\right) \quad \text{(B.53)}$$

The number of molecules per component N_i can be further decomposed into number of guests per cage type, whose total recuperates N_i according to

$$N_i = \sum_j\left(N_{ij}\right) \quad \text{(B.54)}$$

Therefore it can be shown that the number of molecules a component i in a cage of type j is

$$N_{ij} = \nu_j \, N_{\mathrm{w}} \, \frac{q_{ij}\lambda_i}{\sum\limits_i \left(q_{ij}\lambda_i\right) + 1} \tag{B.55}$$

from which it is convenient to define the occupancy fraction (Θ_{ij}) of type j cages by molecules of type i as

$$\Theta_{ij} = N_{ij}/N_{\mathrm{w}} = \frac{q_{ij}\lambda_i}{\sum_k \left[q_{kj}\lambda_k\right] + 1} = \frac{C_{ij}f_i}{\sum_k \left[C_{kj}f_k\right] + 1} \tag{B.56}$$

We can use this definition to conveniently rewrite the partition function

Demonstration. Let a_i and b_j be arrays.

$$\begin{aligned}
a_i &= \frac{b_i}{\sum_k [b_k] + 1} \\
\sum_i [a_i] &= \frac{\sum_i [b_i]}{\sum_k [b_k] + 1} \\
1 - \sum_k [a_k] &= 1 - \frac{\sum_k [b_k]}{\sum_k [b_k] + 1} \\
1 - \sum_k [a_k] &= \frac{\sum_k [b_k] + 1 - \sum_k [b_k]}{\sum_k [b_k] + 1} \\
1 - \sum_k [a_k] &= \frac{1}{\sum_k [b_k] + 1} \\
\sum_k [b_k] + 1 &= \frac{1}{1 - \sum_k [a_k]}
\end{aligned}$$

□

Then, for $a_i \Leftarrow \Theta_{ij}$ and $b_i \Leftarrow C_{ij}\,\hat{f}_i$

$$\sum_i \left[q_{ij}\lambda_i\right] + 1 = \frac{1}{1 - \sum_i \left[\Theta_{ij}\right]} \tag{B.57}$$

And the resulting expression for the partition function is

$$\frac{-\Psi}{k_{\mathrm{B}}\,T} = \ln\left(\Xi\right) = -\ln\left(Q^{\mathrm{EL}}\right) - \sum_j \left[\nu_j N_{\mathrm{w}} \ln\left(1 - \sum_i \left[\Theta_{ij}\right]\right)\right] \tag{B.58}$$

Anticipating the need for derivatives of Θ_{ij} for the obtainment of the remaining derived properties we take generic derivatives from Eq. B.56.

$$d\Theta_{ij}\left(V,T,N_{\mathrm{w}},\underline{\lambda}\right)=d\left(\frac{q_{ij}\lambda_i}{\sum_k\left[q_{kj}\lambda_k\right]+1}\right) \tag{B.59}$$

then

$$\begin{aligned}d\Theta_{ij}\left(V,T,N_{\mathrm{w}},\underline{\lambda}\right)=&\\ \frac{\lambda_i}{\sum_k\left[q_{kj}\lambda_k\right]+1}dq_{ij}-&\frac{q_{ij}\lambda_i}{\left(\sum_k\left[q_{kj}\lambda_k\right]+1\right)^2}\sum_k\lambda_k dq_{kj}\\ &-\frac{q_{ij}\lambda_i}{\left(\sum_k\left[q_{kj}\lambda_k\right]+1\right)^2}\sum_k q_{kj}d\lambda_k\frac{q_{ij}}{\sum_k\left[q_{kj}\lambda_k\right]+1}d\lambda_i\end{aligned} \tag{B.60}$$

Whose terms can be grouped into.

$$\begin{aligned}d\Theta_{ij}\left(V,T,N_{\mathrm{w}},\underline{\lambda}\right)=&\\ \left(\Theta_{ij}\left(1-\sum_k\Theta_{kj}\right)\right)d\ln\left(q_{ij}\right)+&\left(\Theta_{ij}\left(1-\sum_k\Theta_{kj}\right)\right)d\ln\left(\lambda_i\right)\end{aligned} \tag{B.61}$$

B.6 Hydrate pressure

We can calculate the hydrate pressure in the thermodynamic state described by T, V^{H}, N_{w} and λ_i. Pressure is related to the partition function according to Eq. B.21 and B.58

$$\begin{aligned}P^{\mathrm{H}}=&\\ -k_{\mathrm{B}}T\left(-\left(\frac{\partial\frac{-A^{\mathrm{EL}}}{k_{\mathrm{B}}T}}{\partial V^{\mathrm{H}}}\right)_{T,N_{\mathrm{w}}}+\sum_j\left[\left(\frac{\partial\nu_j N_{\mathrm{w}}\ln\left(1-\sum_i\left[\Theta_{ij}\right]\right)}{\partial V^{\mathrm{H}}}\right)_{T,N_{\mathrm{w}},\lambda_i}\right]\right)\end{aligned} \tag{B.62}$$

Where the empty lattice corresponds to the pressure of the theoretical empty lattice with the given volume, and is therefore named P^{EL}.

$$P^{\mathrm{H}}=P^{\mathrm{EL}}-k_{\mathrm{B}}T\left(\sum_j\left[\nu_j N_{\mathrm{w}}\left(\frac{\partial\ln\left(1-\sum_i\left[\Theta_{ij}\right]\right)}{\partial V^{\mathrm{H}}}\right)_{T,N_{\mathrm{w}},\lambda_i}\right]\right) \tag{B.63}$$

We define the difference $\Delta P^{\mathrm{H-EL}}$, which we call the pressure shift,

$$\Delta P^{\mathrm{H-EL}} = P^{\mathrm{H}} - P^{\mathrm{EL}} - -k_{\mathrm{B}}T \left(\sum_j \left[\nu_j N_{\mathrm{w}} \left(\frac{\partial \ln \left(1 - \sum_i \left[\Theta_{ij}\right]\right)}{\partial V^{\mathrm{H}}} \right)_{T,N_{\mathrm{w}},\lambda_i} \right] \right) \quad \text{(B.64)}$$

Taking the chain rule on the differentiation of the logarithm function

$$\Delta P^{\mathrm{H-EL}} = k_{\mathrm{B}}T \left(\sum_j \left[\frac{\nu_j N_{\mathrm{w}}}{1 - \sum_i \left[\Theta_{ij}\right]} \sum_i \left[\left(\frac{\partial \Theta_{ij}}{\partial V^{\mathrm{H}}} \right)_{T,N_{\mathrm{w}},\lambda_i} \right] \right] \right) \quad \text{(B.65)}$$

Where the derivatives of occupancy with respect to volume are taken from Eq. B.60.

$$\left(\frac{\partial \Theta_{ij}}{\partial V^{\mathrm{H}}} \right)_{T,N_{\mathrm{w}},\lambda_i} = \left(\Theta_{ij} \left(1 - \sum_k \Theta_{kj} \right) \right) \left(\frac{\partial \ln q_{ij}}{\partial V^{\mathrm{H}}} \right)_{T,N_{\mathrm{w}},\underline{\lambda}} \quad \text{(B.66)}$$

Then, on substitution

$$\Delta P^{\mathrm{H-EL}} = k_{\mathrm{B}}T \sum_j \frac{\nu_j \, N_{\mathrm{w}}}{1 - \sum_i \left[\Theta_{ij}\right]} \left(\sum_i \left[\left(\Theta_{ij} \left(1 - \sum_k \Theta_{kj} \right) \right) \left(\frac{\partial q_{ij}}{\partial V^{\mathrm{H}}} \right)_{T,N_{\mathrm{w}},\lambda_i} \right] \right) \quad \text{(B.67)}$$

This can be rearranged into

$$\Delta P^{\mathrm{H-EL}} = k_{\mathrm{B}} \, T \sum_j \left(\nu_j \, N_{\mathrm{w}} \sum_i \left(\frac{\Theta_{ij} \, \left(1 - \sum_k \left(\Theta_{kj}\right) \right)}{1 - \sum_k \left(\Theta_{kj}\right)} \left(\frac{\partial q_{ij}}{\partial V^{\mathrm{H}}} \right)_{T,N_{\mathrm{w}},\lambda_i} \right) \right) \quad \text{(B.68)}$$

Where terms $(1 - \sum_k \left(\Theta_{ij}\right))$ in the numerator and denominator cancel out resulting in

$$\Delta P^{\mathrm{H-EL}} = k_{\mathrm{B}}T \sum_j \nu_j N_{\mathrm{w}} \left(\sum_i \left[\left(\Theta_{ij}\right) \left(\frac{\partial q_{ij}}{\partial V^{\mathrm{H}}} \right)_{T,N_{\mathrm{w}},\lambda_i} \right] \right) \quad \text{(B.69)}$$

Recalling Eq. B.29, B.31, and B.32.

$$\Delta P^{\mathrm{H-EL}} = k_{\mathrm{B}}T\left(\sum_j\left[\nu_j\sum_i\left[\Theta_{ij}\left(\frac{\partial \ln\left(C_{ij}\right)}{\partial \overline{V}^{\mathrm{EL}}}\right)_T\right]\right]\right) \tag{B.70}$$

Is the final form of the pressure shift expression.

Where the derivatives of Langmuir coefficients with respect to lattice molar volume is taken from numerical calculations according to Eq. B.47

B.7 Chemical potential of the host component

The chemical potential of water is related to the partition function according to Eq. B.23.

$$\mu_{\mathrm{w}}^{\mathrm{H}} = k_{\mathrm{B}}T\left(\frac{\partial A^{\mathrm{EL}}/k_{\mathrm{B}}T}{\partial N_{\mathrm{w}}}\right)_{V,T} + k_{\mathrm{B}}T\left(\frac{\partial\left(\sum_j\left[\nu_j\, N_{\mathrm{w}}\ln\left(1-\sum_i\left[\Theta_{ij}\right]\right)\right]\right)}{\partial N_{\mathrm{w}}}\right)_{V,T,\underline{\lambda}} \tag{B.71}$$

Taking the chain rule on the differentiation of the logarithm function

$$\mu_{\mathrm{w}}^{\mathrm{H}} = \mu_{\mathrm{w}}^{EL} + +k_{\mathrm{B}}T\sum_j\left[\nu_j\ln\left(1-\sum_i\left[\Theta_{ij}\right]\right)\right] - k_{\mathrm{B}}T\sum_j\left[\frac{\nu_j N_{\mathrm{w}}}{1-\sum_i\left[\Theta_{ij}\right]}\left(\sum_i\left[\left(\frac{\partial\Theta_{ij}}{\partial N_{\mathrm{w}}}\right)_{T,V^{\mathrm{H}},\lambda_i}\right]\right]\right) \tag{B.72}$$

Where the derivatives of occupancy with respect to volume are taken from Eq. B.60, B.32 and B.31.

$$\mu_{\mathrm{w}}(V,T,N_{\mathrm{w}},\underline{\lambda}) = \mu_{\mathrm{w}}^{EL} + k_{\mathrm{B}}T\sum_j\left[\nu_j\ln\left(1-\sum_i\left[\Theta_{ij}\right]\right)\right] + \overline{V}^{\mathrm{EL}}k_{\mathrm{B}}T\sum_j\nu_j\left(\sum_i\left[\left(\Theta_{ij}\right)\left(\frac{\partial\ln\left(C_{ij}\right)}{\partial\overline{V}^{\mathrm{EL}}}\right)_{T,N_{\mathrm{w}},\lambda_i}\right]\right) \tag{B.73}$$

where Eq. B.70 contains a similar term which can be substituted here resulting in

$$\Delta\mu_{\mathrm{w}}^{\mathrm{H-EL}} = k_{\mathrm{B}}T\left(\sum_j\left[\nu_j \ln\left(1-\sum_i\left[\Theta_{ij}\right]\right)\right]\right) + \left(\overline{V}^{\mathrm{EL}}\right)\Delta P^{H-EL} \quad \text{(B.74)}$$

Which is the final form of the relative chemical potential of water in the pressure shift model.

B.8 Internal energy

Internal energy is related to the partition function according to Eq. B.22.

$$U^{\mathrm{H}} = -k_{\mathrm{B}}T\left(-\left(\frac{\partial\frac{-A^{\mathrm{EL}}}{k_{\mathrm{B}}T}}{\partial T}\right)_{V^{\mathrm{EL}},N_{\mathrm{w}}} + \sum_j\left[\left(\frac{\partial\nu_j N_{\mathrm{w}}\ln\left(1-\sum_i\left[\Theta_{ij}\right]\right)}{\partial T}\right)_{V^{\mathrm{H}},N_{\mathrm{w}},\lambda_i}\right]\right) \quad \text{(B.75)}$$

Where the derivatives of occupancy with respect to temperature are taken from Eq. B.60 and B.48.

$$\frac{U^{\mathrm{H}}-U^{\mathrm{EL}}-\sum_i N_i\bar{U}^{\mathrm{PIG}}}{N_{\mathrm{w}}k_{\mathrm{B}}T^2} = \sum_i\left[\sum_j\left[\nu_j\Theta_{ij}\left(\frac{\partial\ln\left(T\,C_{ij}\right)}{\partial T}\right)_{V^{\mathrm{H}},N_{\mathrm{w}},\lambda_i}\right]\right] \quad \text{(B.76)}$$

Where the derivatives of $\left(T\,C_{ij}\right)$ with respect to T is taken from is taken from numerical calculations according to Eq. B.49.

Appendix C

Parameterization of the hydrate modeling framework

In this appendix, we discuss the strategy used in the parameterization of each item in the clathrate modeling framework. We explain the origin of the parameters used and what adjustments were performed. So far, this work did not conduct a parameter regression of the pressure shift model.

C.1 Formation properties for the empty lattice

The parameterization used for the empty lattice is based on the formation properties estimated by Parrish and Prausnitz 1972.

In order to make the parameters used in their expression of the van der Waals and Platteeuw model compatible with our expression, we have addressed some consistency issues.

We choose as T_0 and P_0 values for the reference condition a value that is a known liquid water-ice equilibrium point. This is important because in this way a single value of $\Delta\mu_{w,00}^{EL-Pw}$ is sufficient for the consistent modeling of hydrate in equilibrium with pure water condition being either liquid water or ice, as $\mu_{w,00}^{I} = \mu_{w,00}^{Lw}$, we choose the arbitrary temperature of 273.15 K (0 °C), and the corresponding ice-liquid equilibrium pressure of 1 atm (1.01325×10^5Pa).

However, because the formation properties of Parrish and Prausnitz corresponded to values at a pressure of 0 Pa, we corrected theses values based on

classical thermodynamics relations and approximate molar volume according to

$$\mathrm{d}(\Delta\mu) = \Delta\overline{V}\ \mathrm{d}P \tag{C.1}$$

and

$$\mathrm{d}\left(\Delta\overline{H}\right) = \left(\Delta\overline{V} - \left(\frac{\partial\Delta\overline{V}}{\partial T}\right)_P\right)\ \mathrm{d}P \tag{C.2}$$

for a pure substance.

We corrected the parameters to the new reference condition using Parrish and Prausnitz own estimate of $\Delta\overline{V}^{\mathrm{EL-I}}$ of $3 \times 10^{-6}\mathrm{m}^3\ \mathrm{mol}^{-1}$ and neglecting the $\left(\partial\overline{V}/\partial T\right)_P$ term. In this way, by changing the reference and and correcting the parameters accordingly, we are essentially using the same parameter set as them in our analyses. For the enthalpy of melting of ice to liquid water we used the value presented by HOLDER *et al.* (1988). The corrected parameters values actually varied little after theses calculations as shown in Table C.1.

Table C.1: Formation properties for the empty lattice with respect to ice and pure liquid water.

	s^I-I	Ref.	I-Lw	Ref.
Original				
$\Delta\mu_w\ (0\ ^\circ\mathrm{C}, 0\ \mathrm{atm})\ /\mathrm{J\ mol}^{-1}$	1.26357×10^3	[1]		
$\Delta\overline{H}_w\ (0\ ^\circ\mathrm{C}, 0\ \mathrm{atm})\ /\mathrm{J\ mol}^{-1}$	1.15060×10^3	[1]	-6.00948×10^3	[2]
$\Delta\overline{V}_w\ (0\ ^\circ\mathrm{C}, 0\ \mathrm{atm})\ /\mathrm{m}^3\ \mathrm{mol}^{-1}$	3.0000×10^{-6}	[1]	1.6000×10^{-6}	[2]
Corrected				
$\Delta\mu_w\ (0\ ^\circ\mathrm{C}, 1\ \mathrm{atm})\ /\mathrm{J\ mol}^{-1}$	1.26387×10^3		0.00000	
$\Delta\overline{H}_w\ (0\ ^\circ\mathrm{C}, 1\ \mathrm{atm})\ /\mathrm{J\ mol}^{-1}$	1.15090×10^3		-6.00948×10^3	

References: [1] PARRISH and PRAUSNITZ (1972), [2] HOLDER *et al.* (1988)

C.2 Cell theory cages radii and Kihara potential

We evaluated phase equilibrium for methane, ethane and carbon dioxide using cage radii, coordination numbers and Kihara potential parameters from Parrish and Prausnitz. However, as we changed volumetric properties from a constant difference $\Delta V^{\mathrm{s^I-Lw}}$ of $4.6 \times 10^{-6}\mathrm{m}^3\ \mathrm{mol}^{-1}$ to independent correlations

for lattice and liquid water volumes, even at moderate pressure the phase equilibrium curve changed significantly, so we performed preliminary regressions to the Kihara parameters at pressure conditions below 1×10^7 Pa to be able perform the analyses of our model extension having an approximately good fit in the limit case. It is know that there are severe correlation issues between a_i, σ_i and ϵ_i when fitting all of them to hydrate equilibrium experimental data (MEDEIROS *et al.*, 2018). Therefore, for a preliminary adjustment, we chose to fit only σ_i and ϵ_i, while holding a_i constant based on Tee, Gotoh and Stewart values (JOHN *et al.*, 1985). These are presented in Table C.2.

Table C.2: Parameters for the Kihara cage potential.

	CH_4	CO_2	C_2H_6
a_i/Å	0.26	0.677	0.574
σ_i/Å	3.35	3.1306	3.3173
$\frac{\epsilon_i}{k_B}$/K	148.91	165.0212	178.7843

We consider that the cage radii varies proportionally with the lattice edge parameter, whose cube is proportional to the lattice molar volume as follows

$$R = R_{00}\sqrt[3]{\frac{\bar{V}}{\bar{V}_{00}}} \tag{C.3}$$

Where, in the model we call the pressure shift model, R_{00} are the radii presented by Parrish and Prausnitz and $\overline{V}_{00}$ is the lattice molar volume when $T = T_0$ and $P = P_0$ according to the correlation for the lattice molar volume presented next. On the other hand, in the model we call the volume shift model, the R_{00} are adjusted and $\overline{V}_{00}$ is the lattice molar volume when $T = T_0$ and $P^{EL} = P_0$ according to the correlation for the lattice molar volume with its cubic unit cell parameter a_0 also adjusted, as will be discussed next.

C.3 Volumetric properties of the empty lattice

The calculations of volumetric properties for the empty lattice are performed using correlations based on the works of KLAPPROTH *et al.* (2003) and SHPAKOV *et al.* (1998).

$$V^{\mathrm{H,CH_4}}/N_{\mathrm{w}} = \left(\frac{a_0^{\mathrm{H}}}{\text{Å}} + \alpha_1\left(\frac{T}{\mathrm{K}}\right) + \alpha_2\left(\frac{T}{\mathrm{K}}\right)^2\right)^3 \frac{10^{-30}N_{\mathrm{A}}}{N_{\mathrm{w}}^{uc}} \exp\left(-k\left(\frac{P^{\mathrm{H}}}{\mathrm{Pa}} - \frac{P_0}{\mathrm{Pa}}\right)\right) \quad \text{(C.4)}$$

as function of the hydrate pressure

These correlations correspond to measurements on methane hydrates, all calculations using the pressure shift model have this correlation assigned to the empty lattice, and therefore predict different values of lattice molar volume for the actual methane hydrates.

$$\overline{V}^{\mathrm{EL}} = \left(\frac{a_0^{\mathrm{H}}}{\text{Å}} + \alpha_1\left(\frac{T}{\mathrm{K}}\right) + \alpha_2\left(\frac{T}{\mathrm{K}}\right)^2\right)^3 \frac{10^{-30}N_{\mathrm{A}}}{N_{\mathrm{w}}^{uc}} \exp\left(-k\left(\frac{P^{\mathrm{EL}}}{\mathrm{Pa}} - \frac{P_0}{\mathrm{Pa}}\right)\right) \quad \text{(C.5)}$$

as function of the pressure of the empty lattice reference.

The parameters are presented in Table C.3

Table C.3: Parameter from the methane hydrate molar volume correlation

Parameter	Value
$a_0^{\mathrm{H}}/\text{Å}$	10.18
α_1	5.39×10^{-5}
α_2	1.78×10^{-6}
k/Pa^{-1}	1.098×10^{-10}
P_0/Pa	1.01325×10^5

In order to observe the influence of the pressure shift correction in the phase equilibrium calculations, deducting the change in volume , i. e. to compare a standard and a corrected model being both in agreement with actual methane hydrate volume at T_0, P_0, we introduced the volume shift model.

In the volume shift model we changed the values of a_0 and R_0, the liquid effect being that when the actual hydrate pressure is $P^{\mathrm{H}} = P_0$, the calculated

volume of the adjusted correlation is close to the experimental volume, according to the original correlation at $P = P_0$.

$$\overline{V}^{\mathrm{EL}} = \left(\frac{a_0^{\mathrm{EL}}}{\mathring{\mathrm{A}}} + \alpha_1\left(\frac{T}{\mathrm{K}}\right) + \alpha_2\left(\frac{T}{\mathrm{K}}\right)^2\right)^3 \frac{10^{-30} N_{\mathrm{A}}}{N_{\mathrm{w}}^{uc}} \exp\left(-k\left(\frac{P^{\mathrm{EL}}}{\mathrm{Pa}} - \frac{P_0}{\mathrm{Pa}}\right)\right) \quad \text{(C.6)}$$

Not intending to perform parameter regression at this point, we developed a simple iterative scheme to adjust these parameters to have an exact correspondence solely at T_0, P_0, and approximate correspondence in its vicinity.

C.3.1 Volume shift algorithm

The premise is that, at $P^{\mathrm{H}} = P = P_0$, $\hat{f}_i = P_0$, and $T = T_0$, the volume calculated by the active correlation for the empty lattice, having the parameter a_0^{EL}, should be equal to the volume calculated by the experimental correlation for actual methane hydrate, having the parameter a_0^{H}.

$$\bar{V}^{\mathrm{EL}}\left(a_0^{\mathrm{EL}}, P_0^{\mathrm{EL}}\right) = \bar{V}^{\mathrm{H}}\left(a_0^{\mathrm{H}}, P_0\right) \quad \text{(C.7)}$$

where P_0^{EL} is related to P_0 according to the pressure shift calculation

$$P_0^{\mathrm{EL}} = P_0 - \Delta P_0^{\mathrm{H-EL}} \quad \text{(C.8)}$$

This can be alternatively expressed from the equivalence of values for the edge parameters

$$a^{\mathrm{EL}}\left(a_0^{\mathrm{EL}}, P_0^{\mathrm{EL}}\right) = a^{\mathrm{H}}\left(a_0^{\mathrm{H}}, P_0\right) \quad \text{(C.9)}$$

The same logic is applied for the obtainment of a corrected value for R_0, here called R_0^{VS} such that when $P^{\mathrm{H}} = P = P_0$, $R = R_0^{\mathrm{PP}}$. While

$$R = R_0^{\mathrm{VS}} \frac{V}{V_0} \quad \text{(C.10)}$$

and V_0 is defined as

$$V_0 = V^{\mathrm{EL}}\left(P^{\mathrm{EL}} = P_0\right) \tag{C.11}$$

The proposed algorithm is implemented as follows

Function `calcVolumeShift`(P_0, T_0)**:**

Let the hydrate pressure assume the value of the reference pressure $P^H = P = P_0$;

Estimate the fugacity of the guest component with the system pressure: $\hat{f} = P$

Let the system temperature be the reference temperature: $T = T_0$

Guess the cubit unit cell edge parameter for the correlation for the empty lattice as equal to that for the correlation for the actual hydrate: $a_0 = a_0^{\mathrm{H}}$

Guess the cages radii in the reference condition for the empty lattice as equal to that for the actual hydrate: $R_0 = R_0^{\mathrm{PP}}$

do

Calculate using the pressure shift algorithm: $\left[P_0^{\mathrm{EL}}\right]^k = P^{\mathrm{EL}}([a_0]^k, P_0)$

Calculate a new a_0 and new R_0 for both cage types:

$$\mathtt{fT} = \sum_i \left[\alpha_i T^i\right] \tag{C.12}$$

$$[a_0]^{k+1} = \left([a_0]^k + \mathtt{fT}\right)\left(e^{-k\left(\left[P^{\mathrm{EL}}\right]^k - P_0\right)}\right)^{\left(\frac{1}{3}\right)} - \mathtt{fT} \tag{C.13}$$

$$\left[R_{j,0}\right]^{k+1} = \left(\left[R_{j,0}\right]^k\right)\left(e^{-k\left(\left[P^{\mathrm{EL}}\right]^k - P_0\right)}\right)^{\left(\frac{1}{3}\right)} \tag{C.14}$$

Calculate the residue:

$$\mathtt{RES} \Leftarrow \frac{\left(\left[P_0^{\mathrm{EL}}\right]^k - \left[P_0^{\mathrm{EL}}\right]^{k-1}\right)}{P_0} \tag{C.15}$$

loop while abs (RES) $> 1 \times 10^{-9}$;

Record solution:

$$a_0^{\mathrm{EL}} = a_0^{\infty} \tag{C.16}$$

$$R_0^{\mathrm{VS}} = R_0^{\infty} \tag{C.17}$$

return $a_0^{\mathrm{EL}}, R_0^{\mathrm{VS}}$

The effect of this method is illustrated in Figure C.1

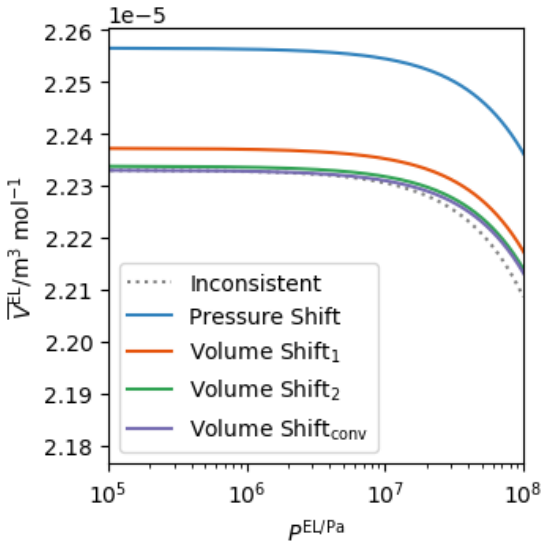

Figure C.1: Volume calculations for four iterations of the volume shift algorithm.

The dotted curve is the correlation based on experimental data for molar volume of methane hydrate. The Pshift curve is the prediction of volume versus system pressure for the pressure shift model, for which the methane hydrate correlation was fed as correlation for the empty lattice. The Vshift 1, 2 and N are the calculated molar volume for the volume shift model after 1, 2 and N iterations, N being a number of iterations required to achieve convergence, which was 4 in this test case.

For applications of the pressure shift model in the design of products and processes, a parameter regression is required to generate an optimized pressure shift model. The parameters in the volume shifted model are useful as initial estimates or references for the setup of search limits in that stage.

C.4 Guest component fugacity

For phase equilibrium calculations with either a gas or liquid phase rich in guest components, we used the equation of state of Peng and Robinson, according to REID *et al.* (1987).

C.5 Volumetric properties for liquid water

The liquid water molar volume was calculated from a correlation based on experimental data of HILBERT *et al.* (1981) and LIDE (2005). The corresponding

parameters are presented in Table C.4.

$$\frac{\bar{V}^{\mathrm{Lw}}}{\left(\mathrm{m}^3\mathrm{mol}^{-1}\right)} = \left(\alpha_0^{\mathrm{Lw}} + \alpha_1^{\mathrm{Lw}}\left(\frac{T}{\mathrm{K}}\right) + \alpha_2^{\mathrm{Lw}}\left(\frac{T}{\mathrm{K}}\right)^2\right)\exp\left(k^{\mathrm{Lw}}\left(P - P_0^{\mathrm{Lw}}\right)\right) \tag{C.18}$$

Table C.4: Parameters of the molar volume correlation for pure liquid water

Parameter	Value
α_0^{Lw}	2.61517×10^{-5}
α_1^{Lw}	5.771157×10^{8}
α_2^{Lw}	1.00453×10^{-10}
$k^{\mathrm{Lw}}/\mathrm{Pa}^{-1}$	3.30859×10^{-10}
$P_0^{\mathrm{Lw}}/\mathrm{Pa}$	1.01325×10^{5}